STUDY OF PULSED LASER SEAM WELDING AND PULSED LASER-GTA HYBRID WELDING ON AISI 316 STAINLESS STEEL

By

A. MASILAMANI CHELLADURAI

(ENGG02200904024)

INDIRA GANDHI CENTRE FOR ATOMIC RESEARCH, KALPAKKAM

A thesis submitted to the

Board of Studies in Engineering Sciences

In partial fulfilment of requirements

For the Degree of

DOCTOR OF PHILOSOPHY

of

HOMI BHABHA NATIONAL INSTITUTE

AUGUST, 2015

Homi Bhabha National Institute

Recommendations of the Viva Voce Committee

As members of the Viva Voce Committee, we certify that we have read the dissertation prepared by **A. Masilamani Chelladurai** entitled "**Study of Pulsed Laser Seam Welding and Pulsed Laser- GTA Hybrid Welding on AISI 316 Stainless Steel**" and recommend that it may be accepted as fulfilling the thesis requirement for the award of Degree of Doctor of Philosophy.

Chairman – Dr. G. Amarendra	**Date:** March 3, 2016
Guide / Convener – Dr. S. Venugopal	**Date:** 2/3/2016
Examiner – Prof. M. Kamaraj	**Date:** 3/3/2016
Member 1 – Dr. S. Murugan	**Date:** 3/3/2016
Member 2- Dr. Shaju K. Albert	**Date:** 3/3/2016

Final approval and acceptance of this thesis is contingent upon the candidate's submission of the final copies of the thesis to HBNI.

I hereby certify that I have read this thesis prepared under my direction and recommend that it may be accepted as fulfilling the thesis requirement.

Date: 3/3/2016

Place: Kalpakkam

3/3/2016

Guide

STATEMENT BY AUTHOR

This dissertation has been submitted in partial fulfillment of requirements for an advanced degree at Homi Bhabha National Institute (HBNI) and is deposited in the library to be made available to borrowers under rules of the HBNI.

Brief quotations from this dissertation are allowable without special permission, provided that accurate acknowledgement of source is made. Requests for permission for extended quotation from or reproduction of this manuscript in whole or in part may be granted by the Competent Authority of HBNI when in his or her judgment the proposed use of the material is in the interests of scholarship. In all other instances, however, permission must be obtained from the author.

A.M. Chelladurai

(A. Masilamani Chelladurai)

DECLARATION

I, hereby declare that the investigation presented in this thesis has been carried out by me. The work is original and has not been submitted earlier as a whole or in part for a degree /diploma at this or any other Institution/ University.

A. M. Chelladurai

(A. Masilamani Chelladurai)

List of Publications arising from the thesis

Journal

1. Energy Transfer Modes in Pulsed Laser Seam Welding, A. M. Chelladurai, K. A. Gopal, S. Murugan, S. Venugopal and T. Jayakumar, *Materials and Manufacturing Processes*, **2015**, *30* (2), 162-168.
2. Effect of Energy Transfer Modes on Solidification Cracking in Pulsed Laser Welding, A. M. Chelladurai, K. A. Gopal, S. Murugan, S. Venugopal, S.K. Albert and T. Jayakumar, *Science and Technology of Welding and Joining*, **2015**, *20* (7), 578-584.

Conferences

1. A comparative study of GTAW and Laser Welding of Austenitic Stainless Steel Tubes, A. M. Chelladurai, K.A. Gopal, S. Murugan and S.K. Albert, *National Welding Seminar*- **2011**, Bhilai.
2. Development of Pulsed Laser- GTAW Hybrid Welding, A. M. Chelladurai, K.A. Gopal, S. Murugan, S. Venugopal and T. Jayakumar, *International Institute of Welding – International Welding Congress 2014 Proceedings*, **2014**, New Delhi, 171-176.

Award

Best technical paper in 'Automation for Process Development' presented in *International Institute of Welding*- International welding Congress 2014 (IC-IIW 2014) held at New Delhi.

A.M. Chelladurai

(A. Masilamani Chelladurai)

DEDICATED TO

My beloved parents

Mr. Asirvatham & Mrs. Koyil Asirvatham

For their untold sacrifices veiled behind my academics

ACKNOWLEDGMENT

It is my pleasure and privilege to thank everyone who rendered their help and support during this course. First of all, I thank my Lord Jesus Christ for His enduring love and blessings showered throughout my life. I am especially thankful for this opportunity and for providing all the grace to accomplish this project.

I express my sincere gratefulness to my thesis supervisor, Dr. S. Venugopal, Director, Metallurgy and Materials Group for his constant encouragement and unconditional support. I owe a debt of gratitude to my technical advisor, Dr. S. Murugan, Head, Innovative Design Engineering and Synthesis Section (IDEAS) for his technical guidance, persistent support and industrious efforts all through my research work.

My heartfelt thanks to Mr. K. A. Gopal for his technical support in handling Laser welding system and establishing hybrid welding facility.

I am grateful to Dr. Shaju K. Albert, Head, Materials Technology Division for his help, encouragement and fruitful discussions. I thank the doctoral committee members, Dr. T. Jayakumar, former Director, Metallurgy and Materials Group and Dr. G. Amarendra, Head, Materials Physics Division for their valuable comments and suggestions during review meetings.

I sincerely thank Department of Atomic Energy (DAE) for the award of research fellowship in Indira Gandhi Centre for Atomic Research, Kalpakkam. I also thank Dr. Baldev Raj, former Director and Dr. P. R. Vasudeva Rao, Director, IGCAR for their inspiration and support. I express my sincere gratitude for the comfortable accommodation and all the administrative support rendered by Dr. M. Saibaba, Director, Recourse Management Group and Dr. G. Sasikala, Dean, Engineering Sciences, HBNI.

I am thankful to Mr. Rajesh Saxena for his lively technical support in establishing and experimenting hybrid welding system. I thankfully acknowledge the friendly ambience I received from all the members of IDEAS, Mr. Sekar, Mr. P.K. Chaurasia, Mr. M. Muthuganesh, Mr. N. Mahendra Prabhu, Mr. R. Ravikumar, Mr. Manam Sambasiva Rao, Ms. Romali, Mr. Ramesh and Mr. K. Purushothaman.

I profusely thank Dr. B. Arivazhagan, MTD for the several prolific discussions on various aspects of welding metallurgy. I sincerely thank Dr. M. Vasudevan, Head, AWPM&MS for his kind support in GTAW experiments. I thank Mr. Mahadevan and Mr. Arun Kumar, NDED for their arduous experimentation on residual stresses measurements. I am grateful to Mr. J. John Swamidoss, ESG for his timely help in providing three-phase power supply for hybrid welding system. I extend my thanks to Mrs. Sreevidya for her help and support in carrying out SEM-EDS analysis.

I express my sincere thanks to Mr. Palani, Mr. Kalai Selvan, Mr. Sakthivel, Mr. Tamilvanan and Mr. Manivannan for their assistance in carrying out experiments.

I cherish the charming friendship of Mr. Dhanasekaran, Mr. Shashwat Kumar Swain, Mr. Sadu Venkatesu, Mr. Srinivasan, Mr. Shuaib Ahmed, Mr. Santhosh Kumar, Mr. Mahendra Chinthala, Mr. Suresh, Mr. Praveen, Mr. Jobby C. Johnson, Mr. Solomon and all the juniors and seniors who journeyed with me during this course.

It is a genuine pleasure to express my deep sense of thanks and gratitude to all the members of the Canaan Church for their loving fellowship and endowing me a homely environment during the stay at Kalpakkam. I relish the rapport with Dr. E. Isaac Samuel and Mrs. Cynthia Isaac for their brotherly love and affection. I am delighted in the fellowship with the families of Mr. N. Theivarajan, Dr. K. I. Gnanasekar and Mr. K. Stanley for their love, counsels and prayers.

I joyfully appreciate the warmth amity with beloved brethren Mr. John Bosco, Mr. Kirubakaran, Mr. John Lawrence, Mr. Christopher, Mr. Stephen, Mr. Manovah David, Mr. Mannsingh and Ms. Johanna.

Finally, I appreciate my beloved Sisters Ms. A. Stella Baby and Ms. A. Melcyba and Brother Mr. A. Jeba Prabakar for their patient and lovely support throughout my life.

A.M. Chelladurai

(A. Masilamani Chelladurai)

TABLE OF CONTENTS

SYNOPSIS .... **I**

TABLE OF CONTENTS .... **IX**

LIST OF FIGURES .... **VI**

LIST OF TABLES .... **X**

CHAPTER 1 INTRODUCTION **1**

1.1 Laser beam welding 1

1.1.1 Working principle of Laser welding 2

1.1.2 Mechanism of laser-material interactions in welding 4

1.2 Energy transfer modes in laser welding 7

1.2.1 Conduction mode 8

1.2.2 Keyhole mode 8

1.3 Classification of energy transfer modes 12

1.4 Hot cracking in austenitic stainless steel 14

1.4.1 Theories on hot cracking 15

1.4.2 Solidification of austenitic stainless steels 17

1.4.3 Weld microstructures and hot cracking 19

1.4.4 Constitutive diagrams 19

1.4.5 Weldability diagrams for pulsed laser welding 21

1.5 Limitations of pulsed laser beam welding 24

1.6 Laser- Arc Hybrid welding 25

1.6.1 Classification of Hybrid welding 28

1.6.2 Weldability of various materials 28

1.6.3 Hybrid welding parameters and their influence on weld geometry and quality 29

1.6.4 Physical mechanisms of laser- arc interaction 34

1.7 Objective of the study 38

1.8 The outline of dissertation 40

CHAPTER 2 MATERIAL AND EXPERIMENTAL METHODS 41

2.1 Material 41

2.2 Nd: YAG Pulsed laser System 42

2.3 Pulsed laser- arc hybrid welding system 45

2.4 Metallography 46

2.5 Scanning electron microscope 48

2.6 XRD-Residual stress measurements 48

2.7 Tensile test 49

CHAPTER 3 ENERGY TRANSFER MODES IN PULSED LASER SEAM WELDING 50

3.1 Pulsed laser seam welding parameters 50

3.2 Experimental Procedure 52

3.3 Experimental results 53

3.4 Discussion 56

3.4.1 Conduction mode 56

3.4.2 Transition mode 59

3.4.3 Penetration mode 60

3.4.4 Keyhole mode 61

3.5 Optimisation of pulse duration 61

3.6 MODES OF LASER SEAM WELDING AND SURFACE CONDITIONS 63

3.7 Conclusions 64

CHAPTER 4 SOLIDIFICATION CRACKING IN PULSED LASER SEAM WELDING 66

4.1 Introduction 66

4.2 Experimental procedure 68

4.3 Results 70

4.3.1 Microstructural analysis of solidification Cracks 70

4.4 Discussion 79

4.4.1 Effect of energy transfer modes on solidification cracking 79

4.4.2 Effect of heat input on solidification cracking 80

4.5 Conclusions 83

CHAPTER 5 STUDIES ON PULSED LASER-GTA HYBRID WELDING 84

5.1 Introduction 84

5.2 Experimental procedures 85

5.3 Results and discussion 87

5.3.1 Energy transfer modes in Pulsed Laser- GTA Hybrid Welding Process 87

5.3.2 Interaction of pulsed laser-GTAW arc in keyhole mode hybrid welding 90

5.4 Position and distance between heat sources 92

5.5 Effect of defocusing on weld geometry 95

5.6 Influence of arc current in pulsed laser-arc hybrid welding 98

5.7 Microstructural and mechanical properties of hybrid, laser and GTA welds 102

5.7.1 Weld geometry 102

5.7.2 Microstructural Analysis 105

5.7.3 Tensile properties of weldments 108

5.7.4 Residual Stress Measurements 110

5.8 conclusions 112

CHAPTER 6 CONCLUSIONS & FUTURE DIRECTIONS 114

6.1 Summary 114

6.2 Suggestions for future works.. 116

REFERENCES 118

SYNOPSIS

Laser beam welding process which utilizes high power, monochromatic, coherent laser light is concentrated using focusing lens system and made to interact on material surface. When the focused laser beam is applied, very low heat input is given as compared to arc welding processes. Hence, the resultant welds are deeper and narrow in geometry and HAZ width is reduced substantially. The consequent thermal load is much lower than in arc processes, and so residual stress development and distortion due to welding thermal cycles is greatly reduced. Further, laser process can be automated easily and high production rate can be achieved as a result of enhanced welding speed. Therefore, laser beam welding finds applications in many fields and industries like power plant, automobile, aerospace, nuclear, ship building, medical etc [1-3]. In the wide range of available lasers, CO_2, Nd: YAG and Fibre lasers are more often used for laser welding applications. Pulsed laser welding is a variant of laser beam processes where laser energy is applied in pulsed mode. Pulsed laser operation gives advantages such as flexibility in applying laser energy, low heat input, very narrow welds with reduced thermal effects etc, [4]. Due to its nature of confined heat affected area, this process can be applied for micro and thermal sensitive welds like heart pacemakers, thin foils etc. While pulsed lasers are largely employed as spot welds in manufacturing industries, continuous, seam welding is performed in lower thickness materials by overlapping spots made by individual pulses.

Laser beam welding is known to have two modes of operation with respect to the manner of transferring laser energy into material, namely, conduction and keyhole. In conduction mode, the power density of laser beam is low and so insignificant or no vaporisation occurs. The heat deposited is conducted to base metal by heat conduction phenomenon. As more heat is conducted in radial direction than in depth direction, these welds are shallow in shape and have low aspect ratio (weld depth/ weld width). Further laser energy absorption is remarkably low at this mode as most of the incident laser photons are reflected on metallic surfaces. Keyhole mode welds are characterised by the formation of characteristic keyhole and resultant drastic enhancement of laser energy absorption. When the power density of laser beam is capable of vaporising material surface, vapour filled hole or depression is formed in weld pool. This characteristic 'keyhole' absorbs laser energy in great proportion which produces welds with high depth of penetration and aspect ratio (depth/ width).

As the energy transfer mode phenomenon influences pulsed laser seam welds altogether, it is necessary to define them with respect to process parameters. In literature the energy transfer mode is classified roughly based on power density of laser beam. It is generally defined that when the power density of laser beam exceeds 10^6 W/cm^2, then mode transforms from conduction to keyhole [5, 6] . However this categorization is very approximate as it is well known that laser process parameters such as beam diameter, focus position, traverse speed determine physical phenomena of laser-material interactions. Further this definition considers that the transition from conduction to keyhole mode is abrupt and no transition regime is present in between conduction and keyhole modes. But a few literature on continuous wave lasers report that the changeover of energy transfer mode from conduction to keyhole is not sudden and there is a transition regime in between these two modes [7, 8]. In case of pulsed laser seam welding, more process parameters are involved. Therefore, energy transfer modes in pulsed laser seam welding are required to be understood and the effect of process parameters on the transition is to be studied.

Further, pulsed laser welding on fully austenitic stainless steel has been reported to encounter solidification cracking issue due to its rapid cooling rate and crack susceptible chemical composition. Since this issue is critical to the integrity of welded structures, it has been addressed by many researchers. Different techniques such as reducing impurity contents, maintaining 3-7% δ- ferrite in weld microstructure, keeping high Cr_{eq}/ Ni_{eq} ratio base metal chemical composition, proper joint design etc, have been proposed to resolve the solidification cracking issue [9-11]. But these methods are not feasible in autogeneous, pulsed laser welding process. Pulsed laser welding of hot cracking susceptible aluminium alloys, super alloys and fully austenitic stainless steels has been attempted with different methodologies. Milewski et al. observed crack-free microstructures under high duty cycle (>60%) conditions [12]. As the susceptibility to hot cracking is closely related to welding conditions, influence of heat input on solidification cracking and HAZ cracking has been studied for laser welding. The tendency for HAZ cracking was observed to reduce with increasing heat input in laser welds of ATI Allvac 718Plus superalloy [13] and Haynes 282 super alloys [14]. Reduced thermal stresses and formation of thick intergranular liquid film were reported as the causes for crack-free welds at higher heat input. However, in contradiction to this, studies on type 316 stainless steel [15] and AZ61 magnesium alloy [16] showed increasing heat input may enhance cracking susceptibility. In all these studies, effect of energy transfer modes of laser welding is not considered. In the work of Montazeri et al. [17], variation of liquation cracking susceptibility of IN738LC superalloy with energy transfer modes has been studied and conduction mode is found to be more susceptible for cracking than keyhole mode. The weld geometry was also found to play an important role in liquation cracking. In the work of Nishimoto et al. on high nitrogen 304 stainless steel, hot cracking susceptibility of conduction mode welds was found to be greater than keyhole welds as nitrogen distribution in welds varies for different modes [18]. Though solidification cracking has been studied extensively, influence of energy transfer modes on hot cracking in pulsed laser welding of fully austenitic stainless steel is not reported much.

The laser-arc hybrid welding process is a variant of laser welding process where laser and electric arc are coupled together and applied on the common molten zone to obtain synergistic advantages and to eliminate the drawbacks of both processes. Hybrid welding experiments are generally carried out using high power lasers and found advantages such as increase in depth of penetration, aspect ratio, welding speed, improved fit-up gap tolerance etc. The process is also performed with low power lasers, and here the benefits are augmentation of keyhole formation, improved arc stability, and increase in welding speed [19-21]. Pulsed laser has been employed in hybrid welding where it has been synchronised with pulsed GTAW for micro welding applications and advantages have been drawn [22]. The study of interaction of pulsed laser with arc and its influence on energy transfer modes is vital in understanding pulsed laser-arc hybrid welding. The interaction of laser and arc influences the weld's geometry and quality. Moreover, several studies are limited to conduction mode welds and keyhole mode pulsed laser welding is seldom reported. Though few experiments have been carried out in pulsed laser welding of stainless steels on optimisation of parameters, weld geometry, microstructures etc, these aspects have not been dealt with adequately [23-25]. In the present study, pulsed laser beam welding of fully austenitic stainless steel of AISI 316 grade has been studied on energy transfer modes and solidification cracking. In addition to that hybrid welding was established by combining GTAW arc with laser beam and experiments have been performed on basic hybrid welding parameters. A comparative study was carried out to analyse the microstructural and mechanical properties of laser, GTA and hybrid welds.

In the present study, pulsed laser beam welding of fully austenitic stainless steel of AISI 316 grade has been studied on energy transfer modes and solidification cracking. In addition to that hybrid welding was established by combining GTAW arc with laser beam and experiments have been performed on basic hybrid welding parameters. A comparative study was carried out to analyse the microstructural and mechanical properties of laser, GTA and hybrid welds. The present work discusses energy transfer modes and its influence on solidification cracking in pulsed laser seam welding of stainless steels. It also comprises the studies on the development of pulsed laser-GTA hybrid welding, hybrid process parameters and comparative study of hybrid, laser and GTAW processes. The study clearly reveals that the conventional classification of modes derived from power density of 10^6 W/cm^2 is not applicable to pulsed laser seam welding. In a systematic study, different zones of energy transfer have been observed based on weld geometry and microstructures. The optimum pulse parameters have been identified to choose appropriate mode and to achieve deeper welds with efficient laser-material interaction. In addition to that for the first time, the effect of modes on solidification cracking has been elucidated. Hybrid welding facility was developed and the effect of basic hybrid parameters on weld geometry has been studied to broaden the application window of pulsed laser seam welding. Drastic enhancement in depth of penetration, tolerance in fit-up gap, crack free welds have been observed. The mechanisms of augmentation in keyhole formation, pulsed laser-arc interaction and arc constriction under the influence of laser have been highlighted and discussed.

LIST OF FIGURES

Figure 1-1 Schematic of Nd: YAG Laser welding 3

Figure 1-2 Flowchart- Transformation of laser energy into thermal energy 5

Figure 1-3 Schematic of plasma formation in laser welding 6

Figure 1-4 Influence of material, wavelength and temperature on laser- material interaction, a) Reflectivity with different materials b) Absorption with different temperatures 7

Figure 1-5 Schematic of a) Conduction and b) Keyhole modes in laser welding 7

Figure 1-6 Mechanisms in keyhole mode welding a) Fresnel absorption and b) Inverse Bremsstrahlung effect 9

Figure 1-7 Schematic of forces acting on keyhole in keyhole mode laser welding 12

Figure 1-8 Stages involved in solidification cracking- Borland's generalized theory 16

Figure 1-9 Pseudo binary phase diagram of 70-30 % austenitic stainless steel alloy... 18

Figure 1-10 WRC-1992 constitutive diagram 20

Figure 1-11 Suutala- cracking susceptibility diagram 21

Figure 1-12 Cracking susceptibility diagram developed by Lienert for 300 series stainless steel pulsed laser welds 23

Figure 1-13 Schematic of arrangement of Laser and arc a) Tandem and b) Hybrid processes.. 26

Figure 1-14 Influence of laser plasma in arc current and voltage A) Decrease in arc resistance due to presence of laser, B) Laser stabilization of fluctuations in arc voltage 26

Figure 1-15 Interaction of laser and arc on material surface in Laser- GMA hybrid welding 36

Figure 1-16 Schematic of interaction of heat sources under the surface of weld pool at two different arc currents 38

Figure 2-1 The CNC Laser workstation used for movement of workpiece........................44

Figure 2-2 Pulsed Laser- Arc hybrid welding experimental setup 45

Figure 2-3 Metallography- polishing machine 47

Figure 2-4 Metallurgical microscope..47

Figure 3-1 Schematic diagram of Laser square wave pulses with illustrations of pulse parameters..51

Figure 3-2 Macrostructures of pulsed laser welds in different energy transfer modes, a) Conduction, b) Transition, c) Penetration and d) Keyhole 56

Figure 3-3 Peak power versus depth of penetration for different pulse durations.............57

Figure 3-4 Peak power density versus aspect ratio for different pulse durations..............57

Figure 3-5 Aspect ratio versus energy density for different pulse durations......................58

Figure 3-6 Method of linear curve fitting- Depth of penetration versus peak power plot 62

Figure 3-7 Penetration depth per unit peak power at different pulse durations along with interaction time 63

Figure 3-8 Surface profiles of a) conduction, b) Transition, c) Penetration and d) Keyhole mode welds...64

Figure 4-1 Microstructures of surface profiles of a) conduction, b) transition/ penetration and c) keyhole mode welds..72

Figure 4-2 Changeover in geometry and cracking severity along weld line in transition/ penetration welds A) At starting position, B) At 'steady condition' 72

Figure 4-3 Microstructures of weld cross sections at root sides of a) Conduction,...........74

Figure 4-4 SEM microstructures of a) conduction, b) transition and c) Keyhole mode welds sectioned at root side of weld 75

Figure 4-5 A) Micrograph depicting SEM-EDS line scan across crack filled region, ...76

Figure 4-6 Effect of heat input and energy transfer modes on cracking severity..............76

Figure 4-7 Effect of heat input and energy transfer modes on mean cell size ... 77

Figure 4-8 Effect of heat input on cooling rate achieved in welds of different energy transfer modes ... 78

Figure 5-1 Macrostructures of conduction mode pulsed laser and hybrid welds ... 88

Figure 5-2 Macrostructures of (a) GTAW, (b) Laser, and (c) Hybrid welds indicating synergistic effect at keyhole mode ... 89

Figure 5-3 Schematic of Pulsed laser- GTA hybrid welding (a) Arc only acting before laser started (b) Both laser and arc plasma interact at laser pulse ON (c) Laser plasma extinguishes in laser pulse OFF time ... 91

Figure 5-4 Macrostructures of A) Arc leading & B) Laser leading hybrid welds at same process parameters ... 92

Figure 5-5 Images of laser-arc interaction A) Laser and arc plasmas interaction during pulse ON time, B) Maintenance of molten pool during laser pulse OFF time ... 93

Figure 5-6 Macrostructures of arc and laser leading welds at inter heat source distances of 4 and 5 mm ... 94

Figure 5-7 Macrostructures of welds at positive defocusing A) Laser alone, B) Hybrid ... 96

Figure 5-8 Macrostructures of welds at negative defocusing- Laser weld's A) surface and B) cross section, Hybrid weld's C) surface and D) cross section ... 97

Figure 5-9 Effect of arc current on pulsed laser- GTA hybrid weld geometry ... 100

Figure 5-10 Macrostructures of a) Laser alone (Mean power 180W), b) GTAW alone (arc current 70 A) and c) hybrid (coupled) welds ... 101

Figure 5-11 Weld geometries of full penetration a) Laser, b) Hybrid and c) GTA welds ... 104

Figure 5-12 Microstructures of full penetration Laser, Hybrid and GTAW welds ... 106

Figure 5-13 Traverse tensile test samples of Laser, GTA and hybrid welds ... 108

Figure 5-14 Tensile test results of laser, GTA and hybrid welds-(a) Joint strength, (b) Ductility 109

Figure 5-15 Residual stress distribution in Laser, GTA and Hybrid welds across weld line 111

LIST OF TABLES

Table 2-1 Chemical composition of AISI 316 stainless steel plate 42

Table 2-2 Specifications of pulsed laser used in experiments 43

Table 3-1 Pulsed laser seam welding parameters 55

Table 4-1 Laser pulse parameters used in experiments 69

Table 5-1 Range of hybrid welding parameters studied in experiments 86

Table 5-2 Process parameters used in Laser, GTA and hybrid processes 103

Table 5-3 Comparison of Microstructures of Laser, GTA and hybrid welds 105

CHAPTER 1 INTRODUCTION 1

Austenitic stainless steels are the structural materials in fast breeder reactor applications due to their better mechanical properties, high temperature strength, low neutronic cross section for fast neutrons, corrosion resistance etc. Components such as fuel clad tubes, wrappers, reactor vessels are fabricated using austenitic stainless steels of different grades like AISI 316, 316L, 316LN and D9 [26-28]. In fabrication of components, welding process is primarily employed. Electric arc processes such as Shielded metal arc welding (SMAW), Gas tungsten arc welding (GTAW), Gas metal arc welding (GMAW) , Flux cored arc welding (FCAW), and Plasma arc welding (PAW) are the commonly used processes. Though these processes are simple and cheaper, due to the low power density of electric arc, high heat input is given on the material, which results in wider weld beads and enlarged heat affected zones (HAZ). In addition, the excessive thermal load may induce high residual stresses in these welds. Further, the productivity is confined as the welding speed of these processes is limited. The application of high energy beams such as electron and laser beams as welding heat sources is observed to provide potential advantages over these limitations.

1.1 LASER BEAM WELDING

Laser beam welding process is an advanced joining process which utilizes high energy laser beam as heat source and promises many advantages over conventional arc welding processes. In this process, monochromatic, coherent laser light is concentrated using focusing lens system and made to interact on material surface. When fine, focused laser beam is applied, very low heat input is given on the material as compared to arc processes. Hence, the resultant welds are deeper, narrower in geometry and the HAZ width is reduced substantially. The consequent exertion of thermal load is much lower than arc welds, and so distortion and residual stress development due to welding thermal cycles is greatly reduced. Further, laser process can be automated easily and high production rate can be achieved because of enhanced welding speed. Therefore, laser beam welding finds applications in many other fields like power generation, automobile, aerospace, ship building, medical, pipelines etc [1-3, 29-33]. In the wide range of available lasers, CO_2, Fibre and Nd: YAG lasers are more often used for welding applications. The unique advantage of laser welding process is that it can be used in micro welding of very thin foils of few micro meters thickness to deeper welds. Pulsed laser welding is a variant of laser beam process where laser energy is applied in pulsed manner. Pulsed mode of laser operation gives advantages such as flexibility in applying laser energy with time, low heat input, very narrow welds with reduced thermal effects, etc [4, 34]. Due to its nature of restricted heat affected area, this process is well suited for micro and precision welds in critical applications like heart pacemakers, thermocouples [35], sensors, detectors [36]. Pulsed lasers are largely employed in spot welds for the advantages of non-contacting nature and high productivity. Continuous seam welds are made by overlapping of spots made by individual laser pulses. This type of continuous seam welds can be used for low thickness materials effectively. Pulsed laser seam welding has been experimented in variety of alloys.

1.1.1 Working principle of Laser welding

Laser welding is performed by focusing high power laser generated from laser resonator and applying onto the joining material surface as shown in Figure 1-1 [37]. The lasing action taking place inside the laser generator and the output laser is characteristic of lasing medium. With respect to the lasing medium used, lasers are classified into solid state

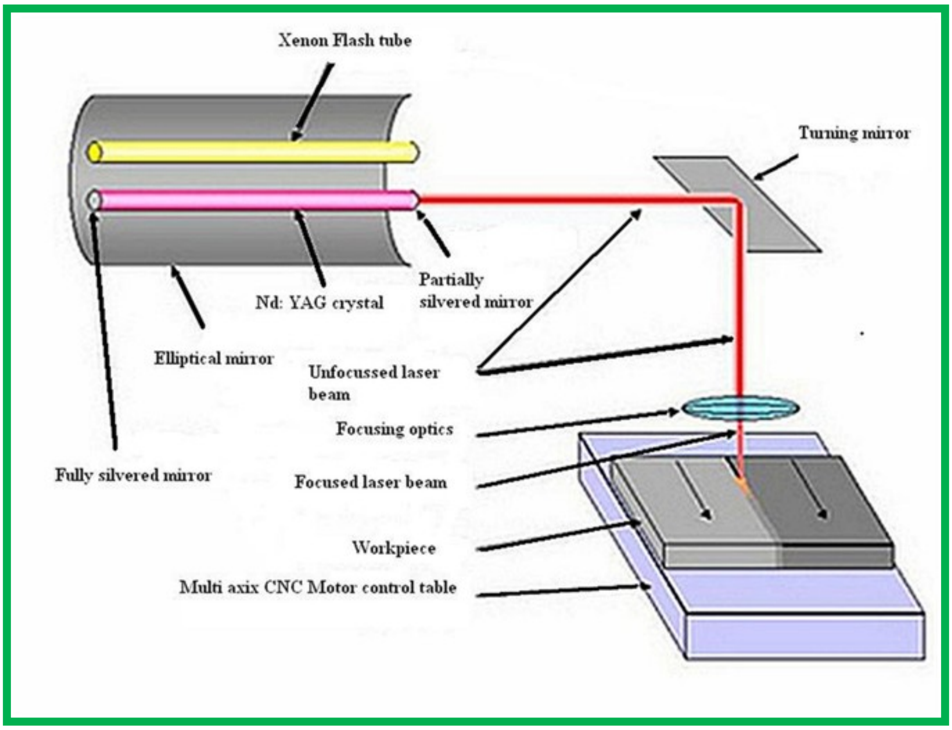

Figure 1-1 Schematic of Nd: YAG Laser welding [37]

lasers, gas lasers, fibre lasers, semiconductor lasers etc. CO_2 gas and solid state Nd: YAG lasers are widely used in laser welding applications. Nowadays fibre lasers also find applications for its low wavelength, compactness and ability to produce high power. The wavelength of the laser photons is decided by lasing medium, and the wavelength of CO_2 laser photons is 10.6 µm and of Nd: YAG laser is 1.06 µm. Laser beam is transmitted either by optical fibre cable or by metallic mirror system. Nd: YAG laser with short wavelength of 1.06 µm can be handled using fibre cable. But, CO_2 laser with wavelength of 10.6 µm cannot be transmitted through fibre cables as long wavelength laser is absorbed by fibre cable and damage it.

Laser welding process is also carried out in pulsed mode to obtain specific advantages. Heat input can be reduced still further when laser is applied in pulsed pattern than continuous mode. This produces welds with narrow weld pool and narrow HAZ. Pulsed lasers are advantageous in spot welds, and very precise applications such as welding of foils, medical devices, sensors, batteries, and microwave enclosures etc. are realized [34]. The flexibility to shape laser pulses by varying power and time yields better quality welds which can be widely used in many engineering applications. Pulsed laser produces short pulses and so less amount of heat is transferred to the work piece. The advantages are low heat input, reduced distortion and higher efficiency in comparison to the continuous laser [4, 38].

Pulsed lasers are used in spot and continuous seam welds. Spot welds are made by either single or more pulses and they find applications in automotive industries etc. In pulsed laser seam welding, joints are made by overlapping of spots formed by consecutive pulses along the weld line. The transformation of laser energy into useful thermal energy for joining is discussed below.

1.1.2 Mechanism of laser-material interactions in welding

The thermal energy required for joining is achieved from the complex interaction of laser with material surface. When the laser light is applied on the material surface, sequence of events takes place. Part of the incident energy is getting reflected away and small percentage is absorbed. The tendency of metal surfaces to reflect light reduces effective absorption of laser energy on metal surfaces. The interaction of laser electro- magnetic radiation with material surface is complicated as it is influenced by many parameters. The conversion of laser-electromagnetic radiation into thermal energy involves a series of physical phenomena as shown in flowchart given in Figure 1-2 [39]. In metals and alloys, the absorption of laser energy occurs by photon-electron interactions. As the laser photon energy is low, it does not vibrate atomic nucleus but excite only free or bound electrons. This process of photons being absorbed by electrons is known as the 'inverse Bremsstrahlung (IB) effect' [5]. These excited electrons collide with lattice phonons or re-radiate in all directions. The collision action causes the structure to vibrate and this vibration is detected as heat energy. When the energy absorption increases sufficiently to the extent of stretching the molecular bonds incapable of withstanding mechanical strength, the material is melted. On further enhancement in energy absorption, the material is evaporated and creates metal vapours above the material surface as explained in Figure 1-3 in schematic form [40]. Metal vapours produced from this laser-material interaction and part of shielding gas are ionised and form plasma known as 'laser induced plasma'. Plasma formation is an essential physical phenomenon in laser welding and it influences resultant weld beads.

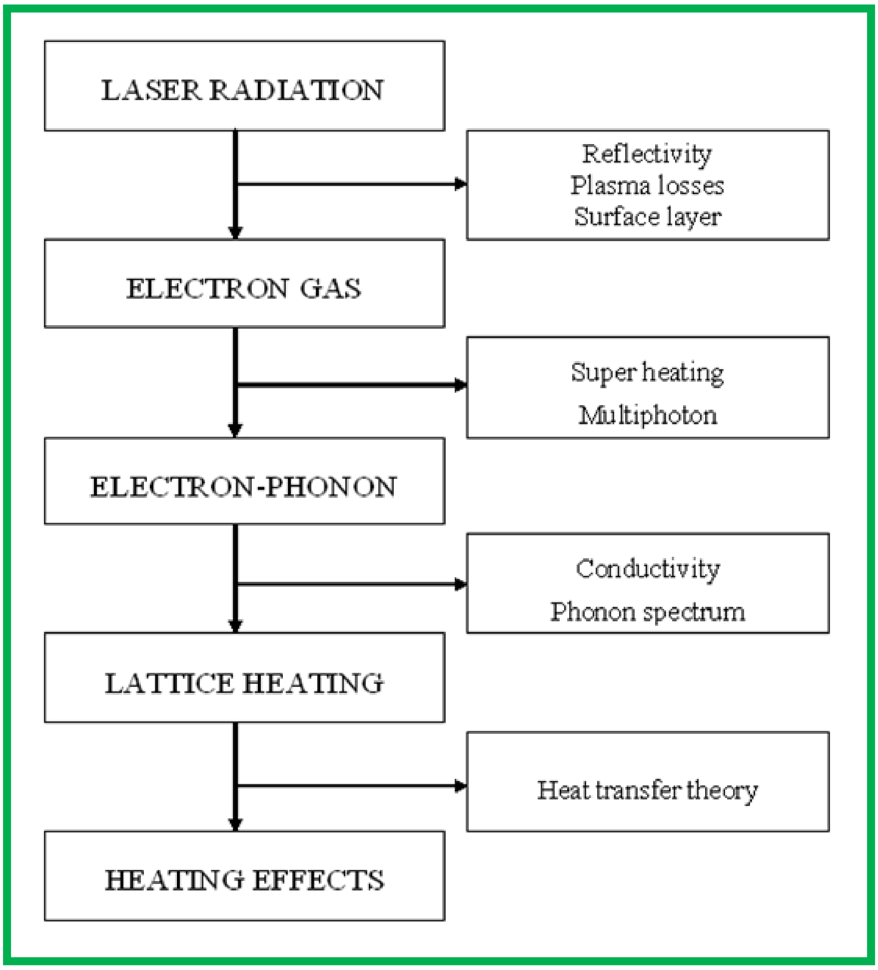

Figure 1-2 Flowchart- Transformation of laser energy into thermal energy [39]

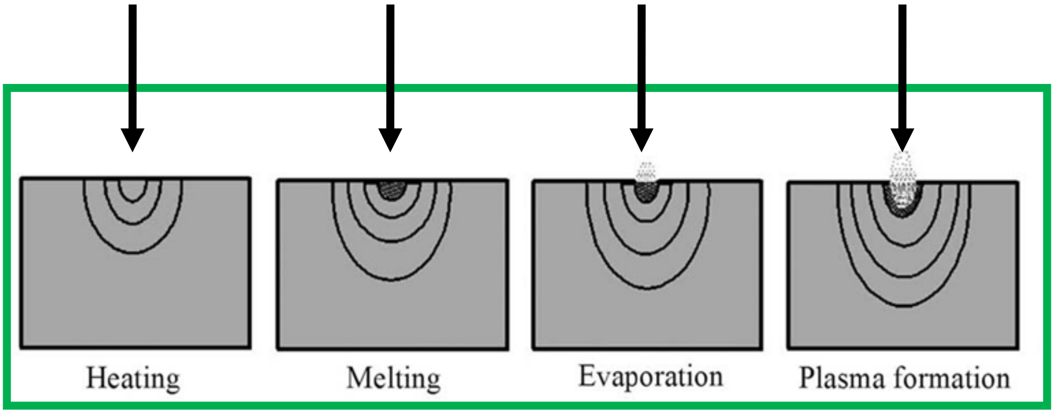

Figure 1-3 Schematic of plasma formation in laser welding [40]

The absorption of laser energy depends on wavelength of laser, nature of materials, material's surface conditions and temperature. Metals and alloys which have high reflectivity tends to reflect most of the incident laser energy and little energy only utilized for melting. Since aluminium and copper alloys are good reflectors, it is difficult to weld them with long wavelength CO_2 laser as shown in Figure 1-4.a [41]. At short wavelength, as more energetic photons can be absorbed by a greater number of bound electrons, the reflectivity drops and the absorptivity of the surface is increased in Figure 1-4.a. Laser with short wavelength is more efficiently absorbed than long wavelength as seen in Figure 1-4.b. In addition, laser energy absorption enhances with increase in surface temperature of material as shown in Figure 1-4.b. As the temperature of the material surface rises, there will be an increase in the phonon population, causing more phonon-electron energy exchanges. Thus, the electrons are more likely to interact with the structure rather than oscillate and re-radiate. Therefore, with a rise in temperature, laser energy absorptivity enhances [5]. When the material surface reaches melting point, absorptivity is rapidly increased. Therefore methods which modify surface roughness or preheat the material surface are employed to enhance laser energy absorptivity [42, 43].

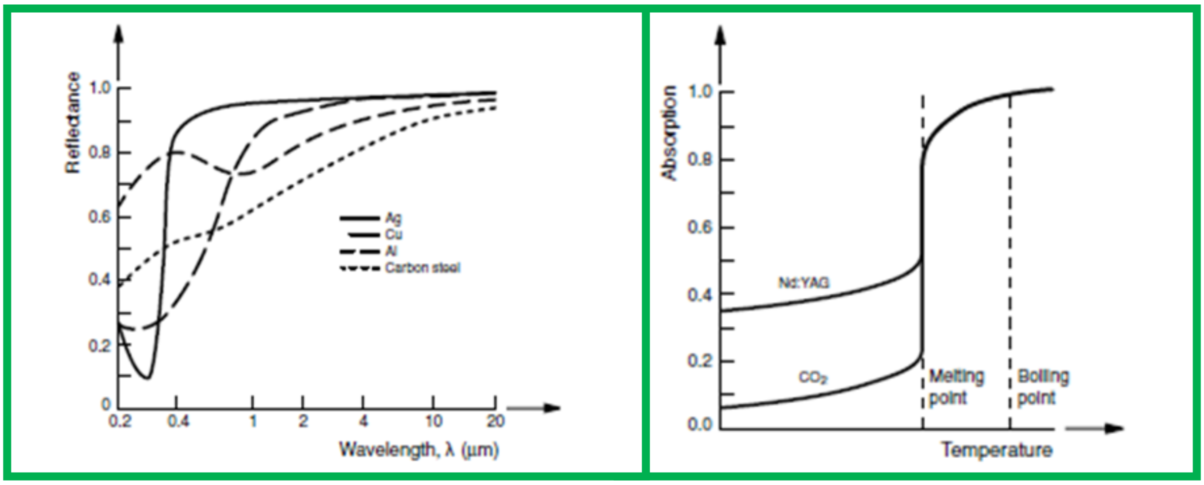

Figure 1-4 Influence of material, wavelength and temperature on laser- material interaction, a) Reflectivity with different materials b) Absorption with different temperatures [41]

1.2 ENERGY TRANSFER MODES IN LASER WELDING

There are two major operational modes in laser welding, namely conduction and keyhole modes. Figure 1-5 shows both the modes of operation in schematic diagram [44].

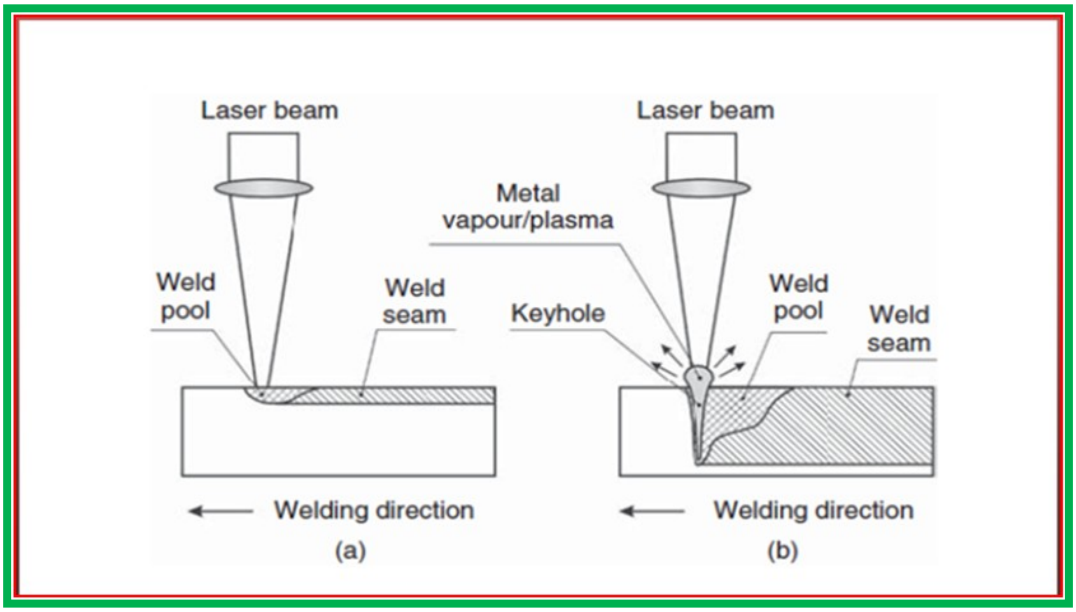

Figure 1-5 Schematic of a) Conduction and b) Keyhole modes in laser welding [44]

1.2.1 Conduction mode

Conduction mode transfer occurs at low laser beam powers where no or insignificant vaporisation occurs. The deposited laser energy on the material surface is transmitted through heat conduction to the surroundings. As the laser absorptivity is very low at this condition, melting efficiency of this mode of operation is lower compared to keyhole mode. Hence conduction welds are observed to have shallow geometry with low depth of penetration. But, these welds are found free from defects like porosity, undercut, spattering, and loss of alloying elements as vaporisation does not occur. Though low penetration depth is anticipated in general applications, in a recent work 6.35 mm penetration depth has been achieved in conduction mode by suitable selection of parameters [45]. One of the major drawbacks of this mode is low coupling efficiency (% of energy absorbed on the material surface to energy delivered from laser generator). It has been experimentally observed to be just 15% for stainless steel, while in keyhole mode 65% of energy is coupled [46]. Metals with high light reflectivity index such as aluminium and copper absorb very little energy in this mode of operation. Apart from heat conduction phenomenon, depth of penetration is also influenced by Marangoni convective flow. These forces are resulted from variation in surface tension in weld pool due to variation in temperature distribution in welds. Presence of surface active elements can change the direction of Marangoni flow and influences the depth of penetration. The welds made in this mode of operation show aesthetic appearance with low or no material loss [47, 48].

1.2.2 Keyhole mode

When laser with high power density is applied, keyhole mode welds are obtained. At this condition, the material surface evaporates and vapour filled cavity or depression called keyhole is formed. This keyhole acts like black body and absorbs laser energy. Thus, the laser absorptivity increases drastically once the keyhole absorbs laser photons. It results in deeper welds of high aspect ratio (depth of weld/ width of weld) leading to narrow HAZ. Unlike conduction mode welds, the coupling efficiency is reported to shoot even above 90% [41, 49]. Light reflecting metals can be welded in this mode of operation with better melting efficiency. Keyhole mode welding has the following drawbacks: The formation of keyhole is highly complex phenomenon, and so the stability of keyhole involves various factors. Instability in keyhole mechanism causes variation in weld geometry and porosity [50]. As vaporisation of alloying elements is involved in this mode, alloys with low melting points such as aluminium and magnesium, encounter issues like loss of alloying elements, spattering, undercut etc., [51-56].

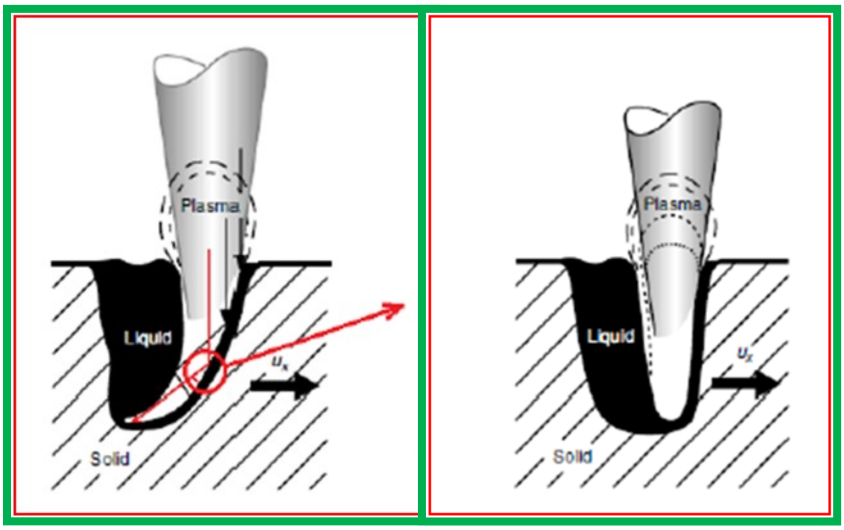

Figure 1-6 Mechanisms in keyhole mode welding a) Fresnel absorption (Red circle and arrows indicate multiple reflections on keyhole walls) and b) Inverse Bremsstrahlung effect [41]

Keyhole is wider at top side and towards bottom narrows down like the shape of keyhole and filled with vapours and ions containing metals from base metal and shielding gas. As the laser beam is traversed, the keyhole also moves along the joint. The keyhole entraps the laser energy efficiently by two major mechanisms namely, Fresnel absorption and inverse Bremsstrahlung (IB) effect as shown in Figure 1-6 [41]. When the keyhole is formed, the incident laser beam is effectively entrapped in keyhole cavity and gets reflected multiple times within keyhole walls as shown in Figure 1-6.a. As this multiple reflection action proceeds, energy is more efficiently absorbed. The multiple reflections inside the keyhole called as Fresnel absorption entrap laser energy efficiently and enhances depth of penetration and melting efficiency of keyhole welds.

1.2.2.1 Plasma formation in keyhole mode welding

Plasma formation is a characteristic phenomenon in keyhole mode welding. Plasma is seen both inside and above the keyhole cavity. The plasma inside the keyhole is denoted as 'keyhole plasma', and above the surface is known as 'laser induced plasma'. The electrons in the plasma can absorb laser photons by inverse Bremsstrahlung (IB) effect. When high power laser beam is introduced, both types of plasmas are formed. In the initial stage, the small amount of 'laser induced plasma' formed above the material surface absorbs laser energy effectively instead of reflecting the laser beam away from material surface (Figure 1-6.a). This is known as 'plasma enhanced energy coupling' [57, 58]. Nevertheless, as the laser power increases, plasma is built up and it blocks the incident laser energy. The energy of laser (I) which passes through the plasma of thickness 'x' and absorption coefficient 'α' is given from Beer-Lambert law in equation 2.1.

$$I = I_0 \exp(-\alpha x) \qquad (2.1)$$

where, I_0 is the incident laser energy (W), α- absorption coefficient of plasma, x- thickness of plasma. The absorption coefficient, α depends on many parameters including electron temperature and density is given as equation 2.2 [59].

$$\propto = \frac{n_i n_e Z^2 e^6 \lambda^2 \ln\left(\frac{2.25 K T_e \lambda}{hc}\right)}{24\pi^3 \varepsilon_0{}^3 c^3 K T_e \sqrt{2\pi m_e K T_e}} \qquad (2.2)$$

where, n_i and n_e are density of electron and ion (m^{-3}) respectively, Z is the ion charge number, e is electron charge (C), K is Boltzmann's constant ($J.K^{-1}$), T_e is the electron temperature (K), h is Planck's constant (Js), c is the speed of light (ms^{-1}), e_0 is the dielectric constant and m_e is the mass of electron (kg). From this equation, it is obvious that the laser beam wavelength, λ has apparent influence on absorption coefficient (α). Therefore, absorption of the laser energy by the plasma is more significant in CO_2 laser welding of wavelength 10.6 μm than in solid-state Nd: YAG laser welding of wavelength 1.06 μm [59]. In order to suppress this unfavourable effect, a laterally injected assisting gas is used in high power CO_2 laser welding [60]. On the other hand, Nd: YAG laser with short wavelength can permeate laser induced plasma without loss of energy. The 'keyhole plasma' present inside keyhole walls effectively couples laser photons and enhances energy absorption.

The keyhole welding process involves complex physical phenomena such as plasma formation, molten pool flow around keyhole, and thermal cycles in molten pool etc. Keyhole is assumed to have shapes like conical or cylindrical. Since these welds are determined by the attributes of stable keyhole, the mechanisms involved in keyhole dynamics have been studied extensively. The geometry of keyhole has influence on Fresnel absorption and IB effect, thereby determines resultant weld quality. There are forces acting on keyhole which can collapse or retain it as shown in Figure 1-7 [41]. Vapour pressure inside the keyhole and ablation pressures tend to maintain the keyhole open. But, pressure due to surface tension at the interface between the molten metal and plasma, hydrodynamic and hydrostatic pressure of the molten pool tend to close the keyhole. The balance between these opposing forces determines keyhole dynamics and which in turn influence the resultant welds [41, 59]. It is experimentally observed that keyhole is constantly fluctuating during welding process [61-63]. Hence, the laser welding parameters such as power density, focal point, shielding gas composition and flow rate, welding speed, nature of material have strong influence on keyhole stability and consequently on keyhole mode welds [64, 65].

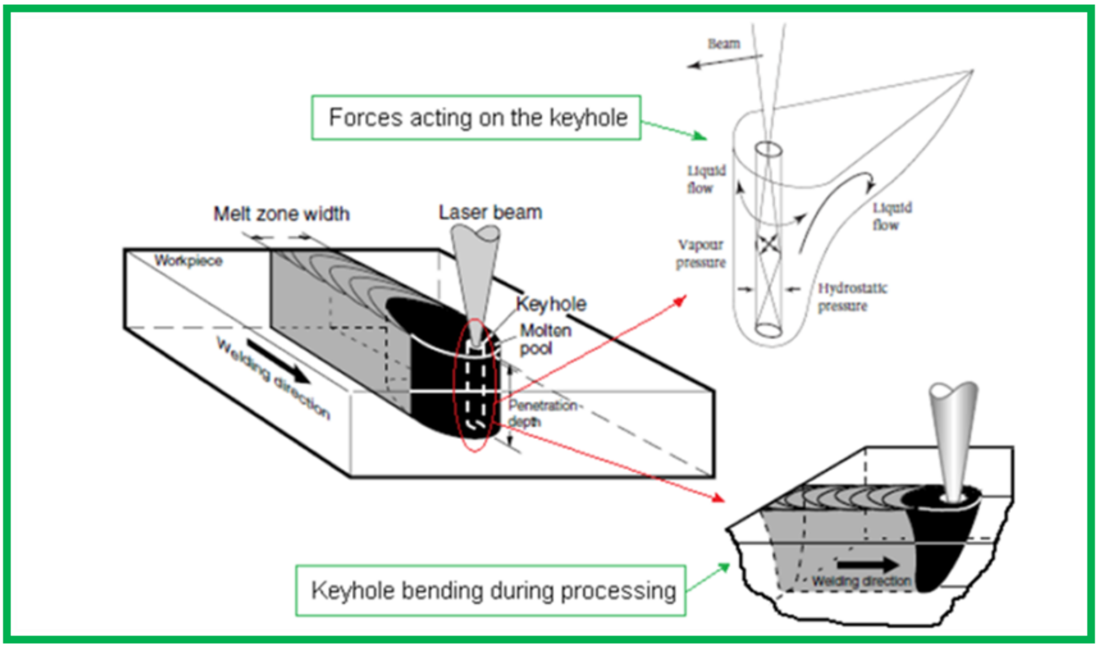

Figure 1-7 Schematic of forces acting on keyhole in keyhole mode laser welding [41]

As explained in the above passages, the change in energy transfer modes from conduction to keyhole alters the laser beam welding mechanisms altogether. The welds produced from different energy transfer modes have variation in weld geometry, microstructures and mechanical properties. Therefore, much work has been carried out on this aspect of laser welding. Many analytical and numerical models have been formulated to understand the process better [66-75]. Most of the works focus on either conduction or keyhole mechanisms. The switchover from conduction to keyhole and the influence of laser welding process parameters have not been discussed adequately in literature.

1.3 CLASSIFICATION OF ENERGY TRANSFER MODES

The work reported on changeover of energy transfer modes with process parameters is reviewed here. Power density of laser has been considered as the parameter to define laser welding modes. The threshold value is taken as roughly 10^6 W/cm^2 [59, 62, 76, 77]. It is considered that above this threshold value the mode changes to keyhole mode and below this value laser welding is limited to conduction mode. Laser power is also used as a parameter to distinguish modes. Laser power above 1 KW is considered to produce keyhole welds and below this value conduction welds [6]. This definition is very approximate and it assumes that above 1 KW power, the formation of keyhole can be ensured. Aspect ratio (depth to width) of welds also has been regarded for classification of modes. When this value is above 0.5, keyhole mode is presumed [78]. All these definitions are based on approximated values and they do not take account of other welding parameters such as traverse speed, beam diameter, etc. These definitions also indicate that there is an abrupt transition from conduction to keyhole mode at the threshold value. But a few studies have shown that this changeover is not sudden and a transition zone is present between conduction and keyhole modes [65-68].

Only a few studies have focussed on the transition from conduction to keyhole mode in laser welding. In continuous laser welding, transition zone between conduction and keyhole modes has been observed and focal position is reported to influence the transition regime [8]. Buvanashekaran et al. have also identified transition from conduction to keyhole mode [7]. This transition to keyhole mode is reported to occur at 400 W of laser power and 1000 mm/min of welding speed. However, no transition regime has been observed [7]. Colegrove et al. identified three different regimes in pulsed laser welding based on drilling models. The mixed mode in between conduction and keyhole modes is found to have significant evaporation similar to keyhole mode but limited depth of penetration as conduction welds [79]. Sibillano et al. also distinguished a mixed mode, but it seems to be describing unstable keyhole welding [80]. The three regimes in laser beam welding have also been indicated by W. M. Steen and Ahmed [5, 81].

Though both conduction and keyhole modes are functional in pulsed laser welding, a very few studies only have considered energy transfer modes in case of pulsed laser welding [4, 5, 38, 82]. Energy transfer modes in single spot welding of AISI Type 304 stainless steel has been studied by Bransch et al. [83]. In their work, conduction to keyhole mode transition was observed by sudden increase in penetration and melt area, and so sharp transition from conduction to keyhole mode is derived. Also, it was reported that threshold power density to form keyhole is 4×10^6 W/cm^2 for stainless steel and 1×10^6 for Aluminium. The power density at which keyhole mode starts is independent of pulse duration. But, in the case of pulsed laser seam welding, spots are made to overlap and each spot is influenced by adjacent spots. Due to continuous application of overlapping spots along the weld seam, the temperature dependent laser absorptivity also changes continuously. The effect of raise in temperature of the base metal which will affect the absorption of laser beam is to be considered for overlapping seam welds.

Pulsed laser seam welding can be performed in both conduction and keyhole modes. Very limited works have been carried out in the domain of energy transfer modes in pulsed laser seam welding and the influence of pulse parameters, on any material, including austenitic stainless steels, which is widely used in fast reactor applications.

1.4 HOT CRACKING IN AUSTENITIC STAINLESS STEEL

Austenitic stainless steels are generally weldable alloys and joined by different arc, high energy beam and solid state welding processes. But, austenitic stainless steels with significant amount of impurities such as sulphur and phosphorous tend to crack during the solidification of weld pool. These impurity elements form eutectics of low melting point and segregate on grain boundary regions. They solidify at the terminal stage of solidification and so the lower melting liquid eutectic is surrounded by solidified solid. Since, the thermal conductivity of austenitic stainless steels is low, they induce high solidification shrinkage stresses and thermal stresses during non- uniform heating and cooling occurring in welding processes. Under the action of solidification shrinkage stresses, the liquid film gets fractured and cracks at the final stage of solidification. Apart from chemical composition of alloy and nature of solidification, the external constrain exerted during welding to counteract distortion also enhances cracking. The chemical composition, welding conditions and mechanical restrain during the welding processes are observed to be the factors influencing these kinds of cracks [84].

1.4.1 Theories on hot cracking

Hot cracks are intergranular cracks occur at the terminal stage of solidification, when the developed tensile stresses exceed the strength of almost solidified weld metal [84, 85]. In stainless steels the presence of impurities like S, P and alloy elements such as Ti, Nb leads to formation low melting eutectics which solidifies last and tends to fracture at the final stage of solidification [9]. Many theories have been constructed in the process of understanding the mechanisms of hot cracking. The initial theory by Medovar accounts hot cracking primarily by the segregation of low melting eutectic forming elements present in alloys which has long freezing range. It states that cracking susceptibility is in proportion with liquid to solid freezing range [86]. But, this theory does not account the other influencing factors and exceptional cases which were observed in some alloys. In addition to the freezing range, the influence of distribution of liquid and solid phases during solidification also was considered in ‘generalized theory’ developed by Borland [87]. Based on the distribution of liquid and solid phases, the solidification of alloy was classified into four stages as shown Figure 1-8 [87].

In stage 1, liquid and solid phases can accommodate themselves and no formation of crack occurs. In stage 2, solid dendrites are interlocked by the freely movable liquid. At this stage, cracks can be healed by the refilling action of available liquid. In stage 3, the amount of liquid is reduced and more solids are formed due to the proceeding solidification. Solidification cracks occur at this terminal stage of solidification when the tensile stresses developed across the adjacent grains exceed the strength of the almost completely solidified weld metal. As the small amount of liquid cannot refill the cracks much cracks occur at this stage which is known as critical solidification range (CSR). In the final stage, as solidification is completed no cracks occur. This theory states that along with longer freezing range the distribution of liquid also influences cracking. The wetting ability of liquid film is more when dihedral angle between the solid- liquid interfaces is more than 60°. This depends on the surface tension and interfacial energies of solid- liquid interface. Ferrous sulphide (FeS) is more deleterious than Manganese sulphide (MnS) in this regard. And so presence of sulphur, (S) in austenitic stainless steel will make it prone to cracking.

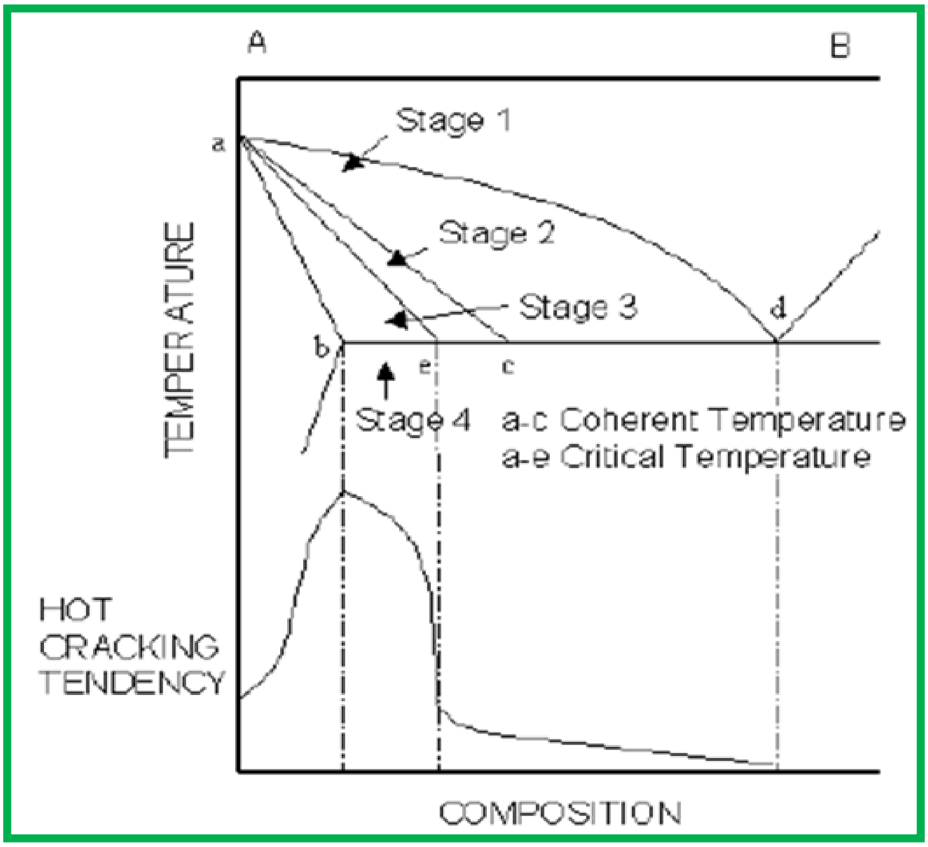

Figure 1-8 Stages involved in solidification cracking- Borland's generalized theory [87]

Although this theory explains liquid distribution and importance of wetting, it does not take account of widening of freezing range by segregation [88]. Further, hot cracks are generally thought to occur at terminal stage of solidification, but some experiments showing occurrence of cracking at the initial stage of solidification [89, 90]. Modification to Borland's theory was proposed by Matsuda and it was suggested that crack initiation and propagation must be considered separately [91]. The third stage of Borland's theory called as critical solidification range (CSR) is divided into two stages. In the first stage which is at higher temperature near liquidus temperature, crack initiation occurs and in the second stage of CSR, cracks are propagated. Thus the solidification cracking is primarily determined by the presence of impurities and pattern of solidification.

1.4.2 Solidification of austenitic stainless steels

Austenitic stainless steels show fully austenitic structure at room temperature. But, due to thermal cycles during welding operation they tend to retain high temperature δ ferrite. Most of the elements present in the stainless steel are on the iron-rich side of the ternary system of Fe- Cr- Ni between 50 and 70 wt. % Fe. The 70 wt. % Fe isopleth of the ternary phase diagram shown in Figure 1-9, is commonly used to identify the primary solidifying phases or solidification modes for various compositions [9]. As shown in Figure 1-9, four distinct modes are normally considered, viz., austenitic (A), austenitic–ferritic or primary austenitic (AF), ferritic-austenitic or primary ferritic (FA) and ferritic (F). Alloys solidifying in the A mode will remain unchanged to low temperatures, while those solidifying as AF would form some eutectic ferrite. Compositions that solidify in the FA mode pass through two phase region (F&A) and may re-enter the single-phase austenite field. This is due to the asymmetry of the two-phase field towards the primary ferritic side of the diagram, as seen in Figure 1-9.

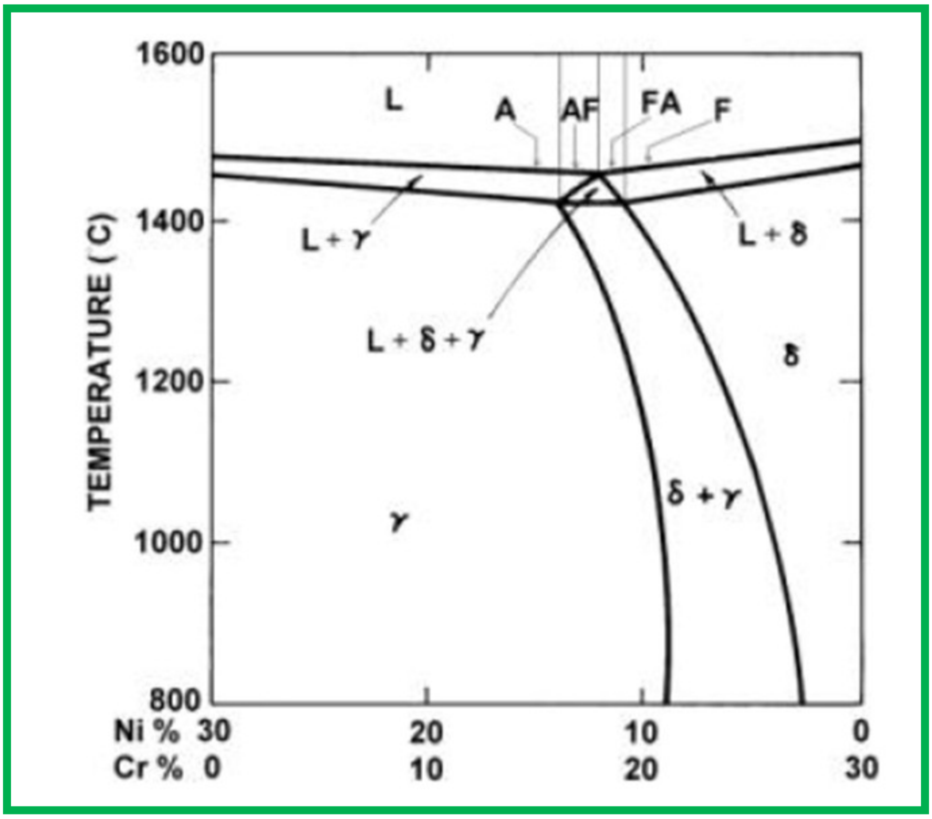

Figure 1-9 Pseudo binary phase diagram of 70-30 % austenitic stainless steel alloy [9]

Thus, alloys such as Type 304 and 316 that are fully austenitic at room temperature enter this two-phase region after AF/FA solidification and may undergo solid-state transformation to a fully austenitic structure. For higher ratios of chromium over nickel, the equilibrium structure at room temperature may retain considerable amounts of δ ferrite. The solidification in lean alloys such as Type 304 or 16-8-2 tends to be peritectic while higher alloyed grades undergo eutectic type of reaction [92]. The occurrence of peritectic reaction is important from the point of view of cracking. It is believed that the heterogeneous grain boundaries, for example austenite and ferrite, formed at liquid junctions in peritectic systems retard wetting and crack formation [93].

1.4.3 Weld microstructures and hot cracking

Welds with fully austenitic microstructures are observed to induce severe cracking. From the study made by Hull in 1967, austenitic stainless steels with 5-30% δ-ferrite are found to be resistant to hot cracking [17]. The reduction in crack susceptibility due to the presence of δ-ferrite has been studied much and many conclusions have been drawn. Studies reported that the composition of 3-7% δ-ferrite in weld metal has resistance to solidification cracking. Masumoto *et al* (1972) witnessed that primary ferritic (both F& FA) solidification mode is essential to reduce cracking rather than residual ferrite content in weld [10]. Few reasons for cracking resistance in the presence of δ-ferrite phase are reduction in segregation of impurities due to high solubility for impurity elements in δ-ferrite phase, arresting of cracks and lower wettability of grain boundaries in duplex austenitic-ferritic microstructure. In order to avoid solidification cracking, δ-ferrite is retained in welds at room temperature. Therefore, quantitative determination of δ-ferrite in welds from chemical composition of base metals is beneficial in predicting hot cracking susceptibility of austenitic stainless steels.

1.4.4 Constitutive diagrams

Constitutive diagrams are used to predict the microstructures of stainless steels using their chemical compositions. Schaeffler's diagram is one of the earliest diagrams used in alloy design [94]. The composition of alloying elements was given as chromium and nickel equivalents. Ferritic and austenitic stabilizing elements have been included in Cr and Ni equivalents respectively. Cr_{eq} is given as % Cr+ 1.5% Si + 0.5 % Nb and Ni_{eq} as % Ni+ 30% C + 0.5% Mn. This diagram was used in the domain of welding for predicting microstructures of welds and selecting suitable filler metals to achieve welds with desirable microstructures. Though Schaeffler's diagram can be used for wide variety of stainless steels, it is not suited under rapid solidification conditions and for stainless steels containing elements which are strong austenitic or ferritic [84]. In order to improve the existing diagram, Cr_{eq} and Ni_{eq} were refined by other chemical elements and their coefficients. WRC-1992 is one of the notable diagrams and usable for many stainless steels where copper was included in nickel equivalent as shown in Figure 1-10 [95]. It also accounts the influence of nitrogen, on stabilising austenitic phase. The numbers denoted with the inclined lines are ferrite number which can be directly measured from magnetic gages. In addition to predicting δ-ferrite phase, this diagram also gives information about the solidification pattern, which is helpful to estimate the susceptibility for solidification cracking. In Figure 1-10, the solidification modes A, AF, FA and F are divided by cross lines slightly inclined to ferrite number lines.

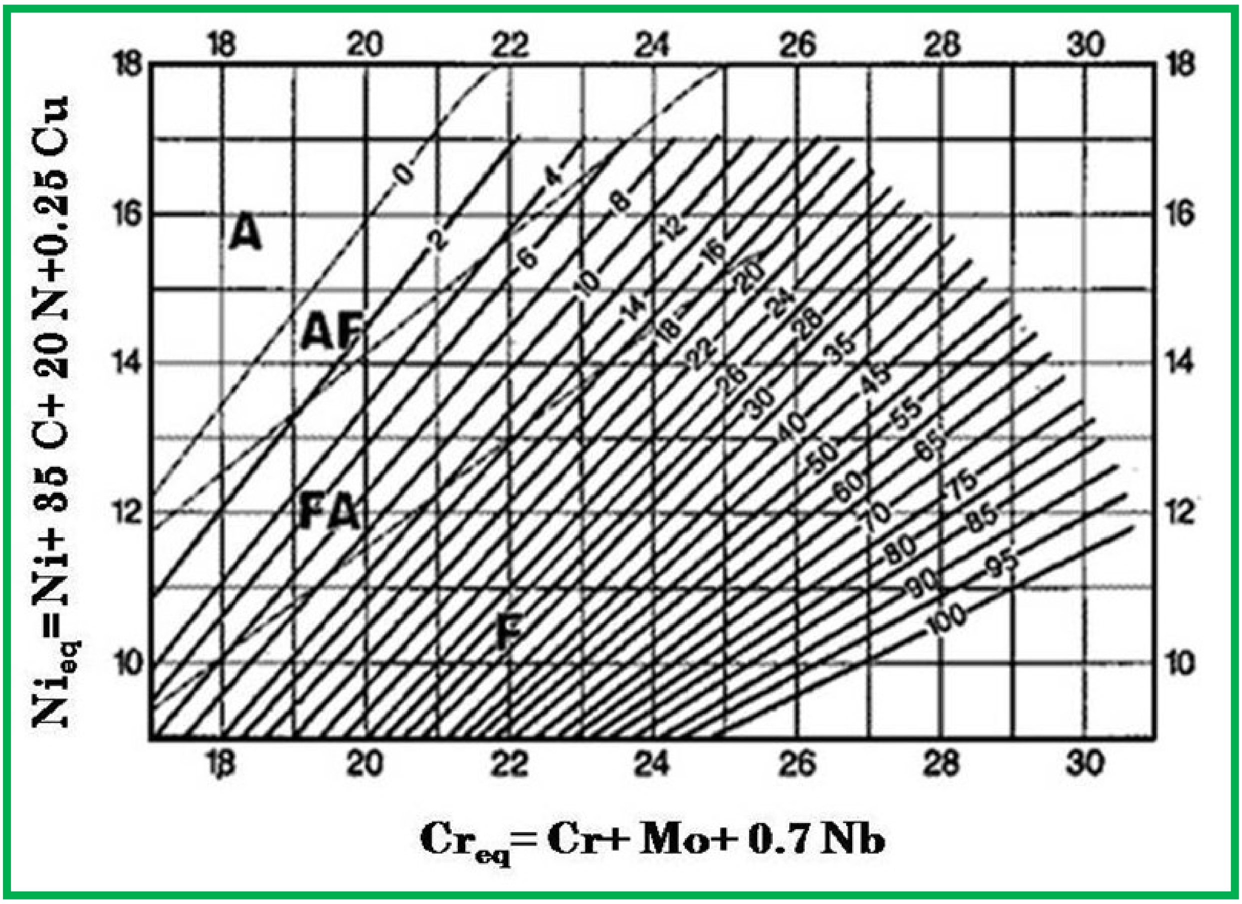

Figure 1-10 WRC-1992 constitutive diagram [95]

1.4.5 Weldability diagrams for pulsed laser welding

The cracking susceptibility of stainless steel is associated with the level of impurity elements [96, 97]. The relationship between cracking susceptibility, alloy composition and impurity concentration was depicted by Suutala et al. as shown in Figure 1-11 [98]. In this diagram, impurity elements sulphur and phosphorous are taken into account and Cr_{eq}/ Ni_{eq} is considered for alloy composition. At extremely low sulphur plus phosphorous (S+P) content, lesser than 100ppm, cracking does not occur for a wider range of Creq/ Nieq. And above this content of (S+P), cracking susceptibility varies with Cr_{eq}/ Ni_{eq}. Cracking susceptibility takes a sharp transition at Cr_{eq}/ Ni_{eq} of 1.48 as beyond this value, no cracking occurs in spite of increase in impurity content. This is attributed to the change in primary solidification mode

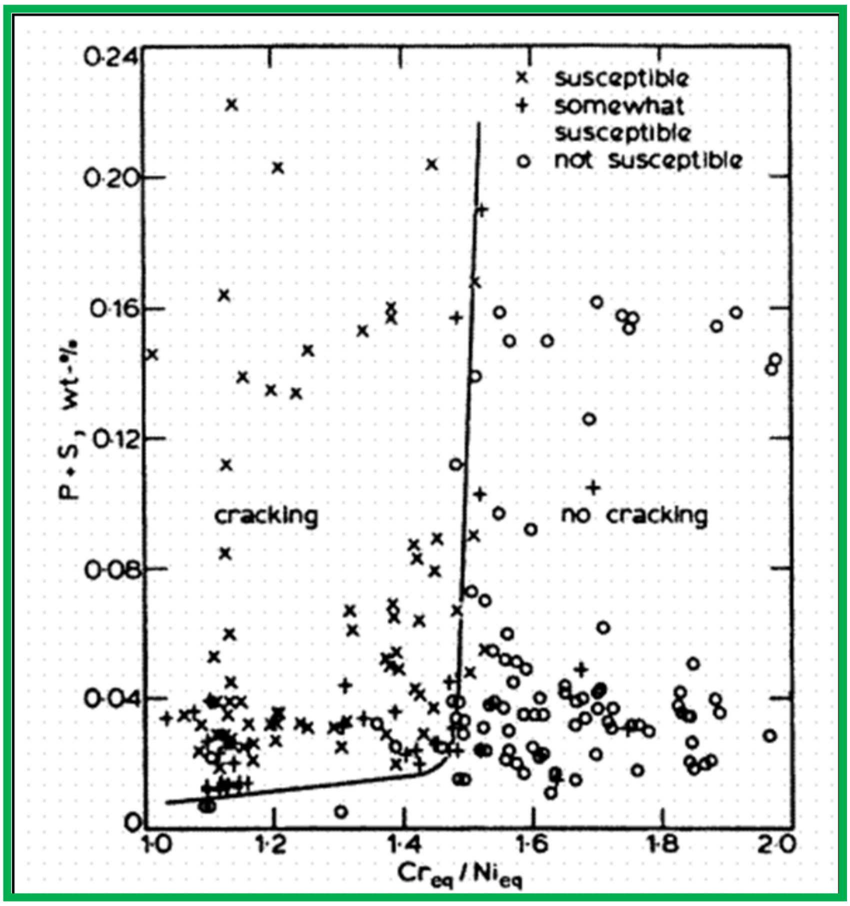

Figure 1-11 Suutala- cracking susceptibility diagram [98]

from primary austenitic to primary ferritic. Thus, welds solidifying in primary ferritic mode have low susceptibility to cracking. The Suutala diagram was developed based on the weldability test data generated using conventional GTAW process.

The prediction of solidification behaviour at rapid solidification processes such as laser, electron beam welding and surface melting treatment does not match with this diagram [99]. At rapid solidification conditions achieved in these processes, shift in primary solidification mode from ferritic to austenitic phase occurs due to dendrite tip undercooling [100]. In order to account rapid solidification and cooling rate, Suutala diagram was modified by Lippold [101]. In this diagram, Cr_{eq}/Ni_{eq} was determined from WRC-1992 equivalents and it takes account of Titanium, a strong ferritic stabilizer. Further, the impurity element Boron is also included with S and P. The critical curve indicating primary ferritic mode solidification is found to be shifting from 1.48 to 1.58 at higher cooling rate conditions [101]. This shows that the cracking susceptibility is getting widened in laser welding process due to rapid solidification and cooling rates achieved in laser welds.

Modified Suutala diagram given by Lippold was made by a few data points and so does not address wide variety of stainless steels. Pulsed laser welding experiments performed by Lienert et al. utilized vast data and accounted primary solidification modes like primary ferritic, dual and austenitic on solidification cracking [11]. The improved weldability diagram for pulsed laser process developed by Lienert et al. is shown in Figure 1-12 [11]. It employs Hammar and Svennson's Cr and Ni equivalents, which predicts solidification modes satisfactorily. The horizontal curve in this diagram shows that alloys with impurities lower than 200 ppm do not crack irrespective of primary mode of solidification. Instead of single demarcation curves used in Suutala diagrams, here two curves are shown which differentiate primary solidification modes into primary austenitic, dual modes and primary ferritic respectively, with respect to increasing Cr_{eq} to Ni_{eq} ratio. Non cracking region (region III) is observed in alloys solidify in primary ferritic mode and obtained in Cr_{eq}/ Ni_{eq} value greater than 1.69. Welds in the mixed mode solidification region (II) found to have variable cracking as some welds are free from cracking while others crack.

Though Lienert's diagram can be used for many varieties of stainless steels, it does not account energy transfer modes in pulsed laser welding. Though most of the welds are carried out in conduction modes, some of the welds reported in literature are found in keyhole or mixed modes. The energy transfer modes influences weld cooling rate as the physical phenomena involved in both modes are distinct. Therefore, the variation in cooling rate due

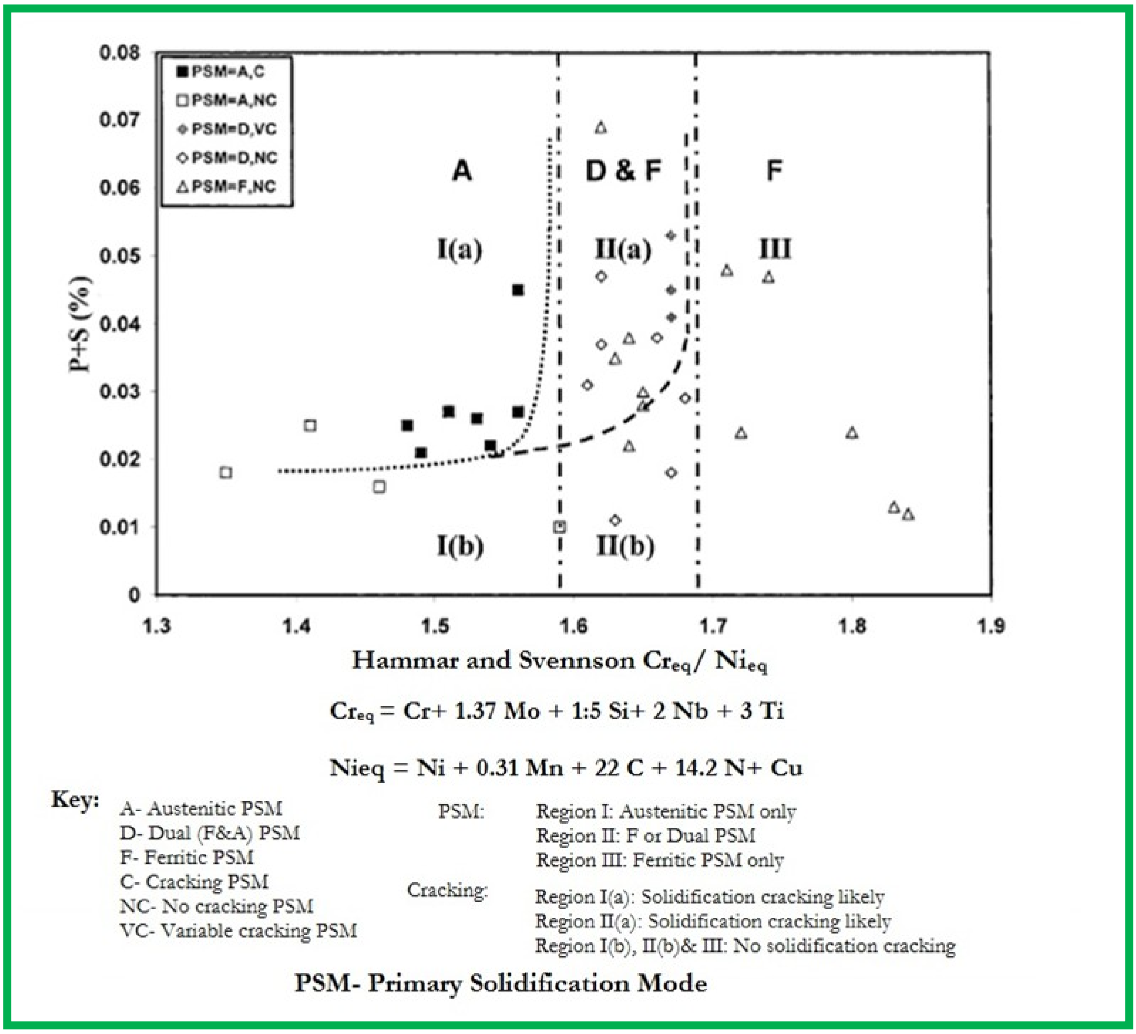

Figure 1-12 Cracking susceptibility diagram developed by Lienert for 300 series stainless steel pulsed laser welds [11]

to energy transfer modes can determine solidification cracking in pulsed laser welding. But this behaviour is not studied enough. Very few experiments take account of heat input given in laser welding on liquation cracking of Nickel and super alloys. The influence of energy transfer modes on solidification cracking in pulsed laser welding of austenitic stainless steels needs to be studied.

1.5 LIMITATIONS OF PULSED LASER BEAM WELDING

Pulsed laser beam welding (PLBW) has advantages and used in many applications as discussed in the previous sections. But like any other welding process, PLBW also has its limitations. The common limitations are the following:

1. The electrical or wall plug efficiency of PLBW is very low as lasing action is a low efficient phenomenon.

2. The capital cost of PLBW system is relatively higher than other processes. Though operating cost is lower, it demands huge initial investment. This may not attract small scale industries.

3. Tight fit up is mandatory due to the usage of fine and focused laser beam. It needs machining of adjoining surfaces and their close fitting which involves additional work and cost.

4. Highly reflective metals such as aluminium and copper reflect incident laser energy, and so melting efficiency is much low.

5. Although using low heat input in laser welding gives advantages such as narrow welds, narrow heat affected zone (HAZ), it also leads to faster cooling of weldment which can promote welding defects such as porosity, solidification cracking and formation of brittle phases.

These limitations have been attempted to be resolved with many techniques such as base metal surface modification, hot wire filler addition, twin beam technique etc. Coupling conventional electric arc heat source with laser beam known as laser- arc hybrid welding process is most promising which eliminates the demerits of laser welding process and keeps the advantages of arc process. In the following sections, laser-arc hybrid welding is reviewed and pulsed laser- GTA welding is discussed in light of information available in the literature.

1.6 LASER- ARC HYBRID WELDING

In hybrid process, both laser and arc heat sources are applied on the same molten zone and act as a single heat source. Tandem welding is another variant of combination of heat sources, where both laser and arc are employed in such a way that interaction of heat sources would not occur as shown in Figure 1-13 [102]. Tandem welding is addition of two or more processes to impart higher heat input or to obtain any specific advantages of multiple heat sources [102-104]. But hybrid welding utilizes a common heat source and achieves synergistic advantages of both processes. While hybrid welding process preserves the advantages of laser beam welding, the demerits mentioned in the previous section are eliminated. The major reported advantages of hybrid welding are increased tolerance in fit up gap, higher depth of penetration, faster traverse speed, controlling heat input etc. It was first demonstrated by W. M. Steen in 1980, and advantages of higher traverse speed, deeper penetration, increase in melting efficiency etc. were observed by him [105]. In this experiment, CO_2 laser was augmented by GTA arc. When arc is applied either on the surface or back side of material, contraction of arc plasma, arc rooting and entering of arc into laser keyhole were observed.

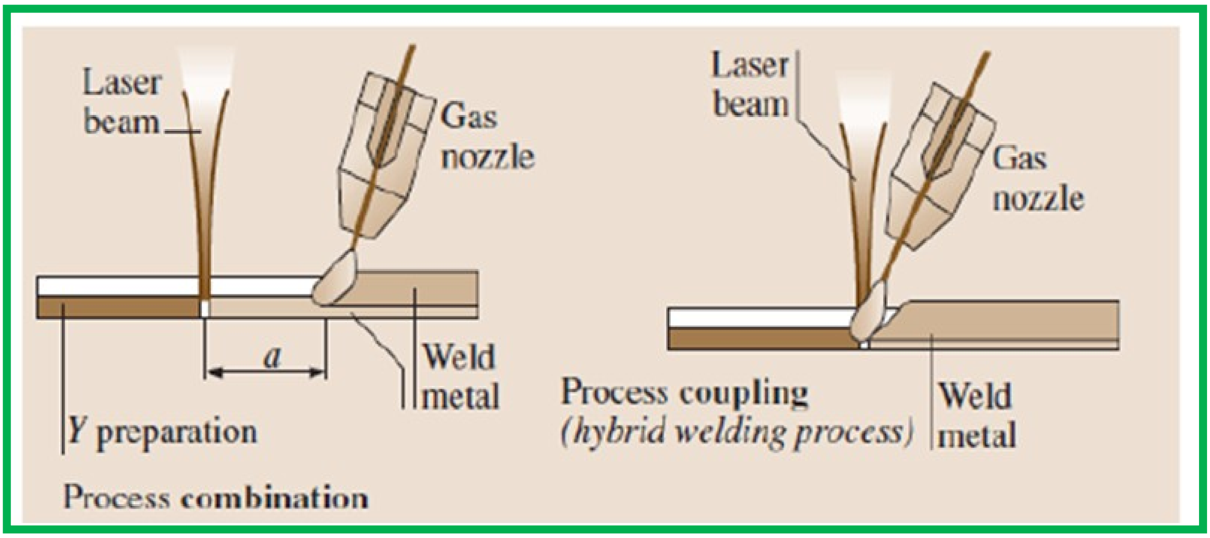

Figure 1-13 Schematic of arrangement of Laser and arc a) Tandem and b) Hybrid processes [102]

Since both the heat sources behave as a single-hybrid heat source, advantages of increase in penetration depth and traverse speed were observed. Lower arc resistance and enhanced arc stabilization in the presence of a laser is shown in the arc current and voltage data in Figure 1-14, A and B [105].

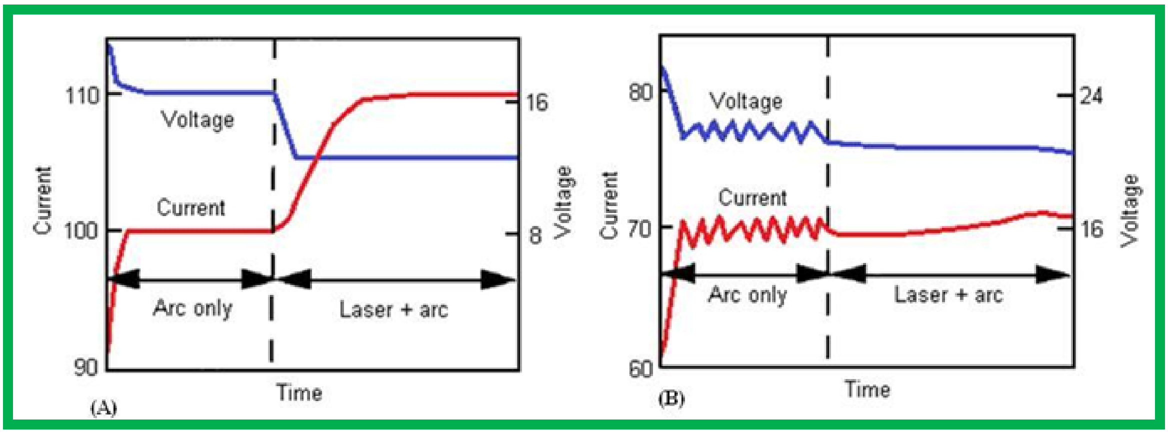

Figure 1-14 Influence of laser plasma in arc current and voltage [92] A) Decrease in arc resistance due to presence of laser, B) Laser stabilization of fluctuations in arc voltage [105]

Figure 1.14 A. shows a decrease in arc column resistance due to laser presence in welding of 3 mm thick mild steel at the speed of 22.5 mm/ s. Figure 1.14 B. shows the stabilization of an unstable arc due to laser presence in the welding of 2 mm thick mild steel at the speed of 45 mm/s. Similarly, unstable and wandering arc was stabilized by laser induced plasma. Arc was also found to root at laser striking spot at conditions of keeping arc heat source both on and below the workpiece surface [105].

Though hybrid welding was found to have such advantages, much attention was not given till recent times. It was because the laser system itself could not find its place as economic user friendly tool in industries [104]. Recently few applications of hybrid welding in ship building and automotive industries have been reported [103, 106-112]. Many works are carried out as it promises advantages that can not be attained by either laser or arc alone. For example, tailor welded blanks in automotive industrial applications cannot be made by high power laser alone due to restricted tolerance in fit up gap [102]. Welding of heavy plates using arc processes in ship building applications needed rework for removing residual stresses build up due to high heat input. In order to exploit the advantages of improved fit-up gap tolerance and deeper penetrations, laser beam welding can be satisfactorily replaced by hybrid welding [109, 110]. Hybrid welding process is complex due to the complicated interaction of arc and laser plasmas and involvement of wide variety of process parameters. Apart from the limited applications, much research works have been carried out on the influence of hybrid process parameters, on the weldability of various materials. The advantages derived from this process are from laser- arc interaction. But, there are few literatures only available to deal with physical mechanisms of laser- arc interaction. In the following section, literature review of works carried out of hybrid welding of various materials, their working parameters and their influence on weld properties is presented. Although the underlying principles of laser-arc interaction and hybrid phenomena are yet to be understood clearly [113], the experiments which attempted to understand these phenomena during hybrid welding also have been reviewed.

1.6.1 Classification of Hybrid welding

Based on the selection of primary heat source, laser- arc hybrid welding can be classified into two major categories as follows:

1. Arc augmented laser welding (Laser is primary source)
2. Laser assisted arc welding (Electric arc is primary source).

In the former, laser welding is enhanced by adding arc heat source with laser and in latter, laser contributes to the improvement of arc heat source. In general, high power lasers are used in former and low power lasers are used in latter. Experiments have been carried out in both types of variants of hybrid welding. When the arc is augmented with high power laser, the increase in depth of penetration, improvement in welding speed, keyhole stability, defect free welds are anticipated. When the laser is assisted to arc, properties of electric arc are improved with the addition of laser into arc acting zone. Arc stability, arc constriction, better metal transfer in GMAW and arc rooting to laser acting zone are few of the reported advantages in laser assisted arc hybrid welding.

1.6.2 Weldability of various materials

The first experiment on hybrid welding process was made on mild steel and many other materials also have been successfully welded. The observed common defects of welding like cracking, porosity, brittleness and hard phase formation can be overcome by hybrid welding [113]. In the literature, hybrid welding of various materials like galvanised steel, stainless steels, dual phase steels, high strength steels, fine grained steel, ship building steels like DH36 and EH36, aluminium, magnesium, titanium alloys have been reported [107, 114-128]. Galvanised steel was hybrid welded in lap joint configuration while arc stability was improved by laser induced plasma. It produced regular, uniform welds at high welding speed with a large gap tolerance [120]. Laser welding of aluminium and its alloys has weldability issues like hot cracking, porosity formation, low efficiency due to its high thermal conductivity, low vaporisation point, and high light reflectivity [129]. These issues can be successfully handled in hybrid welding [130]. Wrought and cast magnesium alloys such as AZ31, AZ61 and AZ 91 were welded successfully with laser- GTA hybrid welding and better property welds were obtained [117, 131-135]. The toughness of welds is found to be improved in CO_2 assisted GMAW than autogeneous laser welding of DH 36 micro-alloyed steel used for ship building [118]. Ultra fine grained steels are best welded with hybrid welding as it reduces HAZ width and grain coarsening effect while retaining weld toughness. Suitable selection of laser to arc power ratio yielded better mechanical properties of these welds [123]. Welding of Duplex steels should ensure equal partition of austenite and ferrite to impart corrosion resistance but it could be modified by faster cooling rates achieved in laser welds. On the other hand, high heat input of conventional arc process develops high distortion due to material's large coefficient of thermal expansion. For these alloys, hybrid welding is suitable process where heat input and cooling rates can be controlled effectively to acquire desirable microstructures with low distortion [136]. Dissimilar joints also have been made with hybrid welding. Aluminium-steel and magnesium-steel dissimilar hybrid welding have been reported in literature [122, 128]. It can be concluded that hybrid welding can be used for welding a variety of materials due to its flexibility in changing welding parameters.

1.6.3 Hybrid welding parameters and their influence on weld geometry and quality

Since hybrid welding employs two distinct heat sources, high energy density laser beam and electric arc, it involves wide variety of parameters. The selection of hybrid welding parameters influences hybrid welds, and an understanding of parameters involved in this process is necessary. The subsequent section deals with experiments carried out on hybrid welding parameters and their effects on resultant hybrid welds. The major parameters which influence hybrid welding process can be classified into four areas as follows:

1. Laser parameters

2. Arc parameters

3. Hybrid parameters (Inter heat source distance, Heat source position)

4. Process related parameters (shielding gas, welding speed etc.)

1.6.3.1 Laser heat source parameters

Nd: YAG, CO_2 and fibre lasers are commonly used lasers in hybrid laser- arc processes. As each laser has its own unique characteristics, the type of laser utilised in hybrid welding affects laser-arc interaction and resultant welds. The wall plug or electrical efficiency of CO_2 laser is much better than Nd: YAG laser and high power can be generated out of gaseous lasing medium compared to Nd: YAG laser. The wavelength of CO_2 laser, 10.6 µm, is ten times higher than that of Nd: YAG, 1.06 µm. The nature of long wavelength in CO_2 laser reduces the absorption of laser energy on the material surface especially by metals like aluminium, copper which have high light reflectivity. Further, due to inverse Bremsstrahlung effect, long wavelength laser is getting attenuated and defocused by laser induced plasma on the material's surface and laser energy is wasted. Also, CO_2 lasers cannot be carried through optical fibre cables as long wavelength CO_2 laser photons can be absorbed and melt the fibre cable. Therefore, it is transported by lens system contains metallic lenses. On the other hand, Nd: YAG lasers have the advantage of short wavelength and result in efficient laser absorption on high reflective metals and negligible attenuation of laser photons by laser induced plasma. As laser can be handled through optical fibre cables, this system is compact and can be used for remote application effectively. The selection of laser for hybrid welding is made on the aspects of material to be welded, thickness, joint design, cost effectiveness etc [34, 137].

The important laser parameters related to laser-material interaction are laser power, beam diameter and focal position. These parameters determine the interaction of laser with material and resultant weld properties. In hybrid welding, laser power is reported to influence weld geometry especially weld penetration [138-142]. At constant arc current, increase in laser power enhances weld penetration. The root side of hybrid weld at high power laser welding is primarily decided by laser power. The increase in depth of penetration is also influenced by arc parameters as the interaction of laser with arc plasma has the effect on laser power. Arc preheating is observed to increase the absorptivity of laser energy on the material surface. When high arc current is used, more arc plasma is generated with increased volume of molten metal and heat input. Presence of large volume of arc plasma attenuate laser energy and so can reduce penetration depth. But, on the other hand, preheating material surface can enhance penetration depth by increasing laser energy absorption. The optimum arc current is also determined by the distance between laser and arc heat sources [143, 144]. When the distance is short, dense arc plasma generated at high arc current can attenuate laser energy. At appropriate distance, the interaction is optimum and utilisation of maximum laser energy occurs.

1.6.3.2 Arc parameters

Arc current and arc voltage are essential parameters to be controlled in hybrid welding. In arc processes, it is generally observed that increasing arc current enhances weld penetration and increasing arc voltage widens weld bead. In hybrid welding, presence of laser is observed to influence arc characteristics. Arc rooting at laser acting spot is reported in the experiments conducted by W. M. Steen [105]. Hu et al. have used this phenomenon and manipulated electric arc in welding of edge, dissimilar and thick-thin combinations [145]. Arc constriction is another phenomenon occurs due to the presence of laser plasma. As the laser plasma has dense metal vapours and ions, arc tends to pass through this 'shortest path' and constricts. When arc is constricted, arc current increases and voltage decreases as reported in W.M Steen experiment as shown in Figure 1-14. The parametric study made on CO_2- GMA hybrid welding by Rayes et al. shows that increasing arc current increases weld penetration in top portion of hybrid weld and increase in voltage widens width of the weld [146]. Electrode tip angle and distance between material and electrode are also noticed to be determining factors. The optimum distance between electrode and material surface is maintained to obtain suitable metal transfer in GMAW aided hybrid processes. In case of GTA assisted hybrid welding, the appropriate distance is retained to avoid electrode damage.

1.6.3.3 Hybrid parameters

The parameters which are essential in combining laser and arc heat sources in hybrid welding are noted as hybrid parameters. Inter heat source distance (D_{LA}), Heat source position and Torch angle are hybrid parameters. These parameters determine hybrid phenomena and the resultant welds.

a) Inter heat source distance (D_{LA})

The distance between laser and arc is the parameter which decides the laser-arc interaction and the extent of coupling. Experiments conducted in different hybrid heat sources show the influence of D_{LA} on weld geometry. According to one definition, hybrid process takes place when laser and arc plasmas do interact [104]. As D_{LA} increases, the interaction of laser and arc plasmas declines. When the heat sources are separated far, the process can be changed to tandem process with respect to the laser and arc powers. On the other hand, when laser and arc are brought close, laser is attenuated or defocused by arc plasma and leads to reduction in depth of penetration. Therefore an optimum D_{LA} is available for every pair of laser and arc heat sources and at this distance (D_{LA}), utmost synergistic effect occurs and maximum penetration depth is achieved. It is reported that D_{LA} is depended on arc current and laser wavelength and power. As arc current increases, the optimum D_{LA} to achieve deep penetration also increases [144, 147]. Since the thorough understanding of laser-arc interaction is yet to be made, optimum D_{LA} is experimentally obtained and no theoretical explanation has not been given in literature. Further, the influence of other hybrid parameters on D_{LA} is also to be considered.

b) Heat source position

In hybrid welding the electric torch can be attached with laser either in coaxial (laser is applied through hallow Tungsten electrode) and in paraxial (Keeping electric torch inclined to laser) fashion. It is reported that coaxial attachment have advantages over paraxial arrangements, but the complexity involved in designing this configuration limits its application [140, 148, 149]. The paraxial arrangement is relatively easier and can be used in all laser systems. In this system, the movement of heat source relative to workpiece is observed to be influencing parameter. When laser is leading the arc, then the process is said to be laser leading hybrid welding and when arc is leading, it is known as arc leading process. Sometimes terms like ‘forehand’ and ‘backhand’ are also used. Arc leading welds are reported to have deeper penetration with poor weld appearance. But, laser leading welds are reported to have better appearance but lesser penetration [144, 150]. Some results which contradict this observation have also been noticed. The variation in heat source position determines laser-arc interaction and physical phenomena involved in the hybrid process which in turn has direct effect on weld geometry. Preheating mechanism is dominant in arc leading arrangement whereas arc constriction and other related mechanisms on arc characteristics are controlling in laser leading position. Heat source position is found to have effect on inter heat source distance [150, 151]. The optimum inter heat source distance (D_{LA}) varies with arrangement of heat sources. Hence, deciding appropriate heat source position is mandatory step in optimising hybrid weld parameters.

c) Torch angle

The angle between laser head and torch noted as torch angle has effects on laser- arc interaction and hybrid weld geometry. Torch angles of 30- 60° are generally practised.

1.6.3.4 Process parameters

Like any other welding process, process parameters like traverse speed, shielding gas have their influence on hybrid welding. The effect of shielding gas in hybrid welding has been studied in few experiments [64, 65, 152-156]. Argon and Helium are the widely used inert gases for shielding of laser and arc welds. As shielding gas is part of laser induced plasma and arc plasma, it affects weld geometry through its action upon laser- arc interaction [152, 155, 157, 158]. In many studies, welding speed is increased when high power laser is assisted with arc. In the experiments of Mahrle [159], the speed of low current (less than 100A) plasma arc welding (PAW) on thin sheets was limited due to PAW arc instability. The stability of arc was improved by coupling of fibre laser and the productivity in terms of traverse speed was enhanced [160, 161]. In high power laser hybrid welding, due to the augmentation of arc, traverse speed is significantly improved and so the productivity can be increased [44, 105].

1.6.4 Physical mechanisms of laser- arc interaction

The synergistic advantages of laser and arc are derived from interaction of laser and arc plasmas. This interaction involves complicated phenomenon in plasma, fluid pool flow, heat transfer, weld metal chemistry etc. Though several experiments have been made on hybrid welding, the interaction of laser and arc is yet to be understood due to its complexity. Therefore, the interaction can be realised in three layers as indicated in [162]. There are interactions above material surface, on material surface and below material surface.

1.6.4.1 Interaction above the material surface

Interaction of both laser induced plasma and electric arc plasma at this region have been studied using tools such as high speed camera, spectroscopy to analyse the hybrid plasma. The composition, electron temperature and density are quantitatively analysed. Arc stability, arc rooting at laser acting spot and arc constriction are the phenomena reported to occur from the interaction of plasmas above material's surface [19, 105, 163]. The commonly accepted explanation for arc rooting is principle of minimum voltage. According to this, arc plasma tends to follow the least resistance electrical conductive path during welding operation. In hybrid welding, as laser induced plasma is denser than arc plasma as intensive laser beam evaporates workpiece. This makes the arc to be attracted towards laser plasma so that arc can pass through minimum electrical resistance channel. This phenomenon is observed to enhance the process efficiency [164]. Also it improves arc stability in low current and high speed welding conditions and increases productivity [160, 165]. Arc rooting is observed to be effective in low arc current (less than 100A) as high current arc is stiffer and cannot be attracted effectively. High laser power evaporates more material and the conductivity of laser induced plasma region increases. It enhances the arc rooting phenomenon. It is observed that shorter the inter heat source distance higher the arc attracting action towards laser acting area.

When laser and arc plasmas interact, arc plasma can absorb laser photons by IB effect. This attenuation of laser energy by arc plasma reduces the effective laser energy input on material surface. IB absorption depends on the wavelength of laser; longer the wavelength more the absorption. As CO_2 lasers have longer wavelength, it is absorbed much more than Nd: YAG lasers. About 40% of CO_2 laser power is attenuated by arc plasma but only 0.3 % of Nd: YAG energy is lost at same welding conditions [166]. Apart from IB effect, energy loss occurs through scattering phenomenon, especially in laser- GMAW processes as fine droplets from metal electrode magnify scattering of electrons [167]. Further, with respect to inter heat source distance (D_{LA}) attenuation of laser energy changes. At optimum distance, the energy loss due to attenuation is low and maximum coupling action takes place.

1.6.4.2 Interaction on material surface

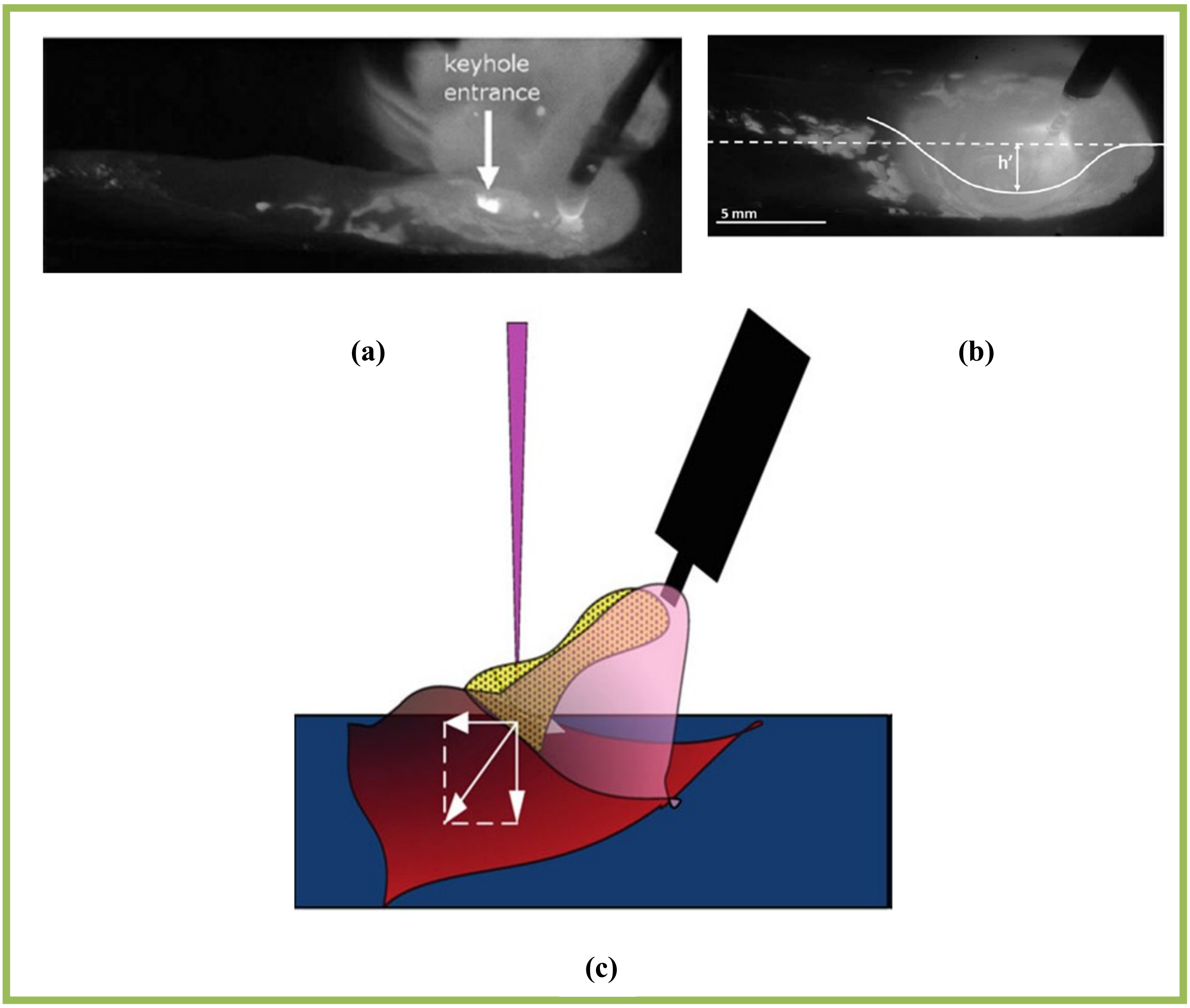

Figure 1-15 Interaction of laser and arc on material surface in Laser- GMA hybrid welding
a) Droplet transfer and keyhole interaction, b) Formation of concave surface,
c) Schematic of interaction of laser and arc plasmas at material surface [123, 168]

Very limited studies only have been carried out on interaction of laser-arc heat sources on material surface [162]. As physical changes at the surface of weld pool affect laser energy absorption and resultant weld's surface quality and geometry, interaction on surface is essential to be considered. High speed video image during laser- GMA hybrid welding shows interaction of laser keyhole- GMAW droplet transfer with material in Figure 1-15.a-c [123, 168]. The mechanisms of keyhole dynamics and molten pool flow in hybrid welding processes are affected by the interaction at weld surface. Further, due to the action of arc on the molten pool, formation of depression or concave surface is observed as shown in Figure 1-15. b. The intensity of this depression, 'h' increases as arc current is raised more than 150A. Due to this change in surface, laser interacting position is modified which leads to shift in focus position and influences resultant welds.

1.6.4.3 Interaction below material surface

The interaction of laser and arc just below material surface is determinant for the molten pool flow which precisely defines weld geometry. The keyhole and molten metal flow under material surface is not visible and cannot be analysed by high speed cameras. The experiments to analyse this interaction were carried out by Katayama et al. using x-ray real time imaging technique on Nd: YAG- TIG (GTA) hybrid welding [169]. The flow of molten pool was analysed by movement of refractory tracers in x-ray imaging system at 100 and 200A arc currents. At low current, wider keyhole was observed and molten pool flow was inward. Due to formation of bubbles in narrow weld pool, porosities were observed. At high current of 200A, keyhole was contracted and the flow pattern changed to outward which leads to wider and porosity free weld [169].

Heat source position is found to influence interaction below the surface and modify molten pool flow in CO_2- GMA hybrid welding [170]. In laser leading position, drag force of the plasma jet and momentum of droplet promote the inward flow and homogenous distribution of alloying elements. In case of arc leading, as the drag force of arc and momentum of droplets are in opposite direction to former, it promotes outward flow. The forces acting on the molten pool flow surrounding keyhole can affect weld penetration. The temperature distribution of keyhole walls is also an influencing factor of hybrid welds.

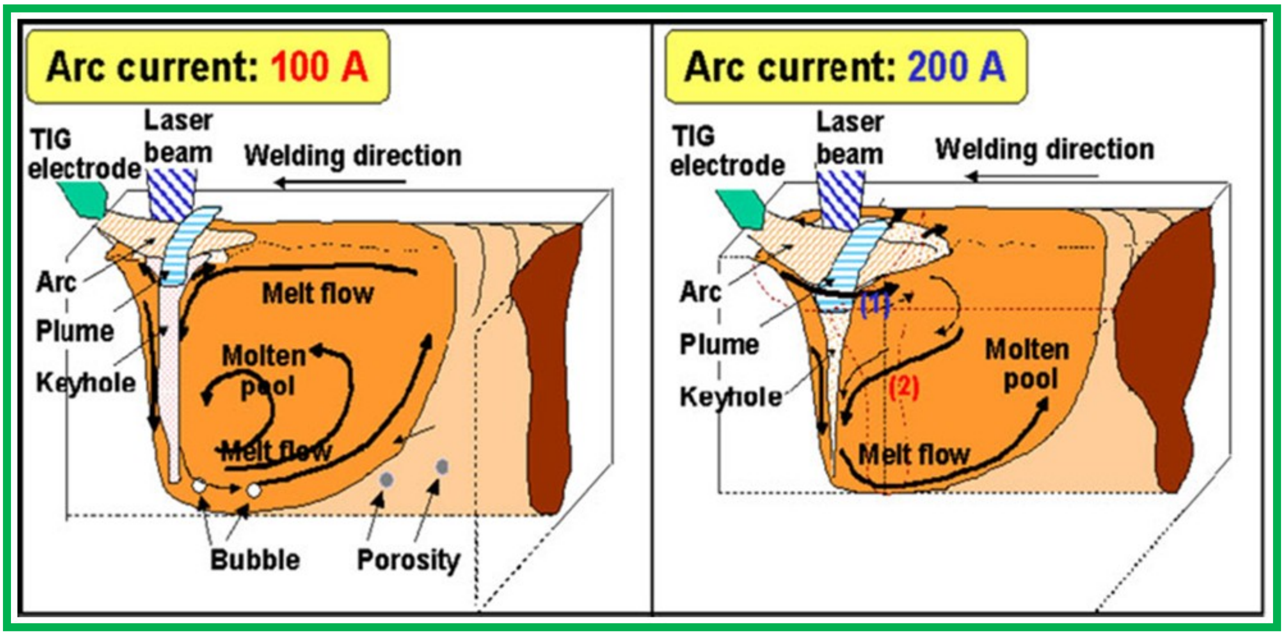

Figure 1-16 Schematic of interaction of heat sources under the surface of weld pool at two different arc currents [169]

1.7 OBJECTIVE OF THE STUDY

As the energy transfer mode phenomena influences weld geometry and characteristics altogether, it must be clearly defined with process parameters. But, very limited studies only have been made on the transition of energy transfer modes with process parameters. Few literature on continuous wave laser reports that the changeover of energy transfer modes from conduction to keyhole is not sudden and there is a transition regime in between these two modes [7, 8]. In case of seam welding using pulsed lasers, many process parameters are involved. Therefore, energy transfer modes in pulsed laser seam welding are required to be understood and the effect of process parameters on the transition is to be studied. Further, pulsed laser welds have been reported to have solidification cracking issue in fully austenitic stainless steels due to its rapid cooling rate and crack susceptible chemical composition. As this issue brings serious damages to the resultant weld structure, it has been addressed by many researchers. Different methods have been used and recommended to avoid cracking in alloys of aluminium, nickel and stainless steels. However, the influence of energy transfer modes on solidification cracking in has not been studied adequately in fully austenitic stainless steels.

Further it is observed that that the applications of pulsed laser have been limited to conduction modes in several studies and very few works report keyhole mode pulsed laser welding. The hybrid process is an advanced variant of laser welding process where laser and electric arc are coupled together and applied on the common molten zone to eliminate the drawbacks of both processes and to obtain their synergistic advantages. Several hybrid welding studies have been carried out using high power lasers, but only a few studies have been made on low power lasers [19-21]. The synchronizing of pulsed laser with pulsed TIG in micro welding has been carried out and the advantages have been reported [22]. In order to widen the application domain of pulsed laser seam welding, more hybrid welding experiments need to be carried out.

Though a few experiments have been carried out in pulsed laser welding of stainless steels on optimisation of parameters, weld geometry, microstructures etc, these aspects have not been dealt with adequately [23-25]. In the present study, pulsed laser beam welding of fully austenitic stainless steel-AISI 316 grade has been studied on energy transfer modes and solidification cracking. In addition to that hybrid welding was established by combining Gas Tungsten Inert Gas (GTAW) arc with laser beam, and experiments have been performed to understand the basic hybrid welding parameters. A comparative study was carried out to analyse the microstructural and mechanical properties of laser, GTAW and hybrid welds.

The review of hybrid welding shows that many process advantages are observed in hybrid welding on various materials and alloy system. Several combinations of laser and electric arc have been employed in experimental studies. But, very few works have been reported using pulsed laser as heat source for hybrid welding. Although pulsed laser welds in conduction mode have been studied extensively, keyhole mode in pulsed processing is not studied adequately. Hence, Pulsed laser-arc hybrid welding and its processing parameters need to be studied and their potential advantages to be identified.

1.8 THE OUTLINE OF DISSERTATION

This dissertation presents the following works (i) Classification of energy transfer modes in pulsed laser seam welding, (ii) Effect of energy transfer modes on solidification cracking, (iii) Investigation of pulsed laser-GTA hybrid welding and comparative study of microstructural and mechanical properties of hybrid with laser and GTA welds. Experimental procedures on pulsed laser and hybrid welding and characterisation of welds have been described in Chapter 2. The results of energy transfer modes and the influence of pulse parameters have been given in Chapter 3. Solidification cracking and the influence of mode transition have been dealt in Chapter 4. In chapter 5, the development of pulsed laser hybrid welding system and experiments carried out in studying basic hybrid parameters have been discussed. The microstructural and mechanical properties of laser, GTAW and hybrid welds have also been described in this chapter. The final chapter summarises the conclusions drawn from the above studies and indicates future directions to expand the present work.

CHAPTER 2 MATERIAL AND EXPERIMENTAL METHODS

2

In this chapter, welding experiments, material and analysis carried out on welds have been described. Pulsed laser seam welding experiments and hybrid welding were performed on AISI Type 316 stainless steel plates. Hybrid welding was established by combining GTAW torch with laser beam paraxially. A torch holder was designed, fabricated and attached with laser focusing head. The microstructures of welds were analysed using optical microscopy. Scanning electron microscope was used to examine solidification cracks in 316 stainless steel welds. Residual stresses developed in the welds were measured by X- ray diffraction system. Mechanical properties of welds were determined in transverse tensile tests. In the following passages, the details of the welding experiments and analysis carried out on welds have been discussed.

2.1 MATERIAL

AISI Type 316 austenitic stainless steel plates were used in all the experiments. The chemical composition was determined using optical emission spectroscopy technique. The chemical composition is given in Table 2-1. In this alloy, Nickel equivalent is more as austenite stabilising elements such as Ni, C, and N are relatively higher than in other alloys. Cr equivalent to Ni equivalent according to Schaeffler, WRC-1992, Lippold and Lienert constitutive diagrams are 1.5, 1.28, 1.33 and 1.44 respectively. As predicted by the above diagrams, the resultant welds tend to solidify in primary austenitic mode and will have fully austenitic microstructures. Though this kind of structure is prone to solidification cracking, the formation of fully austenitic microstructure is required in sub-zero temperature and non-magnetic material applications.

Table 2-1 Chemical composition of AISI 316 stainless steel plate

Element	C	Cr	Ni	Mo	Mn	Si	N	S	P	Fe
Wt %	0.057	15.61	11.66	2.25	1.55	0.62	0.017	0.014	0.038	Balance

In the present study, plates of dimension 75×70×3.3 mm were used. Energy transfer modes and solidification cracking studies were carried out as bead-on-plate welds. In microstructural and mechanical properties comparative study, hybrid, laser and GTA welds were made as butt joints. In all the experiments, plates with same surface finish were used to avoid variations in laser energy absorption.

2.2 ND: YAG PULSED LASER SYSTEM

The pulsed laser and hybrid welding experiments were carried out using Trumpf- Trupulse 556 model Nd: YAG pulsed laser with the capacity of mean power 530W. The specification of the system is given in Table 2-2. Pulsed laser welding system consists of laser generator, beam handling unit, focusing head and workstation for workpiece movement. The laser beam is generated by optical resonator system, which comprises lasing medium, reflectors, pumping source and reflecting mirrors. Neodymium- doped Yttrium Aluminium Garnet rod is used as lasing medium and surrounded by flash lamp, which is employed for optical pumping. The intensity and duration of flash lamp are controlled by electrical system and in turn the laser pulse parameters are determined. The laser photons from lasing medium are reflected and resonated by reflectors arrangement based on stimulating emission of photons. In order to maintain lasing medium at appropriate temperature, Nd: YAG crystal rod is kept in distilled water and which is cooled down by external chiller unit [6].

Table 2-2 Specifications of pulsed laser used in experiments

Lasing medium	Solid state Nd doped YAG crystal
Pumping source	Flash light
Wavelength, μm	1.06
Mean power , W	530
Max. Pulse power, W	10 to 10000
Max. Pulse energy, J	60 to 100
Pulse duration, ms	0.3-50
Beam quality, mm.mrad	25
Focal length, mm	200

Since wavelength of Nd: YAG laser photon is low (1.06μm), it can be carried through fibre cables. Handling Nd: YAG laser through fibre cable is simple and the system becomes compact and flexible to be used in remote applications. The raw laser beam from cable is focused through collimating and focussing lenses in focusing head. The focusing lens in the laser head is safeguarded from excessive arc plasma and any spatters by another protective lens. The lens with 200mm focal length was used. The focused laser beam was applied on the material surface. The CNC workstation used for the movement of workpiece is shown in Figure 2-1. Workpiece is kept on the fixtures of CNC laser workstation and controlled by CNC programmes. Focal length is very important parameter in laser welding as it influences laser- material interaction and weld geometry. The focus point was fixed by visual focus and verified by experimental procedure. The laser spot diameter at the focal point is measured to be 0.8mm.

Figure 2-1 The CNC Laser workstation used for movement of workpiece

According to laser beam safety standards, the employed Nd: YAG laser is of class 4 type, highest and most dangerous class of laser. By definition, a class 4 laser can burn the skin, or cause devastating and permanent eye damage as a result of direct, diffuse or indirect beam viewing [171]. So, all the safety precautions have to be taken during welding process. As the wavelength of Nd: YAG laser is in near-IR range, the laser beam path is not visible. Hence, a He- Ne pilot laser, which is visible to the eyes, is used along with Nd: YAG laser, to focus the laser beam on the workpiece. Argon shielding gas was chosen for all the experiments for its better shielding of molten pool and low cost. Shielding gas nozzle was kept about 45° to the workpiece surface, to obtain better shielding.

2.3 PULSED LASER- ARC HYBRID WELDING SYSTEM

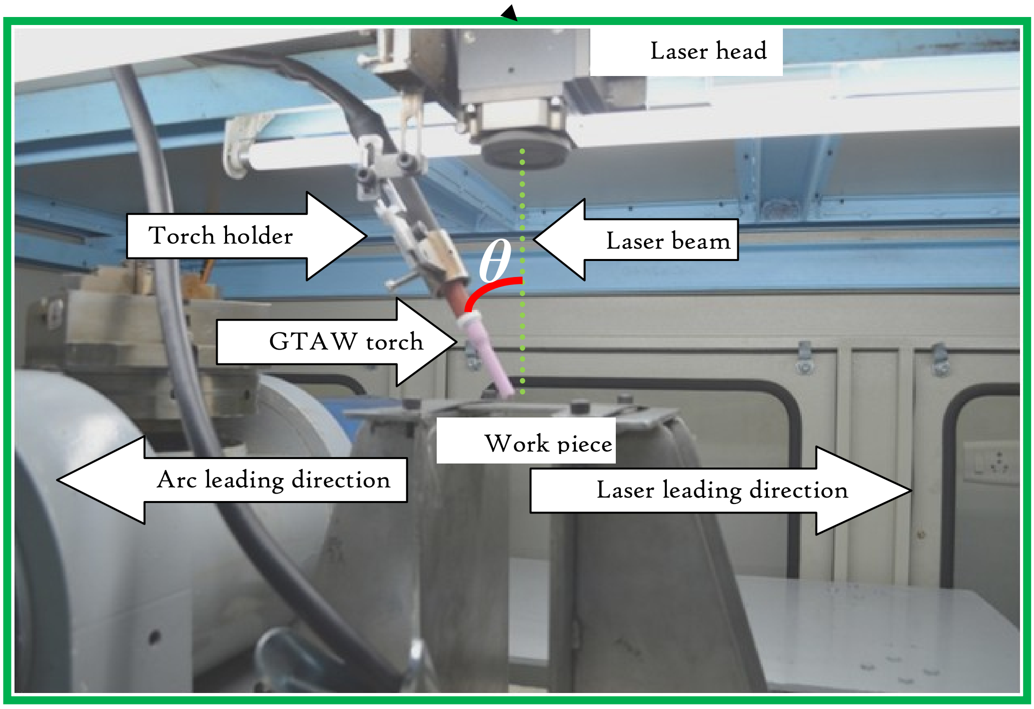

Figure 2-2 Pulsed Laser- Arc hybrid welding experimental setup

Pulsed laser- arc hybrid welding was established by attaching GTA torch paraxial to laser head to apply both laser beam and GTAW arc on same molten zone. GTA torch holder was designed, fabricated and combined with laser head as shown in Figure 2-2. In the design of torch holder, the provisions for varying inter heat source distance (D_{LA}) and torch angle, (θ) were given. Longer ceramic torch nozzle was used to render more tolerance for torch angle and to avoid damage to tungsten electrode. Both laser head and GTAW torch were kept stationary and work piece was moved by CNC workstation. With respect to moving direction, heat source position can be chosen as either arc or laser leading processes. Argon was used as shielding gas for its better arc stability. WC-20 type Tungsten electrode (2% CeO_2 added) of diameter 2.4 mm was used with ground electrode to tip angle of around 20°. Direct current electrode negative (DCEN) polarity was maintained throughout the experiments. GTAW arc was initiated by high frequency (HF) arc starting mechanism in

GTA welding machine. High frequency current during arc starting operation can damage the magnetic parts in CNC workstation. Therefore, electrical insulation was given between workpiece table and CNC controller. This safety precaution is mandatory when hybrid welding is assembled with CNC laser welding workstation.

2.4 METALLOGRAPHY

Metallographic analysis was carried out by following the procedures as per ASTM E3 standard. Weld samples were cut at appropriate places using handsaw. Samples were moulded using cold setting resins. The moulds were ground by silicon carbide (SiC) abrasive sheets in sequence of grid sizes 120, 240, 400, 600 and 800. After grinding, samples were polished with diamond slurry of sizes 9, 6 and 3µm on soft cloths of same size. These procedures were followed until scratch free, mirror finish polished surface is achieved. Both grinding and polishing were carried out using automatic polishing machine ‘Mecatech 234’ which shown in Figure 2-3. The applied pressure, rotation speed and polishing time were optimised for better polished surface. After polishing, samples were cleaned thoroughly using ultrasonic cleaning method.

Etching of austenitic stainless steels is best performed by electrolytic etching in 10% Oxalic acid solution. Macrostructure of welds and microstructure were analysed in Olympus GX-91 metallurgical microscope (Figure 2-4) coupled with image analysis software. Measurement of depth of penetration, weld width and weld area were performed by using image analysing software. In order to understand the influence of energy transfer modes on cracking, total crack length and number of cracks were measured in pulsed laser welds by the special feature of the software.

Figure 2-3 Metallography- polishing machine

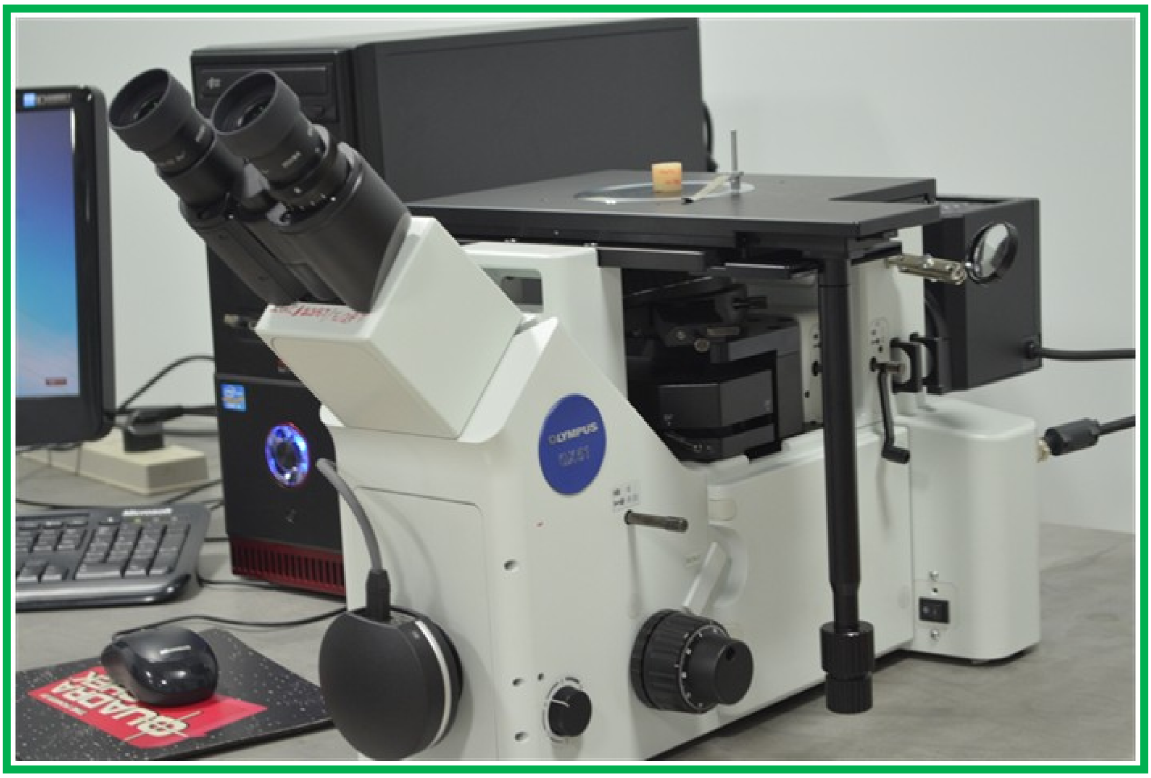

Figure 2-4 Metallurgical microscope

2.5 SCANNING ELECTRON MICROSCOPE

SEM is phenomenal tool in characterisation of various materials. In this technique, electron beam is scanned in raster fashion and made to interact on the material surface. Due to the electron-material interaction, emission of secondary electrons, backscattered electrons, x-rays, Auger electrons etc, occur based on the material's surface and chemistry. These particles are captured by suitable detectors and visualized as digital images. Secondary electrons are detected and imaged which visualise microstructures of material surface. The imaging of X-rays generated from the interactions of electrons with microstructural features shows the elemental composition. This approach is known as Energy dispersive spectroscopy (SEM-EDS) technique. This is used to determine the localised chemical compositions in the fine features of microstructures. In the present work, SEM was used to study solidification cracks observed in pulsed laser welds. The microstructures and chemical compositions across the cracking zones were examined. The samples were prepared by polishing and etching as described in previous section. SEM-EDS analysis was carried out across the crack-filled regions. Both point and line scans were made.

2.6 XRD-RESIDUAL STRESS MEASUREMENTS

X-ray beam with wavelength 'λ' is diffracted at an angle '2θ' when the interplanar spacing 'd' matches the conditions of Bragg's law given by

$$\lambda = 2\mathrm{d}\sin\theta.$$

Where, λ- Wavelength of incident X- rays in Å, θ- Angle between incident or reflected beams and the reflecting planes in degree (°).

X-ray diffraction (XRD) is highly sensitive to interplaner spacing of the lattice which would change in the presence of stresses in a material. While the presence of elastic macro stresses causes a shift in the diffraction peak position, which is dependent on the magnitude, the direction of the shift depends on the nature of the stresses i.e. whether they are tensile or compressive. In this technique, strain in the surface layers of a material is estimated by measuring the shift in the position of the diffraction peak of a set of parallel planes. These strains are then converted into stresses analytically using various assumptions [172]. XRD system was used to determine the residual stress distribution across laser, hybrid and GTA welds. Chromium K_{β} of wavelength 2.0848 Å was used for the measurement. The longitudinal stresses were measured by moving the back reflection type goniometer along the welding direction.

2.7 TENSILE TEST

Transverse weld tensile tests were performed and the mechanical properties of laser, GTAW and hybrid welds were determined. The samples were taken from weld pads across the weld line by milling operation. The dimensions of gauge length and width were chosen according to ASTM E8 standards. Displacement controlled, electromechanical, screw driven universal testing machine (UTM) with the capacity of 100 KN load was employed for tensile tests.

CHAPTER 3 ENERGY TRANSFER MODES IN PULSED LASER SEAM WELDING

3

3.1 PULSED LASER SEAM WELDING PARAMETERS

In this study pulsed laser seam welding parameters have been introduced and the energy transfer modes with respect to these parameters have been discussed. Pulsed laser seam welding is continuous weld made by overlapping of each spot made by single laser pulses. The schematic of laser pulses in conventional rectangular shape is shown in Figure 3-1. The energy of laser pulse (E_p) is the area of laser pulse as shown in Figure 3-1 which is determined by power, pulse duration (t_p) and pulse shape. The maximum power applied is known as peak power (P_{peak}). For rectangular shape pulses, peak power is maintained throughout pulse on time and for other shapes it varies with time and shape. The number of pulses applied per second is pulse repletion rate or pulse frequency. Mean power (P_{mean}) is the term used to indicate average laser power applied per second. The relationship between laser pulse parameters have been described in literature [173-175] and are given below.

Duty cycle (C_D), is the ratio of pulse duration to total pulse cycle time. Duty cycle can be given in many ways as [175]:

$$C_D = \frac{P_{Mean}}{P_{Peak}}; \quad C_D = t_p/t_f\,; \quad \therefore C_D = t_p \times f;$$

Energy density is the energy delivered on the material [175]:

$$E_d = \frac{\text{Pulse energy (J)}}{\text{Spot area (cm}^2\text{)}} = \frac{4E_p}{\pi {d_s}^2}$$

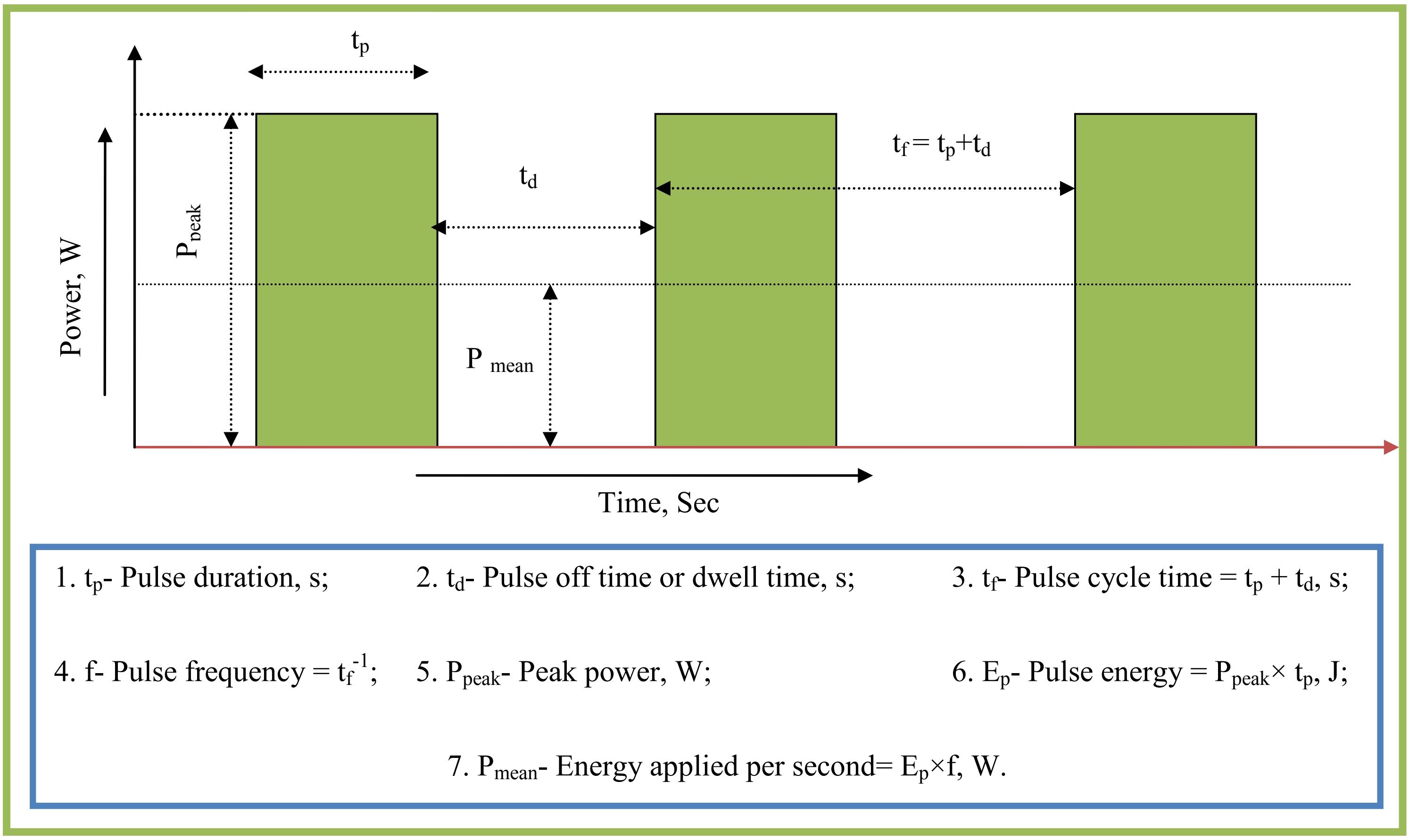

Figure 3-1 Schematic diagram of Laser square wave pulses with illustrations of pulse parameters

The leak tightness of seam welds is examined by a parameter called overlapping factor (Q), which is given below [176].

$$Q_f = \left[1 - \frac{vt_f}{d_s + vt_p}\right] \times 100 \qquad (4.1)$$

For good hermetical sealing, it is recommended that each spot should overlap the nearby spots by more than 70% [6]. It shows that the overlapping factor in percentage (Q_f) depends on traverse speed (v in mm/s), spot diameter (d_s in mm), pulse duration (t_p in s) and pulse cycle time (t_f in s). It implies that traverse speed in pulsed laser seam welding is decided by overlapping factor.

Interaction time (t_i) is the time during which the laser beam interacts with any point on the material. For continuous laser heat source, it is given as, $t_i = \frac{d_s}{v}$ [174].

In pulsed laser seam welding, duty cycle is to be taken into account, since during the dwell time or pulse off- time, no interaction takes place between the laser heat source and the material [105].

$$\therefore \mathrm{t_i} = \frac{d_s}{\mathrm{V}} \times \mathrm{C_D}$$

$$\mathrm{t_i} = \frac{d_s}{\mathrm{V}} \times \mathrm{f} \times \mathrm{t_p} \qquad (4.2)$$

Equation 4.2 shows that interaction time in pulsed laser seam welding involves various pulse parameters.

Specific point energy (SPE) is the actual energy delivered to a point on material surface. In the definition given by Suder et al.[174], all laser parameters are incorporated and laser beam intensity distribution is assumed as constant and the laser beam shape is taken as rectangular or square.

Specific point energy (J) = Laser power × interaction time (t_i)

This relation can be extended to pulsed seam welding by including interaction time as follows:

$$\mathrm{SPE} = \mathrm{P_{peak}} \times \mathrm{t_i}$$

When considering interaction time from equation 4.2, SPE is given as:

$$\therefore \mathrm{SPE} = \frac{\mathrm{P_{peak}} \times \mathrm{d_s} \times \mathrm{f} \times \mathrm{t_p}}{\mathrm{V}} \qquad (4.3)$$

3.2 EXPERIMENTAL PROCEDURE

The welds were made using the Nd: YAG pulsed laser system as discussed in chapter 3. Square wave pulses were used for all the experiments. Beam diameter was kept constant in this study at its minimum possible value of 0.8mm. Argon with 99.99% purity with flow rate of 10 litres per minute was used as shielding gas. In these experiments, laser head was kept stationary and the work piece was clamped to X-Y table which was operated by a CNC workstation. All the welds were made on AISI 316 stainless steel plates of 3.3 mm thickness and bead-on-plate welds were made by keeping same surface conditions.

In this study, to understand the mode transfer and the effect of pulse duration, three sets of experiments were carried out at three different pulse durations, 4 ms, 8 ms and 16 ms, representing short, medium and long pulses respectively. All the other parameters such as pulse frequency, beam spot size, traverse speed, focus position, and pulse shape were kept as constant. For every pulse duration, peak power was varied from lower value to higher possible value. These experimental parameters are given in Table 3-1. It can be seen that the pulse energy and mean power vary linearly as the peak power and pulse duration are changed. Overlapping factor as calculated from the equation 4.1 was kept about 80% in all the cases. After welding, all the samples were cut and polished for metallographic analysis. Each sample was cut and analysed in more than one place to assure the uniformity of penetration. Weld start and end regions were discarded due to transient nature at these domains. Due to transient nature of heat conduction and laser-material interaction phenomena at weld start and regions, weld samples were not taken from these sections. Electrolytic etching was done using 10% of oxalic acid. Weld geometry and microstructures were analysed using metallurgical microscope.

3.3 EXPERIMENTAL RESULTS

In pulsed laser seam welding process, pulse duration is the laser pulse ‘on’ time. During that time, material surface gets melted or vaporized depending on the peak power density. The molten material starts solidifying during the pulse ‘off’ time or dwell time. For constant peak power, increasing the pulse duration will increase the pulse energy and mean power as given in equations in Figure 3-1. The maximum mean power capacity of the pulsed laser welding machine used for the experiments is 530W. As the pulse duration increases, mean power increases linearly. Therefore, wwhen the longest pulse duration in this study, 16ms is experimented, the machine cannot generate laser beam with more than 1.9kW peak power. In other pulse durations 4 and 8ms, above 4kW, spattering was observed. Since spattered weld does not have significance in actual applications the data beyond this limit is not considered.

As the peak power increases, the change in energy transfer modes is anticipated from conduction to keyhole mode. The change in energy transfer mode is reflected in weld geometry and microstructures. Based on the differences in weld geometry and microstructures, different modes were identified, namely, conduction, transition, penetration and keyhole modes as shown in Figure 3-2 (a-d). From the measured dimensions of welds, graphs were plotted between peak power (W) and depth of penetration (mm) for different pulse durations as shown in Figure 3-3. The relationships between depth-to-width ratio (aspect ratio) against peak power density and energy density for three different pulse durations are shown in Figure 3-4 and Figure 3-5 respectively. Except the weld of experimental number 16 (given in Figure 3-2.d), which is a full penetration weld, all the others are partial penetration welds. For this weld, the depth to width ratio is attributed as minimum aspect ratio that can be attained using this pulse parameter.

Table 3-1 Pulsed laser seam welding parameters

[Pulse frequency, f= 15 pulses/ s; Pulse cycle time, t_f= 66.7ms; Spot diameter, d_s= 0.8mm; Traverse speed, V= 2.5 mm/s; Focus position- 0 mm (On top surface)]

Expt. No	Peak power, P_{peak} (KW)	Pulse Duration, t_p (ms)	Pulse energy (J) $E_p = P_{peak} \times t_p$	Mean Power, ($P_{mean} = E_p \times f$) (W)	Peak power density, ($P_d = 4P_{peak}/\pi d_s^2$) ($10^5$ W/ cm^2)	Energy density, ($E_d = 4E_p/\pi d_s^2$) (10^3 J/cm^2)
1.	2	4	8	120	3.98	1.59
2.	2.5		10	150	4.98	1.99
3.	3		12	180	5.97	2.39
4.	3.3		13.2	198	6.57	2.63
5.	3.5		14	210	6.97	2.79
6.	3.75		15	225	7.46	2.99
7.	4		16	240	7.96	3.18
8.	1.25	8	10	150	2.49	1.99
9.	1.5		12	180	2.99	2.39
10.	1.75		14	210	3.48	2.79
11.	2		16	240	3.98	3.18
12.	2.25		18	270	4.48	3.58
13.	2.5		20	300	4.98	3.98
14.	3		24	360	5.97	4.78
15.	3.5		28	420	6.97	5.57
16.	4		32	480	7.96	6.37
17.	0.8	16	12.8	192	1.59	2.55
18.	1		16	240	1.99	3.18
19.	1.2		19.2	288	2.39	3.82
20.	1.4		22.4	336	2.79	4.46
21.	1.6		25.6	384	3.18	5.10
22.	1.8		28.8	432	3.58	5.73
23.	1.9		30.4	456	3.78	6.05

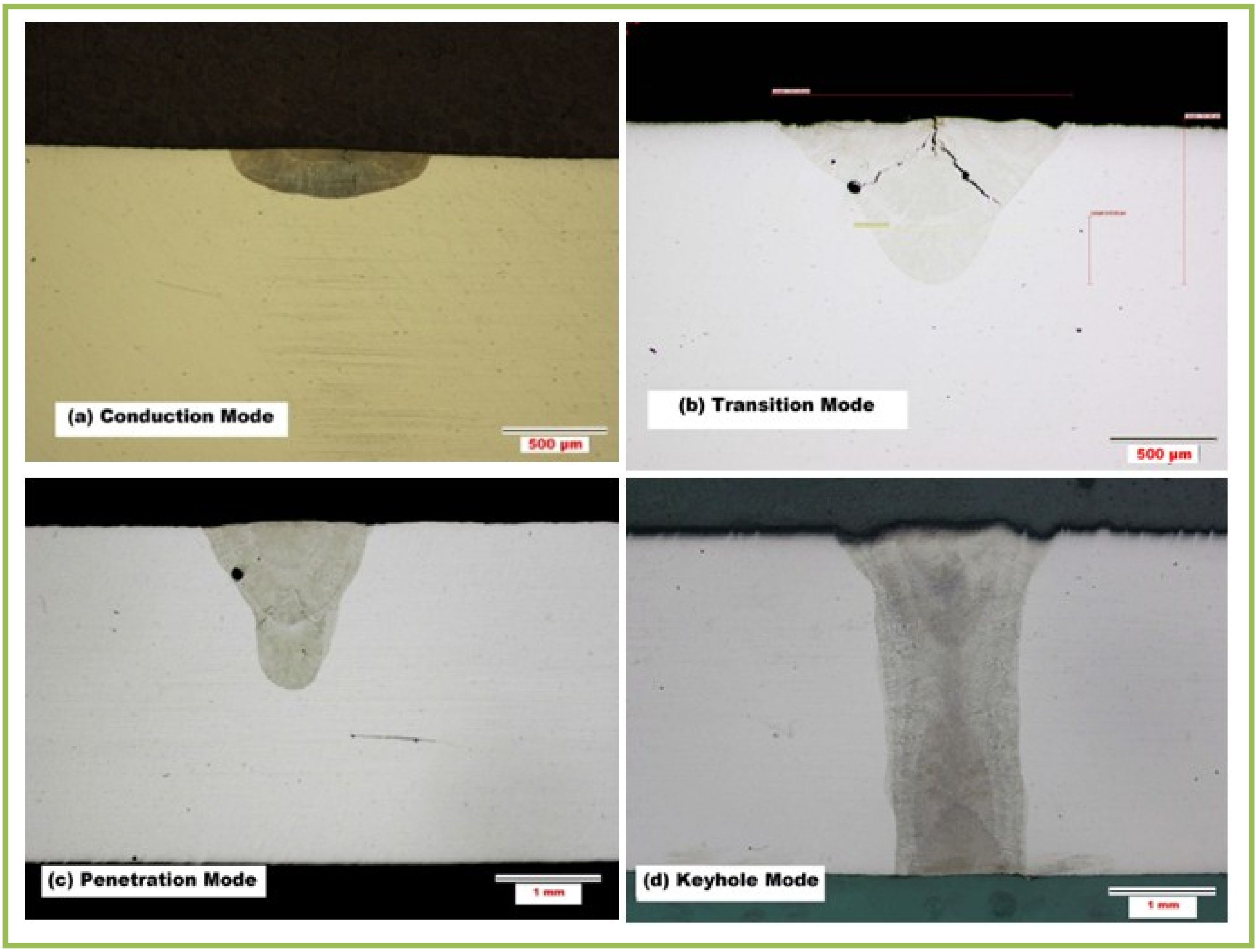

Figure 3-2 Macrostructures of pulsed laser welds in different energy transfer modes, a) Conduction, b) Transition, c) Penetration and d) Keyhole modes

3.4 DISCUSSION

3.4.1 Conduction mode

Conduction mode welds (Figure 3-2 a) are identified by their shallow penetration and flat top surface, characteristic of no or insignificant vaporization. In conduction mode welds, the laser energy absorption is very low as laser light energy is reflected out of the material surface. Further, the absorbed energy via heat conduction mechanism more in radial direction

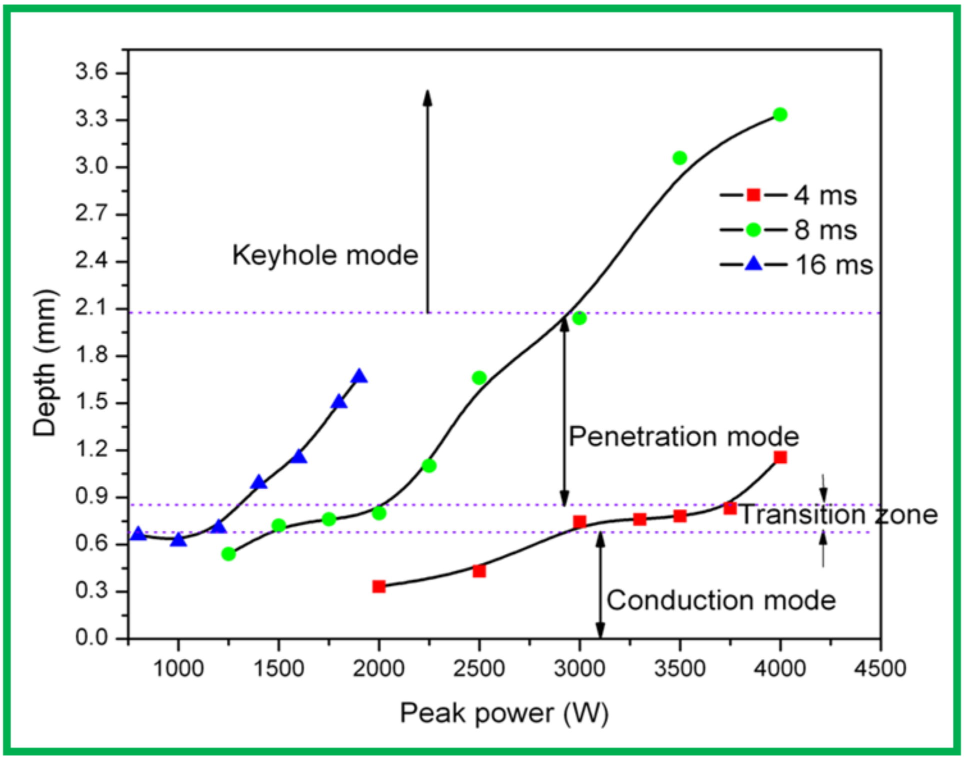

Figure 3-3 Peak power versus depth of penetration for different pulse durations

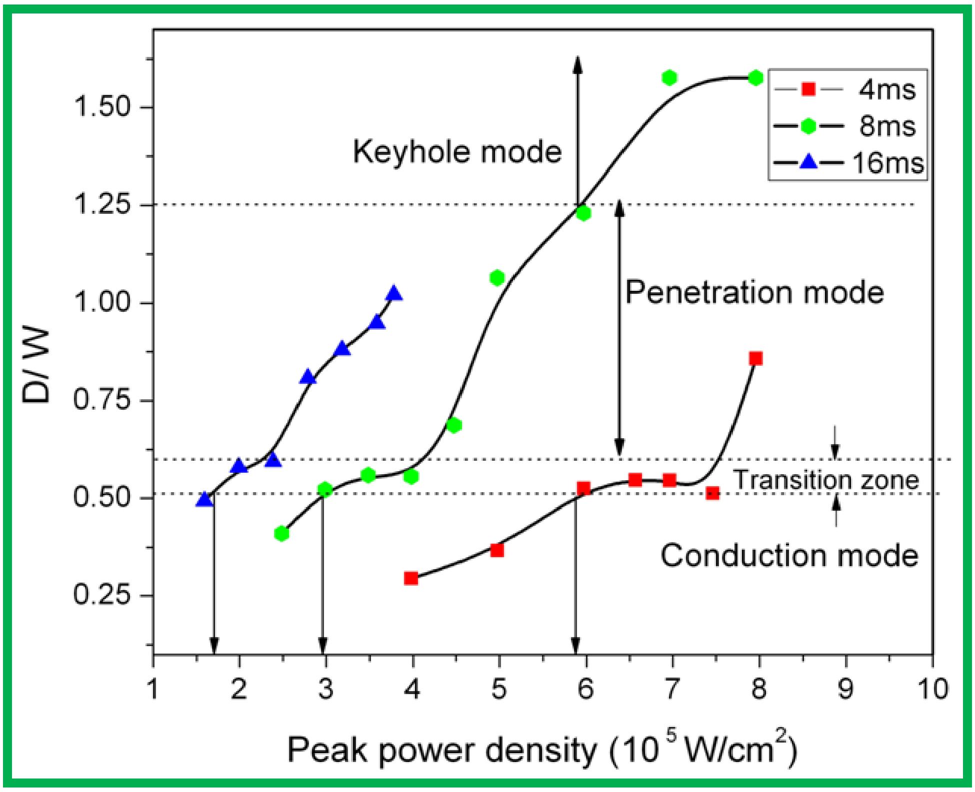

Figure 3-4 Peak power density versus aspect ratio for different pulse durations

than depth direction as a result of Marangoni convection. The gradient in surface tension at the solid/ liquid interface in welds takes place due to variation in temperature distribution, solute concentration along the interface. When the thermal coefficient of surface tension ($\partial\gamma/\partial T$) is negative, the cooler peripheral have a higher surface tension than the centre of the weld pool and the flow will be outwards, creating a wide shallow weld pool. Therefore in conduction welds, as energy density increases although aspect ratio also raises the rate of increase in aspect ratio decreases.The threshold limit of conduction mode (E_{CML}) is more or less same for all the three pulse duration conditions, as seen in Figure 3-5.

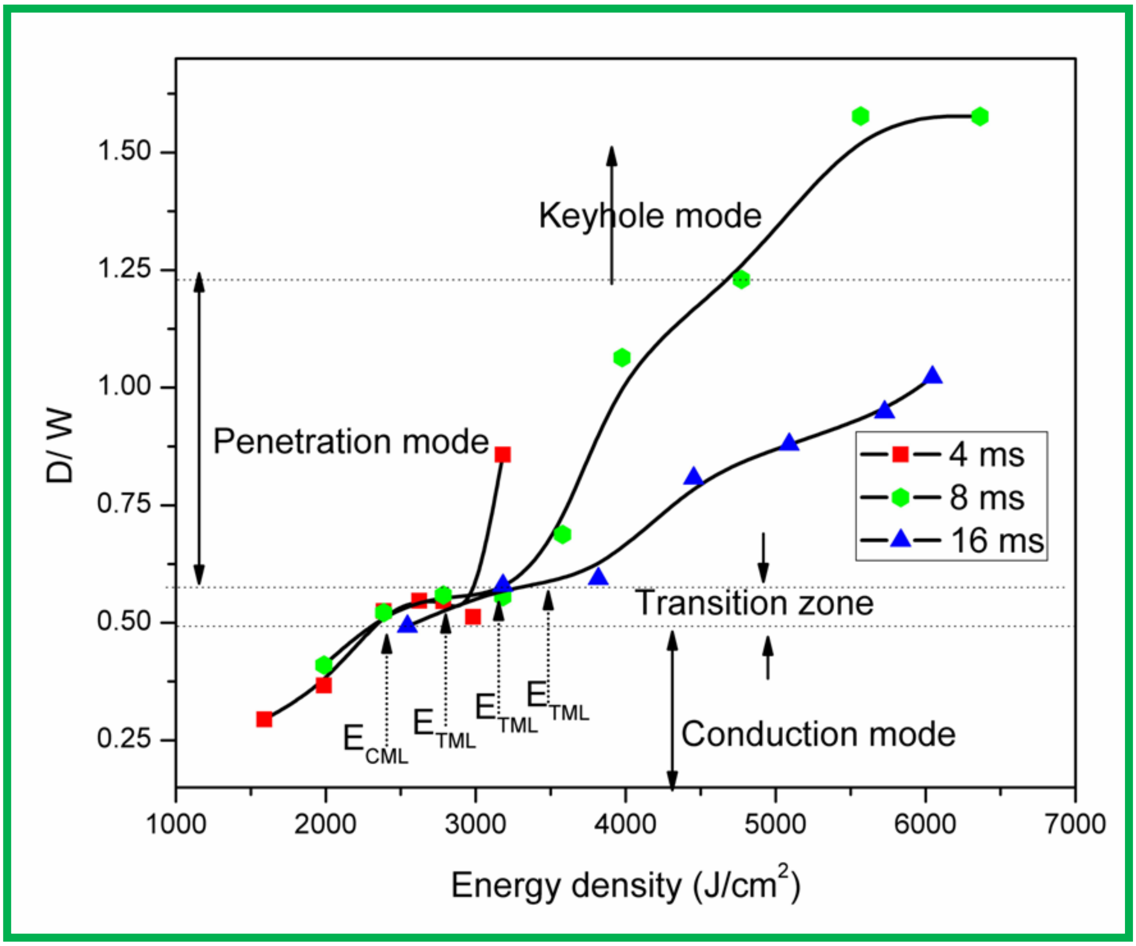

Figure 3-5 Aspect ratio versus energy density for different pulse durations

3.4.2 Transition mode

As the peak power increases further, at the end of conduction mode, keyhole starts forming. In Figures 3-3 to 3-5, all the curves show a flat region known to be transition zone, where depth of penetration increases slowly and the aspect ratio is almost constant. The keyhole is highly unstable and is balanced by the forces which try to open it and the forces which try to close it. The pressure exerted by the vapours inside and above the keyhole keeps the keyhole open. But the surface tension forces and hydrostatic pressure try to close the keyhole. So in order to keep the keyhole open, sufficient vaporization should occur. The added extra energy in the transition zone does not increase depth of penetration, but it is spent to evaporate more material until significant keyhole is formed [80, 113, 177].

From Figure 3-4, it is clear that the threshold peak power density to form keyhole (marked by down arrows in Figure 3-4) is not a constant value but as pulse duration increases this value is reduced. As the pulse duration increases, laser energy is applied for more time. The added energy increases the molten metal surface temperature and results in increased laser energy absorption as laser absorptivity also increases drastically with increase in temperature. These conditions facilitate the earlier formation of keyhole and reduce the threshold peak power density to form keyhole. The peak power densities corresponding to the pulse durations of 4ms, 8ms and 16ms are 5.57×10^5 W/cm^2, 2.79×10^5 W/cm^2 and 1.59×10^5 W/cm^2 respectively. This clearly shows that the formation of keyhole cannot be defined by a single power density value, rather, it depends on other pulse parameters.

However, the relation between the energy density and the aspect ratio, as given in Figure 3-5, shows that conduction mode limit, (E_{CML}) or the threshold energy density to form keyhole in transition zone, lies within approximately 2.4 kJ/cm^2 for all pulse durations. Since the pulse duration in pulsed laser seam welding has influence on the formation of keyhole along with peak power, it is suggested that energy density should be considered along with peak power density to determine the energy transfer modes.

3.4.3 Penetration mode

When the energy density reaches the threshold energy density to form significant keyhole, sudden increase of aspect ratio is observed. This rapid increase of aspect ratio is coupled with the sudden increase of absorption of laser energy into keyhole which is due to multiple reflections of laser inside the keyhole [41, 162, 176]. Welds of aspect ratio about 1 are identified to be of penetration mode, where the formed keyhole is unstable and the molten pool is not maintained continuously [173]. Figure 3-2.c shows the macrostructure of penetration mode weld.

Since the energy absorption inside the keyhole is effective in penetration mode conditions, it can be naturally anticipated that increasing the laser energy will produce deeper welds. But as Figure 3-5 shows, the welds in the penetration mode, for the same energy density but different pulse durations, show much difference in the aspect ratio. Welds with longer pulses have smaller aspect ratio. The reduction in aspect ratio and depth of penetration is due to the attenuation of laser energy by fine particles of the radius less than 100nm in the plume [178]. Since the available time is higher at longer pulse duration conditions, the attenuation increases. Temperature and intensity distribution at the keyhole bottom also seem to be reduced at longer pulse conditions [178]. Hence, lower aspect ratio welds are produced even at higher energy density but with longer pulse durations.

Though higher peak power densities are applied, welds of 4 ms pulses show lower depth of penetration and aspect ratio compared to other welds (Figure 3-3 and 3-4). Normally with increase of peak power, higher penetration is expected. In the present study, the observation of lower depth of penetration at 4 ms pulse shows that the formed keyhole is not deep as expected. It is reported in [179], that within 1.5 ms of laser irradiation, the depth of keyhole reaches its maximum. But in this experiment, even after 4 ms pulse duration, sufficient deep keyhole is not formed, and the penetration achieved in the case of 8 ms pulse shows the formation of deeper keyhole beyond 4 ms irradiation. It gives the information that sufficient pulse duration is also important to achieve maximum penetration.

3.4.4 Keyhole mode

Welds of average peak power 3.5 KW and above with 8ms pulse duration show deeper penetration with aspect ratio greater than 1.5. These weld beads have cylindrical profiles as shown in Figure 3-2.d. The reason for the higher penetration depth and cylindrical profile may be the higher temperature achieved in the molten pool due to the high peak power and optimum pulse duration used. Therefore molten metal is not solidified in the pulse-to-pulse time or dwell time. Laser energy from consecutive pulses is more efficiently gets absorbed on molten metal rather than by fully or partially solidified regions found in other modes. This increases the depth of penetration and aspect ratio, much higher than that achieved in the penetration mode welds. Welds with aspect ratio of more than 1.25 are considered to be of keyhole mode in this discussion, as represented in Figures 3-3 to 3-5.

3.5 OPTIMISATION OF PULSE DURATION

In order to determine the optimum pulse duration for achieving effective deeper penetration welds, the index, ‘depth of penetration per unit peak power’ was used. This was determined by the slope of the curves plotted between peak power and depth of penetration for different pulse durations as shown in Figure 3-6. These slope values were obtained by linear curve fitting method while keeping the R^2 value about 0.9 and more. The calculated depth of penetration per unit peak power (mm/ KW) is plotted with pulse duration and shown in Figure 3-7. In addition, pulse duration is also plotted with interaction time. As given in

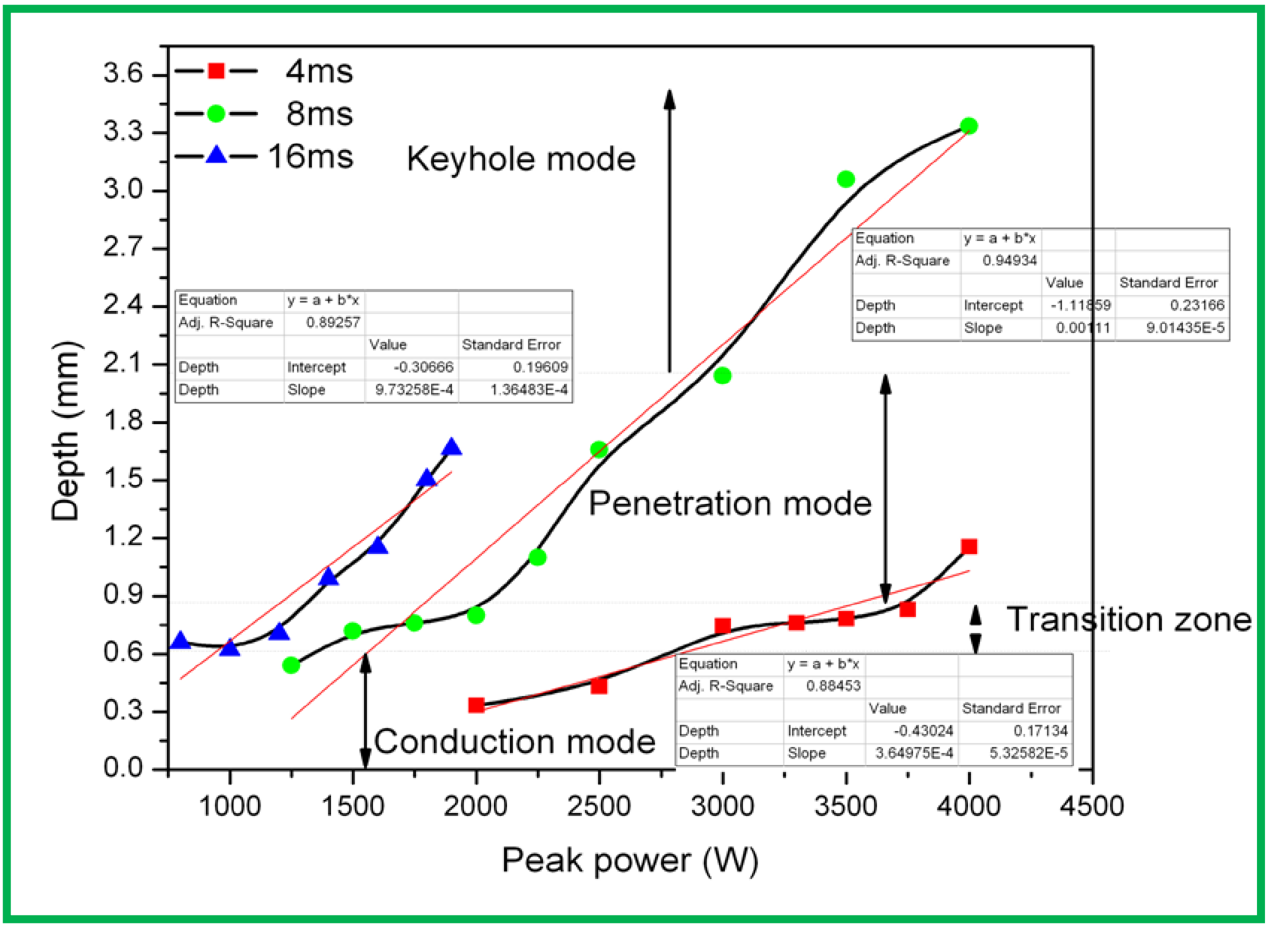

Figure 3-6 Method of linear curve fitting- Depth of penetration versus peak power plot

equation 4.2, interaction time is linear with pulse duration and shown in Figure 3-7. In this figure, the data points of 'depth of penetration per unit peak power' have been polynomial curve fitted and plotted as a B- spline curve. Initially as pulse duration increases, the penetration depth per unit peak power increases and the curve plateaus at about 1 mm/kW and then decrease to 0.9 mm/kW. Though the time of laser-material interaction is more at longer pulse durations, effective increase in penetration depth is not observed at longer pulse durations. As discussed in section 3.4.3, it is due to the energy attenuation by very fine particles in the plume at longer pulse duration conditions [178]. Further, it was verified from another similar experimental study with 6 ms pulse duration that penetration depth per unit peak power lies on the curve between 4 ms and 8 ms and shown in Figure 3-7. It was also observed experimentally that the energy transfer modes and weld geometry are not influenced by work piece width provided the width of the plate is more than about 5 times the thickness of the plate on either side of the seam.

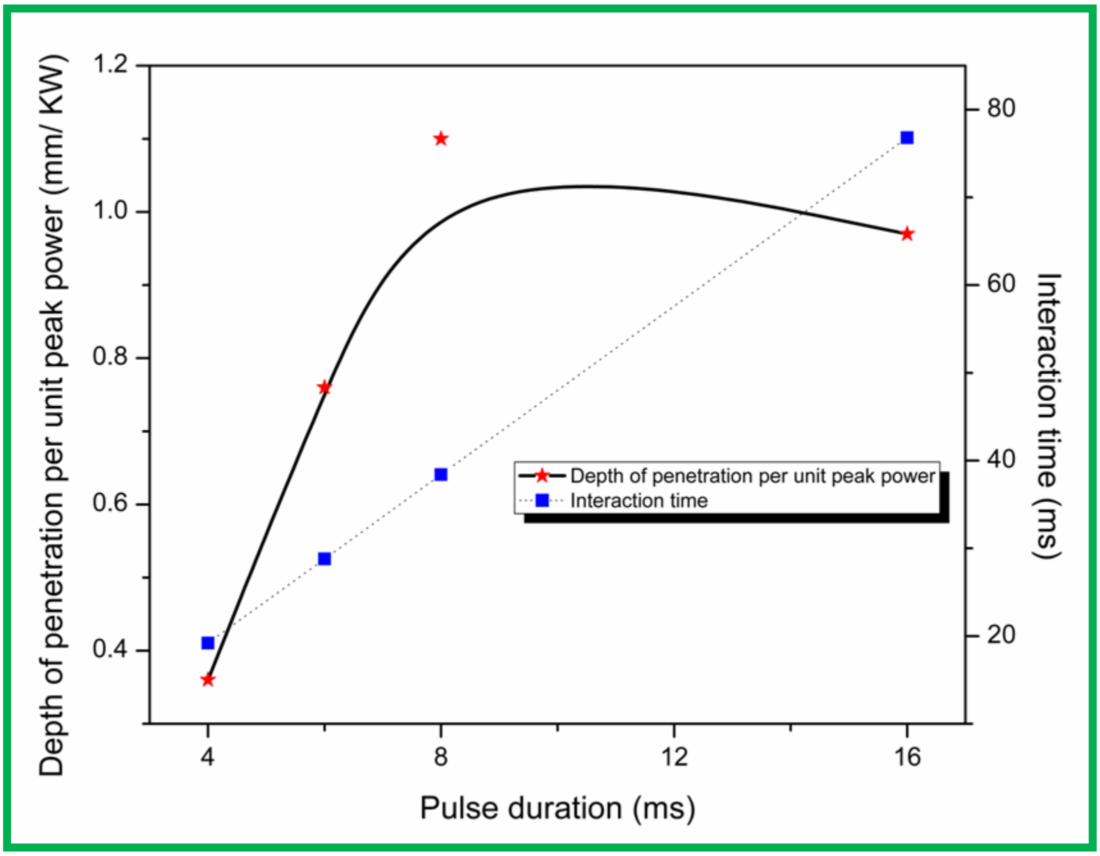

Figure 3-7 Penetration depth per unit peak power at different pulse durations along with interaction time

3.6 MODES OF LASER SEAM WELDING AND SURFACE CONDITIONS

The surface profiles of conduction, transition, penetration and keyhole mode welds were observed and shown in Figure 3-8.a-d. Conduction mode weld surfaces are smooth and the overlapping spots are circular. In this mode, heat is transferred through conduction and no vaporization occurs, and this leads to smooth, aesthetic appearance. But in transition zone, as the keyhole starts to form, weld spots get distorted and show elliptical profile. In penetration mode, the surface gets distorted further and uneven profile is seen. The uneven profile is due to the molten material flow around the keyhole and the evaporation effect. The keyhole mode shows more distorted and slightly spattered profile. These uneven and distorted surface profiles are due to the turbulence created in the molten pool when higher peak powers are used. Thus, observation of the surface profiles in case of pulsed laser seam welding can be used to identify the energy transfer mode undergone by the weld metal.

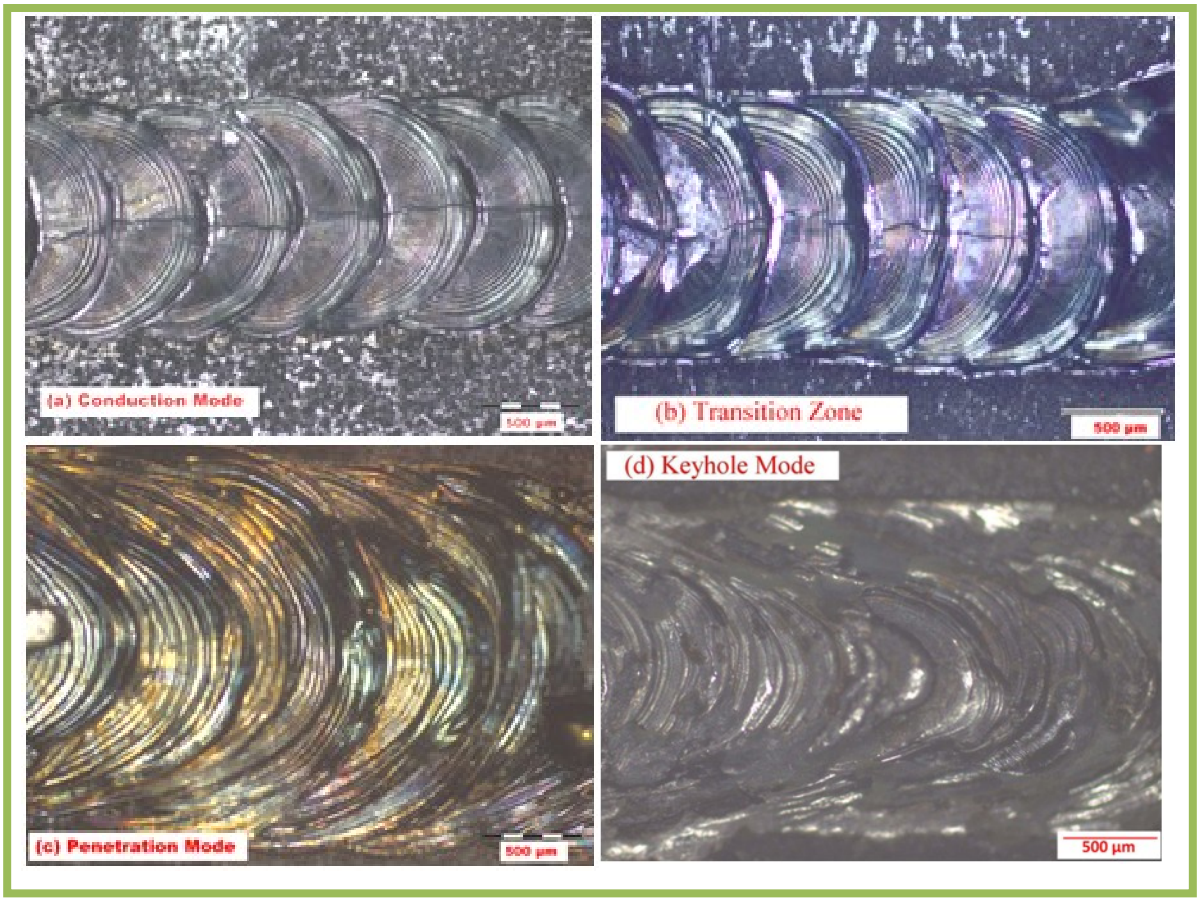

Figure 3-8 Surface profiles of a) conduction, b) Transition, c) Penetration and d) Keyhole mode welds

3.7 CONCLUSIONS

- Energy transfer modes in pulsed laser seam welding are identified as conduction mode, transition mode, penetration mode and keyhole mode based on the weld bead geometry and microstructural observations.

- The formation of keyhole is not defined by single peak power density but it depends on pulse duration. Increasing the pulse duration reduces the threshold peak power density to form keyhole.
- To describe the influence of pulse duration on the mode transition, it is suggested that energy density should be considered along with peak power density.
- In short pulses sufficient keyhole is not formed and in longer pulses laser energy is lost in plume attenuation. Therefore pulse duration to achieve effective welds with maximum depth of penetration is optimised to be around 8-10ms.
- The resultant weld surface profile changes can be used to predict the energy transfer modes in pulsed laser seam welding.

The work presented in this chapter is discussed in [180].

CHAPTER 4 SOLIDIFICATION CRACKING IN PULSED LASER SEAM WELDING

4

4.1 INTRODUCTION

Austenitic stainless steels are generally good weldable alloys except for solidification cracking which occurs during solidification of weld pool with certain chemical compositions. It is caused by formation of low melting eutectics such as FeS, due to the presence of impurities like sulphur, phosphorous and boron in the material, and thermal stresses associated with solidification [15, 97, 99, 181, 182]. Many researchers have studied this phenomenon and reported that solidification cracking can be prevented by reducing the impurities or by ensuring 3-7% of δ- ferrite in weld metal, which has higher solubility than the austenitic phase for elements that form low melting eutectics [15, 97, 99, 183]. For materials in which some of these elements are intentionally specified to exploit the specific advantages such as irradiation stability and improved creep properties, these elements cannot be reduced below specified levels which make these steels susceptible to hot cracking [9]. Introducing δ- ferrite in weld microstructure is not viable for autogeneous welds where no filler addition is made. Further, primary ferritic mode solidification is preferred to primary austenitic mode to avoid hot cracking [10]. But the alloys which has Cr_{eq}/Ni_{eq}, less than 1.48 solidify in primary austenitic mode and are prone to cracking [5]. In addition to this, when high power density laser beam welding (LBW) and electron beam welding (EBW) are used, focused intense energy is applied leading to rapid solidification. At this condition, primary ferritic mode can be shifted to primary austenitic mode due to higher cooling rates encountered in weld metal [182]. Therefore, an austenitic stainless steel, which does not show cracking when low energy density processes like GTAW, GMAW are used for welding, may show cracking tendency for high energy density processes like EBW and LBW.

Pulsed laser welds are much more susceptible to hot cracking than continuous laser welds due to high cooling rates encountered in the former [177]. As per weldability diagram for pulsed lasers [11], welds with impurity content (sulphur + phosphorous) greater than 0.02% and Cr_{eq}/ Ni_{eq}, according to Hammar & Svennson, lower than 1.59 solidify in primary austenitic (A) mode and exhibit cracking tendency. When Cr_{eq}/Ni_{eq} is more than 1.69, primary ferritic (F) solidification mode is obtained and no cracking is observed. In between 1.59 to 1.69, dual modes (A and F) were observed and cracking behaviour varies with the impurity content and welding conditions. Therefore, impurity content and Cr_{eq}/ Ni_{eq} are important factors in the cracking behaviour of pulsed laser welds [11].

Pulsed laser welding of hot cracking susceptible aluminium alloys, super alloys and fully austenitic stainless steels has been attempted with different methodologies. Milewski et al. observed crack-free microstructures under high duty cycle (>60%) conditions [184]. Pulse shaping has been used as effective method in reducing the solidification cracks [97, 185, 186]. Since susceptibility to hot cracking is closely related to welding conditions, influence of heat input on solidification cracking and heat affected zone (HAZ) cracking has been studied for laser welding. The tendency for HAZ cracking was observed to reduce with increasing heat input in laser welds of ATI Allvac [13] and Haynes 282 super alloys [14]. Reduced thermal stresses and formation of thick intergranular liquid film were reported as the causes for crack-free welds at higher heat input. However, some other studies showed increasing heat input may increase crack susceptibility. Studies on type 316 stainless steel [15, 187] and magnesium alloy [16] showed cracking at higher heat input conditions. In all these studies, effect of energy transfer modes of laser welding is not considered. Energy transfer modes depend on pulse parameters of laser beam such as peak power density and pulse duration. In pulsed laser seam welding, modes of energy transfer have been classified as conduction, transition/penetration and keyhole based on weld geometry and microstructures [180]. With increase in the power density, mode changes from conduction to keyhole along with variation in weld metal geometry, and both mode of transfer and power density can influence solidification cracking. In the work of Montazeri et al, [188] variation of liquation cracking susceptibility of IN738LC superalloy with energy transfer modes has been studied and conduction mode is found to be more susceptible than keyhole mode. The weld geometry was also found to play an important role in liquation cracking. In the work of Nishimoto et al. on high nitrogen 304 stainless steel, hot cracking susceptibility of conduction mode welds was found to be greater than keyhole welds as nitrogen distribution in welds varies for different modes [18].

Though solidification cracking has been studied extensively, influence of energy transfer modes on hot cracking in pulsed laser welding of fully austenitic stainless steel is not reported much. In this work, effect of heat input and energy transfer modes on solidification cracking of 316 stainless steels has been studied. The weld microstructures and cracking severity are analysed for different energy transfer modes and influence of weld microstructure on solidification cracking is discussed.

4.2 EXPERIMENTAL PROCEDURE

AISI Type 316 stainless steel solidifies in primary austenitic mode as Cr_{eq}/ Ni_{eq} is 1.44 and impurity content (S+P) is 0.052 wt%. Therefore, as discussed in chapter 2, it is prone to solidification cracking predicted by Lienert's weldability diagram for pulsed laser [11].

Table 4-1 Laser pulse parameters used in experiments

Constant parameters:

†Traverse speed (v) - 2.5mm/s,

Spot diameter (d) - 0.8mm, Shielding gas- 99.99 % pure Argon, Flow rate- 10 lpm.

Sl. No	**Peak power, KW (1)**	**Pulse duration, ms (2)**	**Pulse frequency, pps (3)**	**Pulse energy, J (4)= (1) × (2)**	**Mean Power, W (5) = (3) × (4)**	**Heat input, J/mm (6)= (5) / (v†)**
Conduction Mode- Varying pulse duration with constant pulse frequency						
1	0.7	8	15	5.6	84	33.6
2	0.7	16	15	11.2	168	67.2
3	0.7	24	15	16.8	252	100.8
4	0.7	32	15	22.4	336	134.4
Conduction Mode- Varying pulse frequency with constant pulse duration						
5	0.7	8	20	5.6	112	44.8
6	0.7	8	30	5.6	168	67.2
7	0.7	8	40	5.6	224	89.6
8	0.7	8	50	5.6	280	112
Transition/ Penetration Mode						
9	2.5	8	15	20	300	120
10	2	10	16	20	320	128
11	2	10	20	20	400	160
12	1.7	16	16.3	27.2	443.4	177.3
13	2	10	22.5	20	450	180
14	1.9	16	15	30.4	456	182.4
15	2.2	12	17.7	26.4	467.3	186.9
Keyhole Mode						
16	3.5	8	15	28	420	168
17	3	10	15	30	450	180
18	3.5	10	13	35	455	182
19	4	8	15	32	480	192

Pulsed Nd: YAG laser having the mean power capacity of 530 W was used for making bead-on-plate welds in the present study. The welding parameters were selected suitably to acquire conduction, transition/ penetration and keyhole modes. The pulse parameters used in these experiments are listed in Table 4-1.

All the welds were made as overlapping spot welds by keeping overlapping percentage above 70%. Within the conduction mode, two sets of experiments were carried out. In one set, pulse duration was kept constant and frequency was increased and in the other set keeping frequency constant, pulse duration was increased to higher values. Weld surfaces were examined by optical microscope both in unpolished condition and polished and etched condition under high magnification. The weldments were cut and processed for metallography following the standard procedures. The microstructures of the fusion zone were examined by optical microscope and cross-sectional area of the weld metal was estimated using image analysing software. The total crack length of all the cracks in the weld cross section was measured and cracking severity was determined from mean crack length specified as total crack length per unit area. The mean intercellular size in the fusion zone was measured using optical microscope with image analysis software by employing intercept method. In order to understand the mechanisms involved in the cracking, weld microstructure and solidification cracks were observed under scanning electron microscope (SEM). Energy dispersive X- ray spectroscopy (EDS) was used to check for elemental segregation at the cracked interfaces.

4.3 RESULTS

4.3.1 Microstructural analysis of solidification Cracks

The surface profiles of conduction, penetration and keyhole mode welds are shown in Figure 4-1.a, b and c respectively. Variation in cracking severity is observed in conduction and transition modes along the weld length. Although, keyhole mode weld show very minute cracks at weld starting position and crater cracks at end spots, no cracks are ascertained in other regions. The considerable change in cracking severity along weld line is evidently observed in weld macrostructures of transition/ penetration welds taken in weld starting and middle positions. As shown in Figure 4-2 A and B, the cracking severity is reduced when weld moves from starting position (Figure 4-2. A) to steady conditions (Figure 4-2. B), where stable weld geometries are attained. The increase in weld area in steady conditions is due to enhancement in laser energy absorptivity as weld progress. The microstructures of different mode welds are shown in Figure 4-3.a-d. These micrographs represent the microstructures of welds sectioned at stable, middle region of weld line, where weld microstructures are regular. The weld starting and end regions were not used as these regions undergo unbalanced transient conditions.

Conduction and transition welds show cellular morphology growing from fusion boundary towards weld centre with direction of solidification determined by direction of heat conduction and welding (Figure 4-3.a&b). In contrast, keyhole welds show cellular-dendritic microstructure near the fusion boundary similar to those observed in the conduction and transition mode welds, but at the centre of the welds directionality of the solidification is absent and the microstructure appears to be equiaxed grains (Figure 4-3.c). In order to verify this, microstructure of the surface of fusion zone produced by keyhole mode was examined along the length of the weld and this is shown in Figure 4-3.d. It is clear that even at the centre of the fusion zone, mode of solidification is cellular-dendritic; but the direction of solidification is parallel to the welding direction and almost perpendicular to cellular-dendritic microstructure growing from the fusion boundary. From the cellular boundary microstructure aall the welds are observed to solidify in primary austenitic mode.

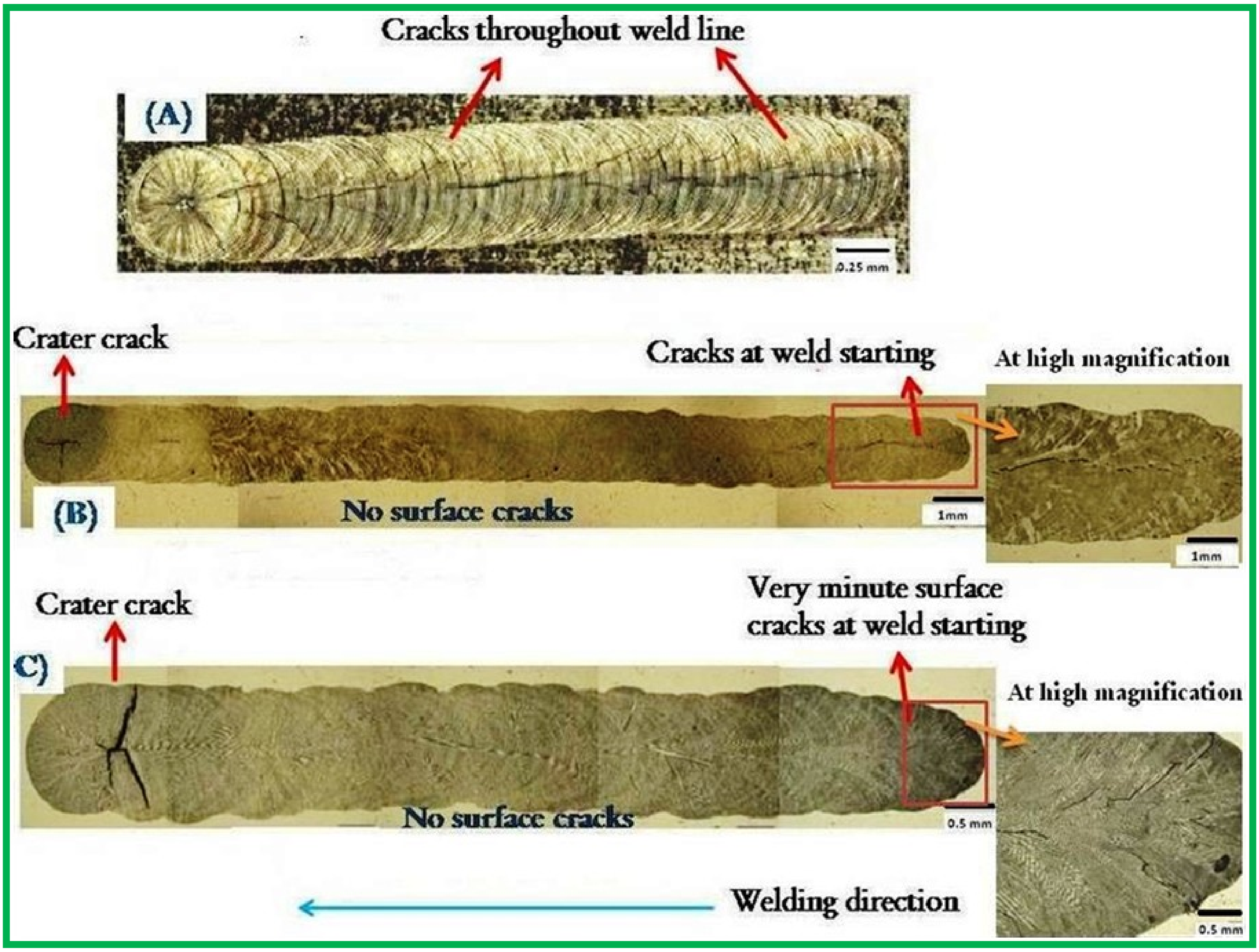

Figure 4-1 Microstructures of surface profiles of a) conduction, b) transition/ penetration and c) keyhole mode welds

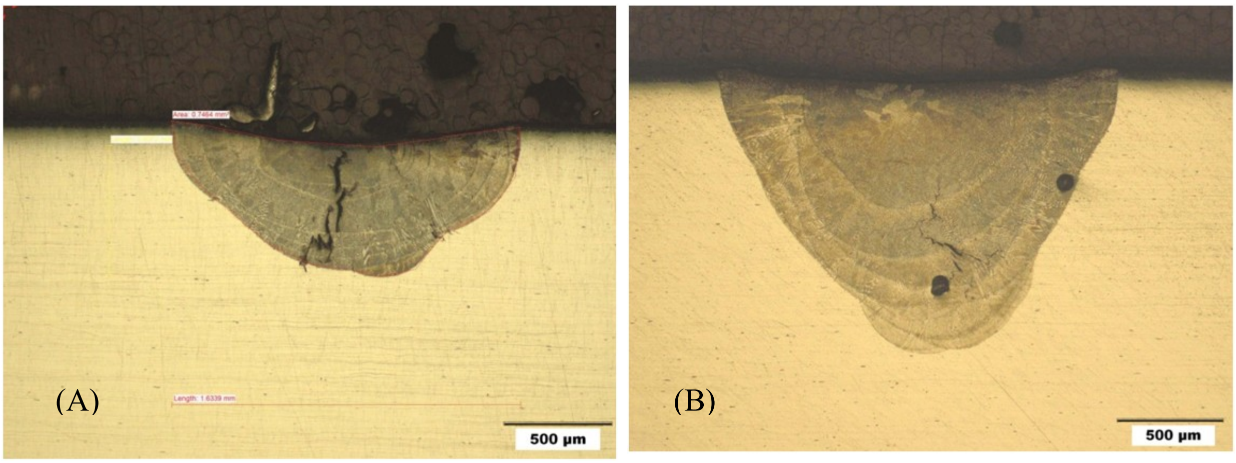

Figure 4-2 Changeover in geometry and cracking severity along weld line in transition/ penetration welds A) At starting position, B) At 'steady condition'

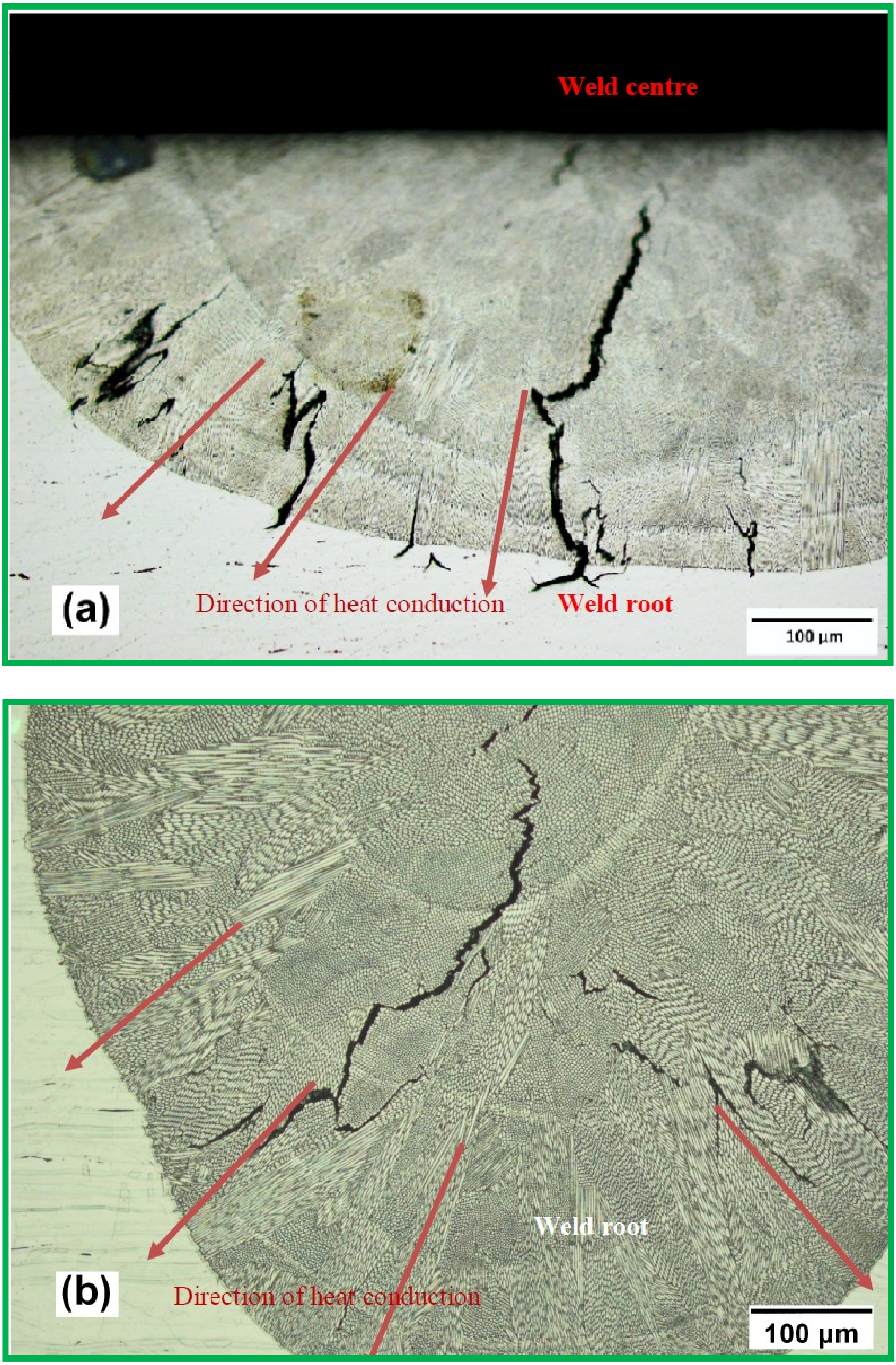
Weld centre
(a)
Direction of heat conduction
Weld root
100 µm
(b)
Direction of heat conduction
Weld root
100 µm

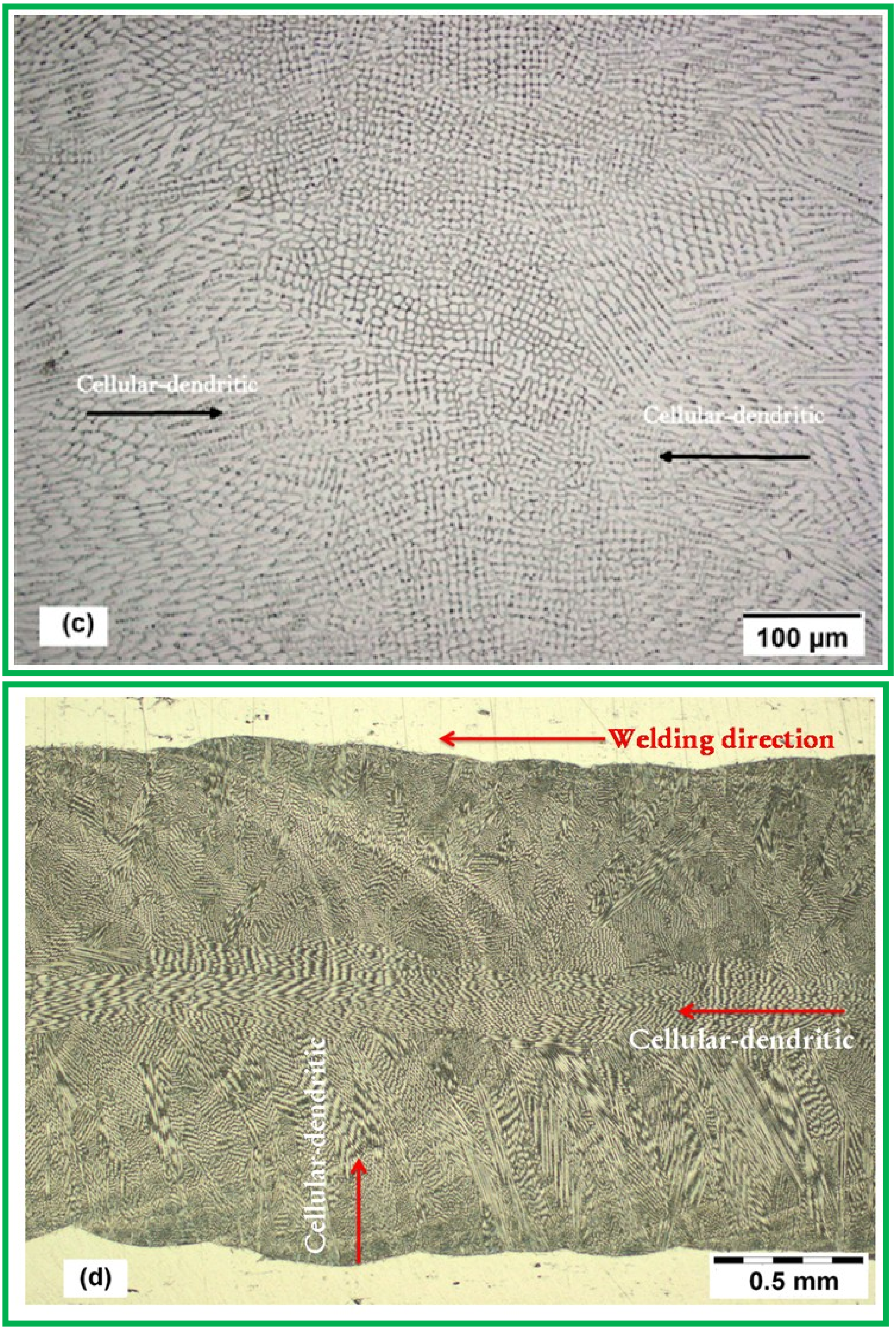

Figure 4-3 Microstructures of weld cross sections at root sides of a) Conduction, b) Transition, c) Keyhole modes d) Microstructure along the length of the weld for keyhole weld surface

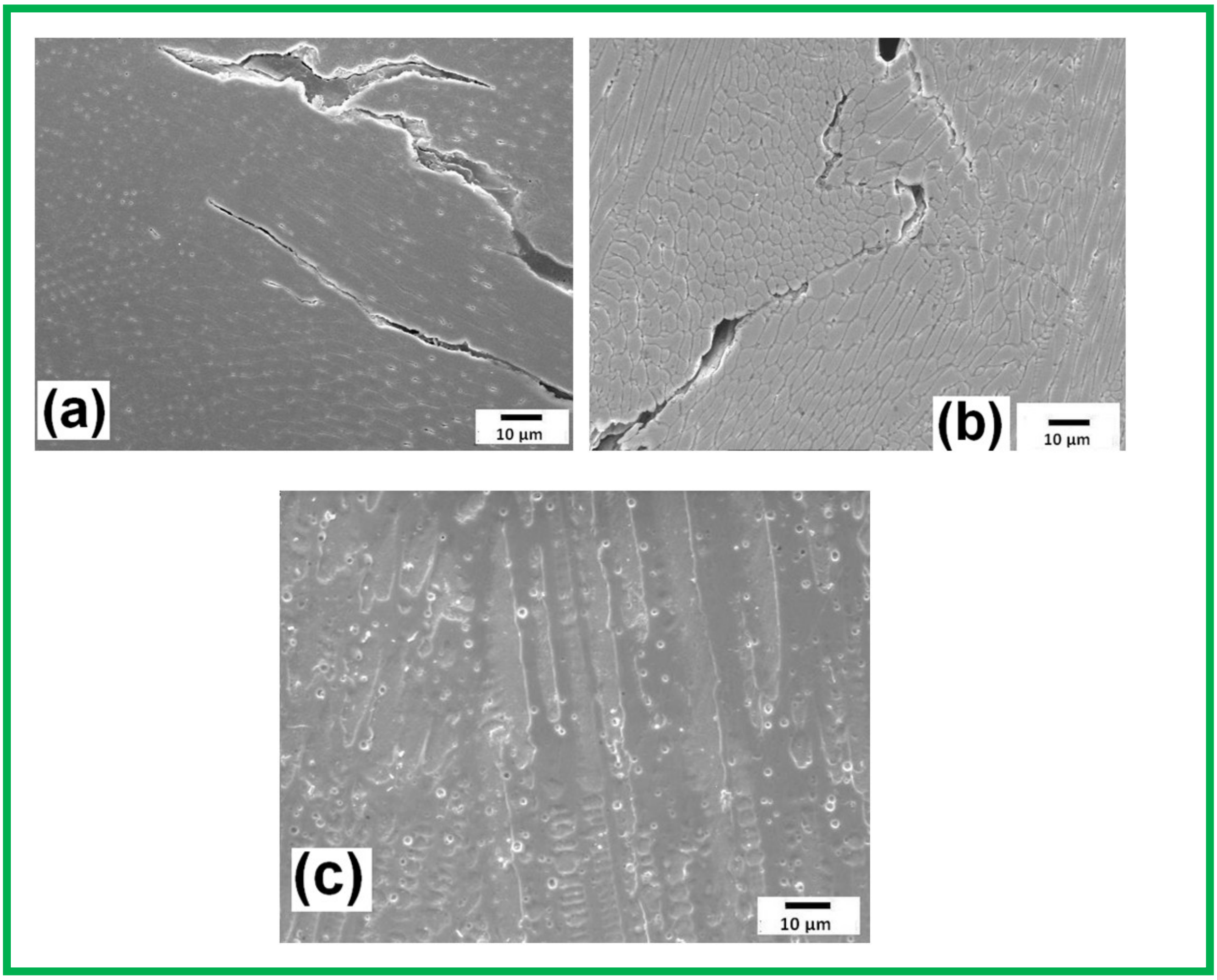

Figure 4-4 SEM microstructures of a) conduction, b) transition and c) Keyhole mode welds sectioned at root side of weld

The absence of δ-ferrite is also established by ferritescope measurements irrespective of energy transfer modes. While conduction weld shows severe cracking and penetration weld shows cracking mainly at root side, keyhole welds were found to be free from cracking.

With the purpose of understanding solidification cracking phenomenon, microstructural studies were made under scanning electron microscope (SEM). Cross-sectional SEM images of different modes are shown Figure 4-4.a-c. It is observed that crack width is more in conduction than penetration welds and intercellular spacing is decreasing from conduction to keyhole welds. No evidence of alloy or impurity segregation across the crack filled region was observed in line-EDS analysis as shown in Figure 4-5.

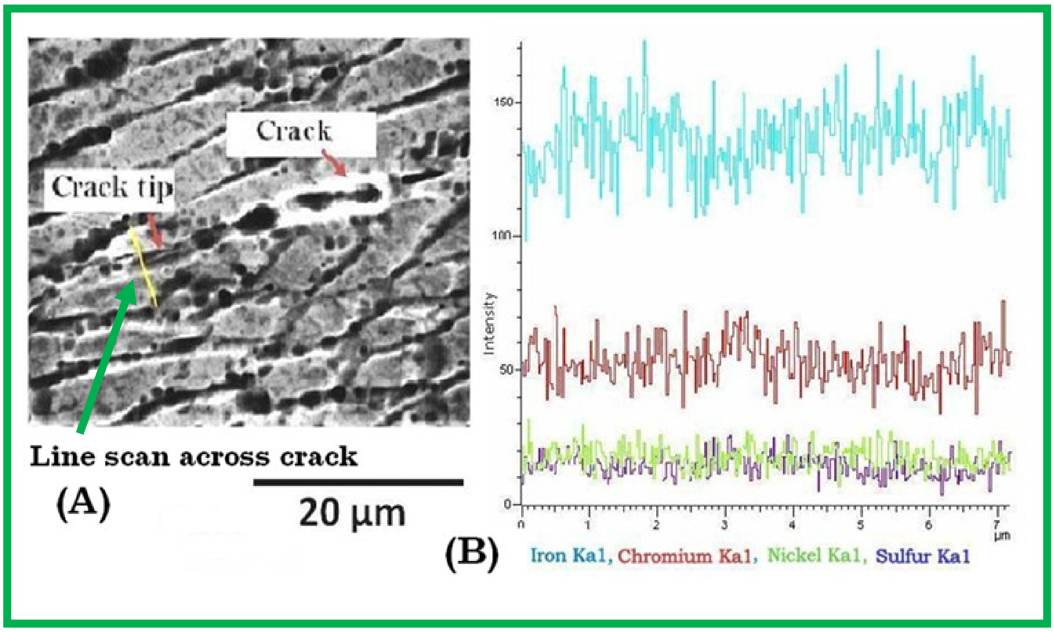

Figure 4-5 A) Micrograph depicting SEM-EDS line scan across crack filled region, B) Line scan- No segregation across crack

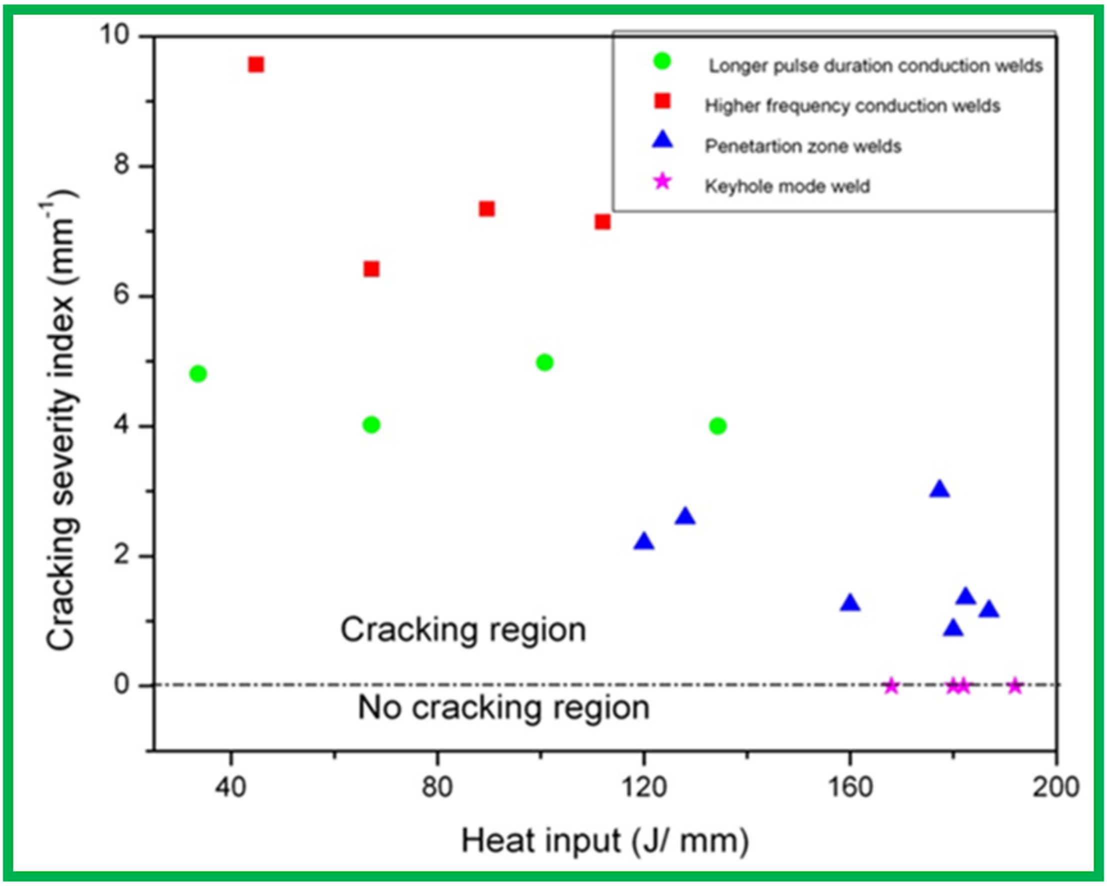

Figure 4-6 Effect of heat input and energy transfer modes on cracking severity

The cracking severity index was determined by total crack length per unit weld area. The plot of heat input versus this index is plotted in Figure 4-6. Since different modes produce welds with varying geometry, cracking severity was determined as total crack length per unit cross-sectional area of the fusion zone. Figure 4-6 clearly shows that, as the heat input increases, cracking tendency reduces. However, at the same heat input condition, cracking severity is influenced by mode of energy transfer. The cooling rates achieved in different energy transfer mode welds were estimated by the relationship between mean intercellular spacing and cooling rate given by Katayama et al [25]. This relation is given as $\lambda=80\Delta T^{-0.33}$, where λ- primary arm spacing given or mean inter cellular size in µm and ΔT- cooling rate in K/s.

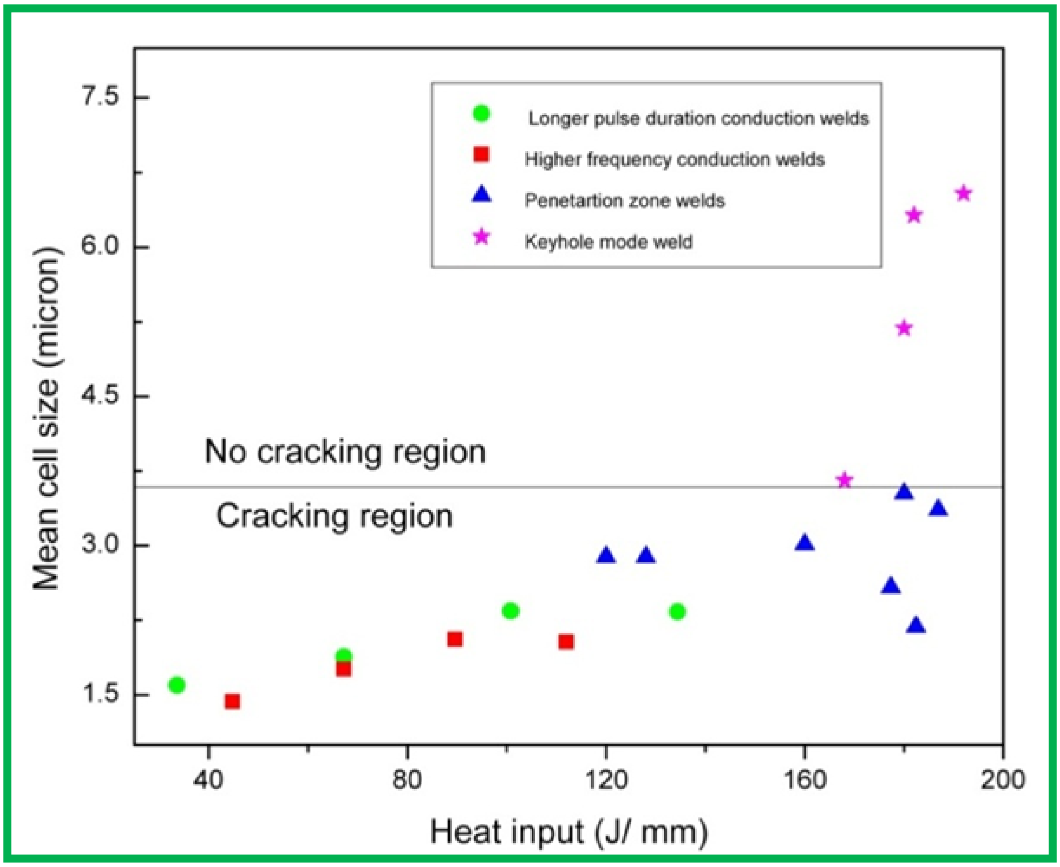

Figure 4-7 Effect of heat input and energy transfer modes on mean cell size

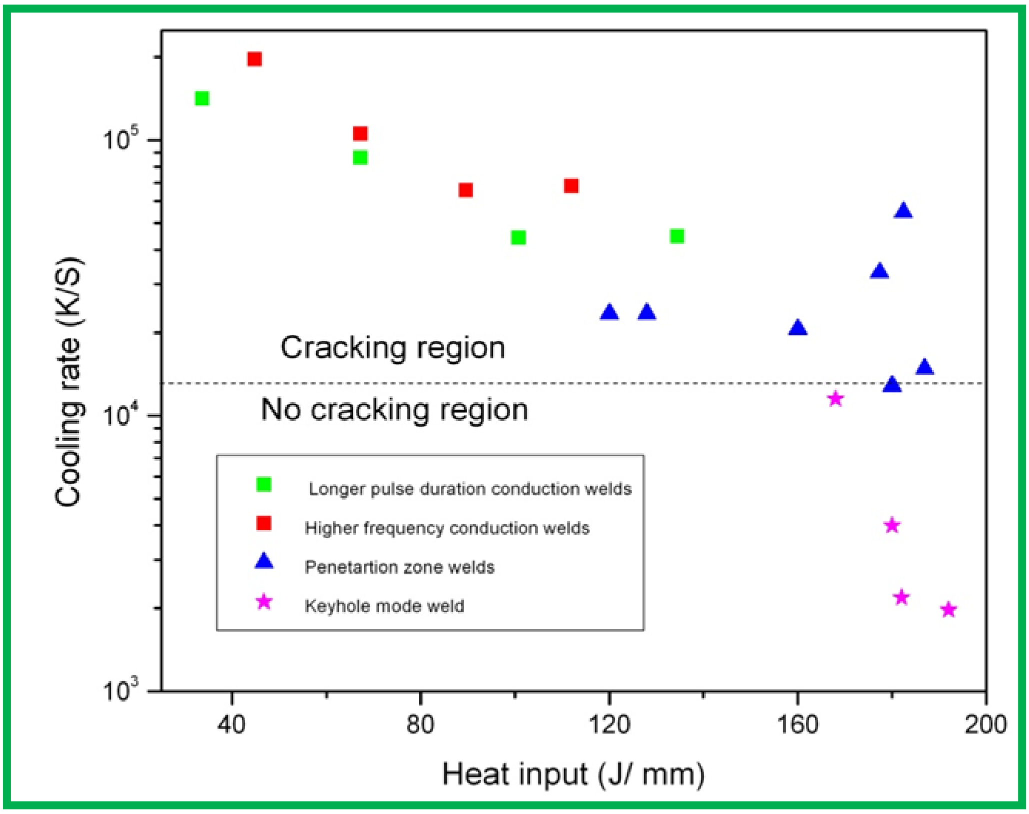

Figure 4-8 Effect of heat input on cooling rate achieved in welds of different energy transfer modes

The intercellular spacing was measured on the cross sectional microstructure of the welds on the cellular and cellular- dendrites growing from fusion line. Since weld centre was found to have different morphologies for different welds as seen in Figure 4-3. a-c, measurements were not made at weld centre. The data measured throughout weld pool except weld centre does not reveal much scatter due to low thickness of workpiece plate. Though, this method of cooling rate determination is indirect, the obtained results are consistent with literature[189, 190]. The measurement of intercellular spacing was made in all the weld samples. Two weld cross-section samples were used to prove consistency in cooling rates. Since the scatter in the measurement was considerably very little, the average values have been used. The relation between heat input and intercellular spacing (λ) is given in Figure 4-7. The calculated cooling rate from mean cell spacing is plotted against heat input in Figure 4-8. As the cooling rate reduces, cracking severity reduces and below certain threshold value, cracking does not occur.

4.4 DISCUSSION

4.4.1 Effect of energy transfer modes on solidification cracking

In the present study, solidification cracks were found to be influenced by nature of energy transfer mode, heat input and weld geometry as stated in section 4.3.1. Solidification cracks are caused by both metallurgical and mechanical factors. The low melting eutectics formed by impurity elements are segregated into solidification boundaries leading to formation of cracks at terminal stage of solidification due to the induced strain. The factors like thermal contraction stresses, solidification shrinkage stresses and mechanical clamping stresses cause strain in solidifying weld pool [9]. In this study, segregation of impurities was not observed in SEM-EDS analysis of crack surfaces (Figure 4-5).

In the case of conduction mode welds, surface cracks are observed throughout weld line, as shown in Figure 4-1.a. But in penetration welds, solidification cracks are observed only in weld starting position (Figure 4-2.A). In conduction mode weld, solidification is completed within a few milliseconds of laser material interaction [177, 179, 190]. It implies that each spot is not affected by previous pulse and the circular shape of single spot is maintained. Also, depth of penetration in conduction mode weld does not vary as weld advances, indicating no increase in laser energy absorption along the weld line. Since the solidification is completed in the interval of consecutive pulses, the temperature gradient between the peak temperature and the material's surface temperature ($\Delta T = T_{Peak} - T_{surface}$) is very high resulting in high levels of solidification shrinkage stresses, sufficient to produce cracks. Since the temperature gradient at solid/ liquid interface, 'G' remains more or less unchanged along the weld centreline, surface cracks continue till the last spot.

Higher peak power pulses than those used in conduction mode are used to attain penetration mode, but during initial pulses, the material surface is not heated up instantaneously. Hence, energy absorbed at the initial stages of bead-on-plate welding is less. Therefore, in this part of the weld, the weld pool solidifies like conduction mode welds and the consequent higher temperature gradient leads to cracking during initial pulses (Figure 4-2.A). But, after a few initial pulses, significant keyhole formation occurs due to the increase in surface temperature and absorptivity. In view of this, temperature gradient decreases along the weld line and hence the centre line cracks formed in the initial stages of welding do not propagate till the end of weld. Further, as the weld moves along weld line, the decrease in cooling rate is observed through widening of inter-cellular spacing. However, cracks are observed at root side of weld cross-section as shown in Figure 4-2.B. The combined action of faster cooling rates encountered at root side of laser weld and the larger strain exerted in root side due to its narrow geometry make the penetration welds crack at root side [191]. In keyhole mode, very fine surface cracks are observed only on the initial few spots and no more cracks are seen along the weld line (Figure 4-1.c). At the end of weld spot, crater cracking is observed as thermal stresses are induced abruptly due to the sudden increase in temperature gradient and consequent solidification shrinkage stresses when the laser pulse is terminated at the final location.

4.4.2 Effect of heat input on solidification cracking

In this study, it is observed that as the heat input applied on the material surface increases, cracking severity reduces as shown in Figure 4-6. Corresponding to the increase in heat input, cooling rate encountered in weld pool reduces as observed from Figure 4-8. The direct influence of cooling rate on solidification cracking is apparently shown in Figure 4-6 and Figure 4-8, where both graphs show very similar trend. In the present experimental conditions, as the heat input increases, cooling rate and temperature gradient decrease. Conduction welds produced with longer pulse duration are less severe in cracking than conduction welds produced with higher frequency pulses. This is due to the reduction in temperature gradient (G) and resultant decrease in solidification shrinkage strain exerted in weld pool when pulse duration is kept longer. Since pulse-off time is not reduced significantly, increase in pulse frequency does not show improvement in hot cracking of conduction mode welds. Cracking severity reduces significantly once the mode changes from conduction to penetration.

For the same heat input applied, pulse parameters can be chosen appropriately to produce welds of different modes. At the same heat input condition, cracking in conduction welds is more severe than penetration welds because cooling rate is more in the former than in the latter. The higher cooling rate and susceptible weld geometry make penetration welds crack at root side of weld bead while surface cracks are eliminated. As observed from penetration mode weld geometry in Figure 4-3.b, heat extraction occurs in all the directions and results in high induced strains leading to cracking. The fact that the cracks observed in both conduction and penetration mode welds are in the direction of heat transfer demonstrates the influence of solidification induced strain on cracking. On the other hand, in keyhole welds, (Figure 4-3.c) heat is extracted in two dimensions; hence cooling rate is low and thus strains induced in the fusion zone during solidification is correspondingly reduced.

It can be considered that high heat input during welding can promote segregation, increase the width of the partially melted zone (mushy zone) and introduce large thermal stresses [187, 192] and thus promote cracking. These are true for arc welding in which heat input is of the order of several kJ/mm and there will be substantial heating of the adjacent base metal resulting in slow cooling of the weld metal during solidification promoting segregation of the alloying elements in the fusion zone. For laser welds made in the present study, heat input is significantly lower than that experienced in a typical arc welds (one order of magnitude lower, Table 4-1) and hence, in the entire range of heat input employed in the present study, the cooling rate is too high to cause any effective segregation of the impurity elements that promote cracking. This is supported by the fact that there is no evidence of segregation at the crack location in the SEM-EDS analysis shown in Figure 4-5. The solidification cracking can be attributed to variation in microstructures with energy transfer modes. Conduction mode welds have cellular microstructure throughout the weld geometry and are found to have highest cracking severity due to high cooling rates encountered inside weld pool. The fine cellular structure oriented in heat flow direction does not capable to withstand high thermal and solidification shrinkage strains. As shown in Figure 4-1, keyhole weld also is observed to have cracks at weld starting and ending regimes, where, cellular- dendritic grains are oriented similar to conduction welds. The microstructure of crack free keyhole weld has wider cellular-dendritic grains with two distinct directions of solidification; one opposite to the direction of heat removal and another parallel to the direction of solidification. This microstructure appears to accommodate the stresses generated during solidification and subsequent cooling. Further, the reduced solidification shrinkage and thermal strains due to low cooling rate also facilitate in achieving crack free welds. Since the keyhole formation in transition weld is unstable, heat transfer through conduction phenomenon prevails which leads to high cooling rate. Thus transition welds are found to have cracks at root side of weld bead. The threshold cooling rate for achieving crack free welds is found to be about 10^4 K/s. The achieved cooling rate inside weld pool is dictated by both heat input and mode of energy transfer.

4.5 CONCLUSIONS

- Solidification cracking in pulsed laser welds of austenitic stainless steel is influenced by both heat input and energy transfer modes which affect the cooling rate and strain induced in weld pool.
- While keyhole mode weld is free from cracking, conduction welds have severe cracking throughout weld bead, and penetration welds show cracks only at root side of weld.
- Conduction welds produced with pulses of longer durations are less severe for cracking than conduction welds with higher pulse frequencies.
- As heat input increases and energy transfer mode changes from conduction to keyhole modes, cooling rate decreases.
- In the entire range of heat input employed in the present study, the cooling rate is too high to cause any effective segregation of the impurity elements that promote cracking.
- The subsequent reduction in shrinkage strain due to low thermal gradient and also the presence of cellular-dendritic microstructure parallel to the weld direction reduce the susceptibility of cracking in keyhole mode welds.
- Crack free welds are obtained when the cooling rate of the weld pool during solidification is lower than 10^4 K/s.

The work presented in this chapter is discussed in [193].

CHAPTER 5 STUDIES ON PULSED LASER-GTA HYBRID WELDING 5

5.1 INTRODUCTION

As mentioned in literature survey in chapter 1, Laser- arc hybrid welding is an advanced welding process where both laser and electric arc heat sources are coupled together and applied on common molten zone to achieve synergistic advantages and eliminate drawbacks of individual processes [104, 105, 113]. After the first hybrid welding experiment of W.M. Steen in 1980, much research works have been carried out on this process [105]. Few applications of laser-arc hybrid welding have also been reported in the fields of automotive, ship building etc. [103, 107-112]. Different combinations of laser and arc heat sources have been employed in hybrid welding experiments [102]. While several works have been carried out using high power lasers as primary heat source, low power lasers also have been used in few experiments [19, 194, 195]. Improved arc stability, increased welding speed and enhanced melting efficiency through facilitation of keyhole formation have been observed in these studies [20, 21, 40, 196].

Few studies have also been made on pulsed laser-arc hybrid welding where pulsed laser and electric arc were used as heat sources [135, 197]. Laser pulse shaping in hybrid welding was observed to influence weld geometry with increase in depth of penetration [135]. A. V. Birdeanua et al. studied hybrid welding by combining pulsed laser with pulsed-TIG for micro welding applications and the flexibility of varying pulse parameters for achieving welds with varying geometries was indicated [197].

Although pulsed laser-arc hybrid welding process promises advantages as mentioned, very limited works have been reported in literature. Also, the preliminary experiments carried out so far have not analysed the microstructural and mechanical aspects of welds and which is essential for employing this process in real applications. In the present work, pulsed laser hybrid welding (Laser arc coupled with GTA arc) experiments have been carried out on AISI 316 austenitic stainless steel sheet, which is widely used material in many fields including critical areas like nuclear, high temperature and cryogenic applications. The interaction of laser and arc in conduction and keyhole modes of energy transfer have been analysed and the hybrid parameters such as power ratio (power of laser to arc), inter heat source distance, heat source position, defocusing distance have been studied. Further the microstructural and mechanical properties of pulsed laser- GTA hybrid welds are compared with pulsed laser and GTA welds.

5.2 EXPERIMENTAL PROCEDURES

The experiments were carried out with the hybrid welding set up developed in our laboratory, discussed in chapter 2. The influence of process parameters such as power ratio (laser power to arc power), heat source position, inter heat source distance, defocusing distance on weld geometry have been studied. In order to understand the influence of energy transfer mechanism on hybrid welding, conduction and keyhole mode hybrid welds were made. Laser and arc parameters were chosen appropriately to achieve conduction and keyhole mode hybrid welds. Laser pulses with lower peak power were used for conduction limited welds producing partial penetration welds. Higher peak power pulses were used to produce keyhole mode welds. The range of parameters used in this study is given in Table 5-1. Experiments were video graphed by high resolution camera and the images were analysed for arc and laser plasma interactions.

Table 5-1 Range of hybrid welding parameters studied in experiments

Heat source	Parameters	Values
Laser	Peak power, KW	0.7 to 4
	Pulse duration, ms	8
	Pulse frequency, pps	15-20
	Focus position, mm	-4, -2, 0, 3, 4
	Pulse energy, J	10.5 -32
	Average power, W	100-300
GTAW arc	Current, A	40, 50
	Voltage, V	10-12
	Electrode arc gap, mm	1
Others	Shielding gas	Argon with 99.99 % purity
	Flow rate, lpm	8
	Traverse speed, mm/s	2.5
	Inter heat source distance, mm	2.5
	Torch angle, °	60

The plates of thickness 3.3 mm were used for all the experiments except for defocusing studies, where 4 mm thick plates were utilized. The presence of δ-ferrite in welds was examined by 'Fischer' ferritescope and is expressed as ferrite number (FN). Welded samples were cut, ground and polished for microstructural studies by following standard procedures of metallography. Samples were etched by electrolytic etching with 10% Oxalic acid solution. Welds were examined under optical microscopy and macro and microstructures of weld surface and cross sections were studied. X- ray diffraction (XRD) system with Chromium K_{β} of wavelength 2.0848 Å was used to measure residual stresses developed in welds of hybrid, laser and GTA welding processes. The direction and magnitude of shift in diffraction peak position determines nature (either tensile or compression) and quantity of residual stresses respectively [164]. The longitudinal stresses were measured by moving the back reflection type goniometer along welding direction. Tensile tests were performed by computer controlled electromechanical, universal testing machine with capacity of 250 KN.

5.3 RESULTS AND DISCUSSION

5.3.1 Energy transfer modes in Pulsed Laser- GTA Hybrid Welding Process

Similar to pulsed laser seam welding, hybrid welding was also carried out in different modes of energy transfer by selection of appropriate process parameters. The interaction of laser and arc heat sources influences laser-material interaction phenomena and can determine the transition of modes. The formation of keyhole and its stability can be enhanced by additional arc. In the present study, conduction and keyhole mode hybrid welds have been made and analysed.

5.3.1.1 Conduction mode hybrid welding (CMHW)

Few welds were made on conduction mode and their surface and cross section profiles are shown with laser weld in Figure 5-1.a-d. As discussed in chapter 4, laser welds exhibit centre line solidification cracks (Figure 5-1.a, b), which occur due to the presence of impurities such as S and P and their tendency to form low melting eutectics during solidification. But, conduction mode hybrid welds does not show solidification cracks in their surface and cross section macrostructures (Figure 5-1.c, d). It can be reasoned that the applied heat input is more than laser and so cooling rates encountered inside the weld pool is reduced. This can be affirmed from coarse cellular-dendritic grains extending from fusion boundary to weld centre. Though addition of arc increases the heat input and widen weld bead, low amperage arc can be used to obtain crack free welds. In addition to that, the enhancement of keyhole formation is observed as the aspect ratio of these welds was observed to raise upto 1. From the surface of weld, it can be understood that hybrid weld has finest weld ripples than laser welding alone. These finest ripples could be due to higher frequency of re-melting in hybrid welding than laser welding. This causes reduced segregation hence the complete absence of solidification cracks.

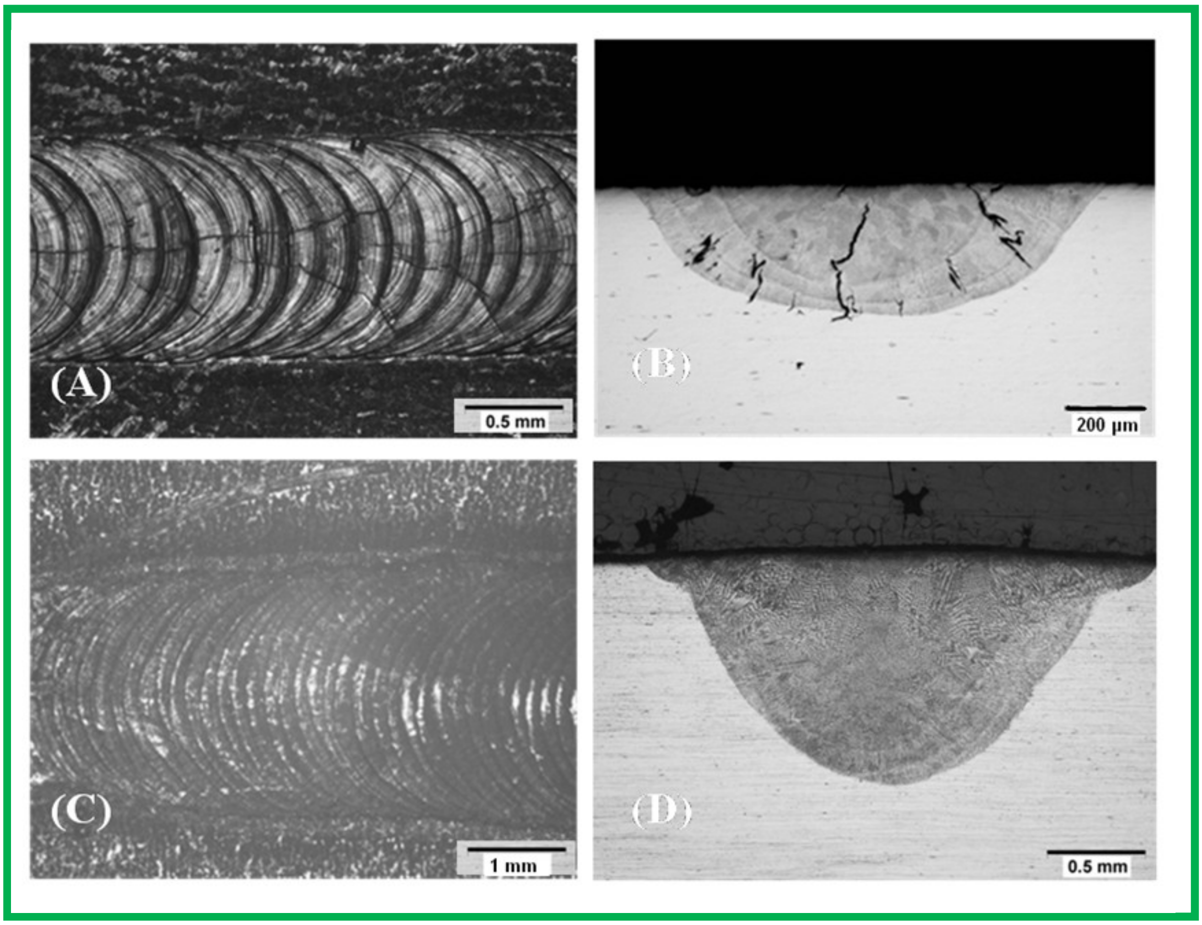

Figure 5-1 Macrostructures of conduction mode pulsed laser and hybrid welds
Pulsed laser weld- A) surface, B) cross section, Hybrid weld- C) surface, D) cross section
Laser parameter- Peak power- 1.25KW, Pulse duration- 8ms, Pulse frequency- 15pps,
Arc parameters- Current- 50A, Voltage- 9.5V, Traverse speed- 2.5mm/s

5.3.1.2 Keyhole mode hybrid welding (KMHW)

Pulsed laser hybrid welds performed in keyhole mode of operation clearly shows synergistic effect of laser-arc interaction. The macrostructures of laser, GTA and hybrid welds are shown in Figure 5-2 a, b and c. From the weld geometries, it is evident that when

Figure 5-2 Macrostructures of (a) GTAW, (b) Laser, and (c) Hybrid welds indicating synergistic effect at keyhole mode (Laser -300W, GTAW- 30A current, D_{LA}- 2.5mm, and arc leading position)

GTAW arc is adjoined to pulsed laser, depth of penetration, aspect ratio and melt area of welds are improved significantly. It is also observed that keyhole mode hybrid welds have characteristic weld profile as seen in Figure 5-2.c. It shows two distinct regions: wide top and narrow bottom zones. As both laser and arc are applied on top side, wider weld beads are observed due to increased heat input. At root side of hybrid weld, laser beam passes through the thickness and yields narrow welds. About 100% increase in depth of penetration is observed when GTA arc is coupled with laser. It shows that laser energy is efficiently absorbed and utilized from laser-arc interaction. The interaction of arc on the laser acting molten pool influences keyhole dynamics and molten pool flow which in turn determines weld geometry and quality. Higher depth of penetration is achieved when keyhole formation is facilitated and molten pool flow is inward.

Despite having better aspect ratio, keyhole mode in pulsed laser welding encounters problems such as spattering, undercut, porosity and uneven top surfaces due to complex keyhole dynamics and associated molten pool flow mechanisms. Similarly, porosity is formed due to the bubble formation in molten pool at root side of keyhole where the cooling rate to be high. Hybrid welds are found to have better surface quality than laser welds. The hybrid weld surface profile is smooth, even and free from spattering and undercut. Further, solidification cracks are not observed throughout the thickness due to increase in heat input and reduction in cooling rate. The shallower temperature gradient and slower solidification rate make hybrid welds free from hot cracks. The wider weld bead formation in hybrid weld appears to enhance the tolerance in fit-up gap before welding.

5.3.2 Interaction of pulsed laser-GTAW arc in keyhole mode hybrid welding

The solidification of molten pool in keyhole mode weld is quite different from conduction welds due to its complex keyhole dynamics and molten pool flow. Further, the interaction of GTAW arc with laser, complicate the hybrid welding process and influence the weld geometry, microstructures and its mechanical properties. In hybrid process, the interaction of laser induced plasma and arc plasma above the material surface is crucial as it determines hybrid phenomena of arc rooting and arc constriction etc [19]. In the Figure 5-3, video-graphed images of hybrid experiments are incorporated in schematic of laser pulses. As shown in Figure 5-3 (a), arc plasma is present when GTAW alone is switched ‘on’. When the laser pulse is activated, the laser induced plasma formation occurs instantaneously as shown Figure 5-3 (b). Above the material surface, the laser induced plasma and arc plasma interact at this pulse ‘on’ time. Once the laser pulse is turned ‘off’, the plasma generated by laser is blew out as seen in Figure 5-3 (c). This pulsed interaction influences the microstructures and mechanical properties of the welds. In this study, the microstructures and mechanical properties of pulsed laser hybrid welds are compared with pulsed laser and GTA welds and the variations are explained on the basis of interaction of heat sources.

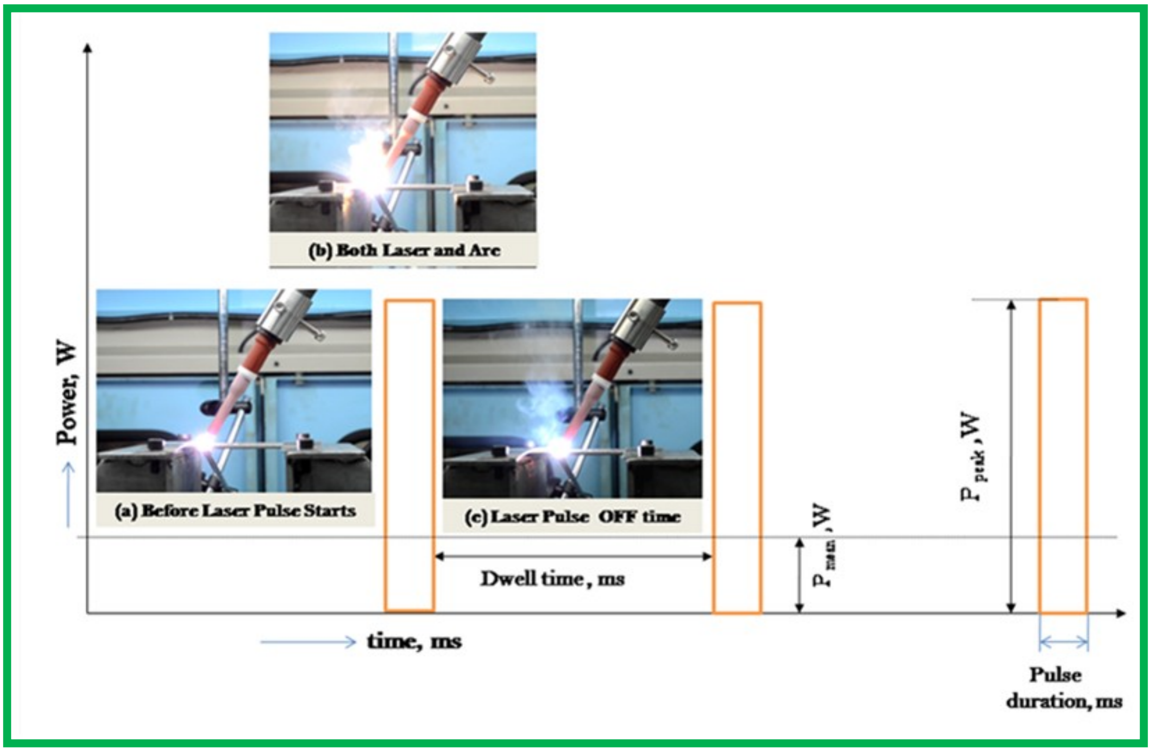

Figure 5-3 Schematic of Pulsed laser- GTA hybrid welding (a) Arc only acting before laser started (b) Both laser and arc plasma interact at laser pulse ON (c) Laser plasma extinguishes in laser pulse OFF time

5.4 POSITION AND DISTANCE BETWEEN HEAT SOURCES

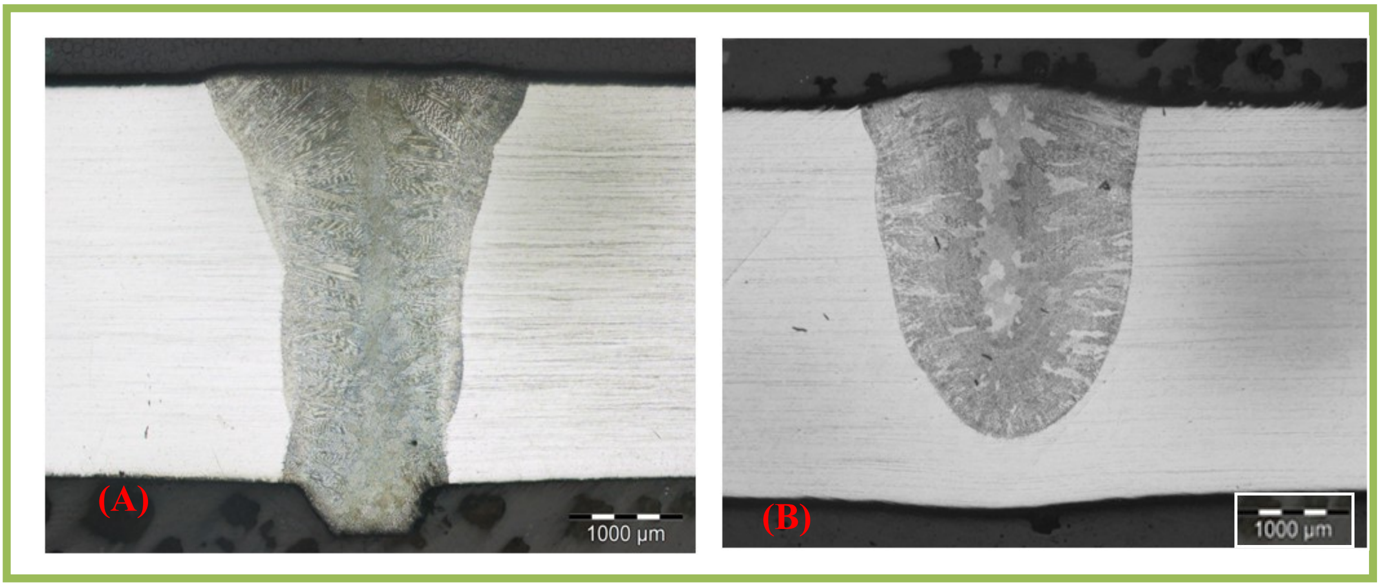

Figure 5-4 Macrostructures of A) Arc leading & B) Laser leading hybrid welds at same process parameters

Laser parameter: Peak power- 2.5 KW, Pulse duration- 8 ms, Pulse frequency- 15 pps,
Arc parameters: Current- 40 A, Voltage- 9.9 V, Traverse speed- 2.5mm/s

Heat source position is an important process parameter in hybrid welding as discussed in chapter 1. The macrostructures of arc and laser leading hybrid weld beads (ALHW& LLHW) at same process parameters are given in Figure 5-4.a and b. In ALHW, the top portion is wide where both laser and arc heat sources are applied and at the bottom side, the bead contour is similar to laser alone. It indicates that when laser and arc heat sources are coupled, the ability of laser beam to penetrate deeper is improved. At this position, the laser energy is applied on the molten pool created by GTAW arc which enhances laser energy absorptivity and results in large melt area and deeper penetration welds. Achieving deeper penetration welds is determined by efficient absorption of incident laser light and its utilization for joining. In keyhole mode welding, though high peak powers are used, the weld bead is kept in 'laser pulse off' stage for most of the time. For example, in pulsed welding with pulse duration of 8ms and frequency 15 pulses per second, pulse 'off' time is around 60ms. Due to the precise, intense heat applied by laser beam, welds tend to solidify rapidly. When the succeeding laser pulse is interacting on partially or fully solidified material surface, laser energy absorptivity is reduced. But, when GTAW arc is leading the laser beam in ALHW condition, the laser beam is indeed employed on the molten pool formed by GTAW arc. It can be clearly perceived from the images of hybrid welding process shown in Figure 5-5.a& b. As shown in Figure 5-5.a, when laser pulse act on the material, laser plasma interacts with arc plasma above the material surface and molten pool is sustained. This molten pool is observed to persist even at laser pulse off time as shown in Figure 5-5.b (the bottom side of workpiece plate). It facilitates the formation of keyhole and enhances laser light absorptivity and results in increased depth of penetration.

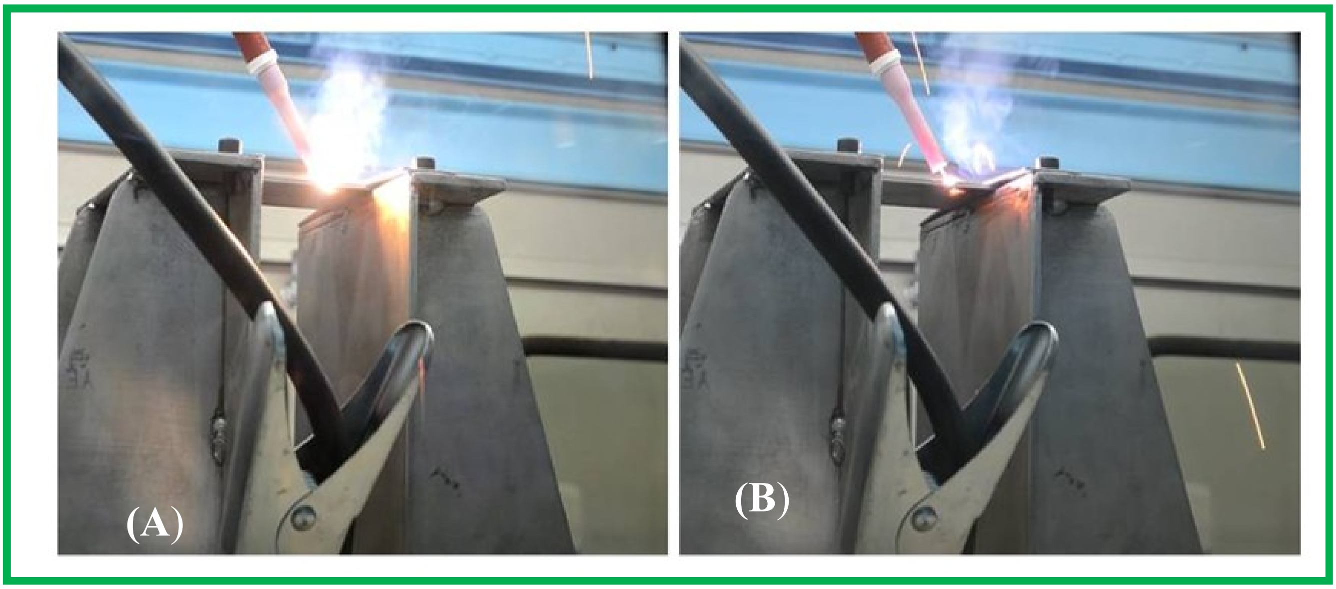

Figure 5-5 Images of laser-arc interaction A) Laser and arc plasmas interaction during pulse ON time, B) Maintenance of molten pool during laser pulse OFF time

In case of LLHW, improvement in depth of penetration and aspect ratio is observed but the development is not as much of arc leading position as seen in Figure 5-4.b. Due to the interaction of laser and arc plasmas, the preceding laser tends to constrict the succeeding

GTAW arc. In laser leading position, the weld pool created by laser beam solidifies rapidly. Therefore increasing laser energy absorptivity through preheating effect is not predominant. The weld geometry appeared in Figure 5-4.b indicates action of combined heat source throughout weld and possible arc constriction. This phenomenon occurs as the arc plasma tends to travel in least resistance path made by the dense laser plasma. The surface profile of LLHW is much smoother and width of the weld bead is also smaller than that of ALHW.

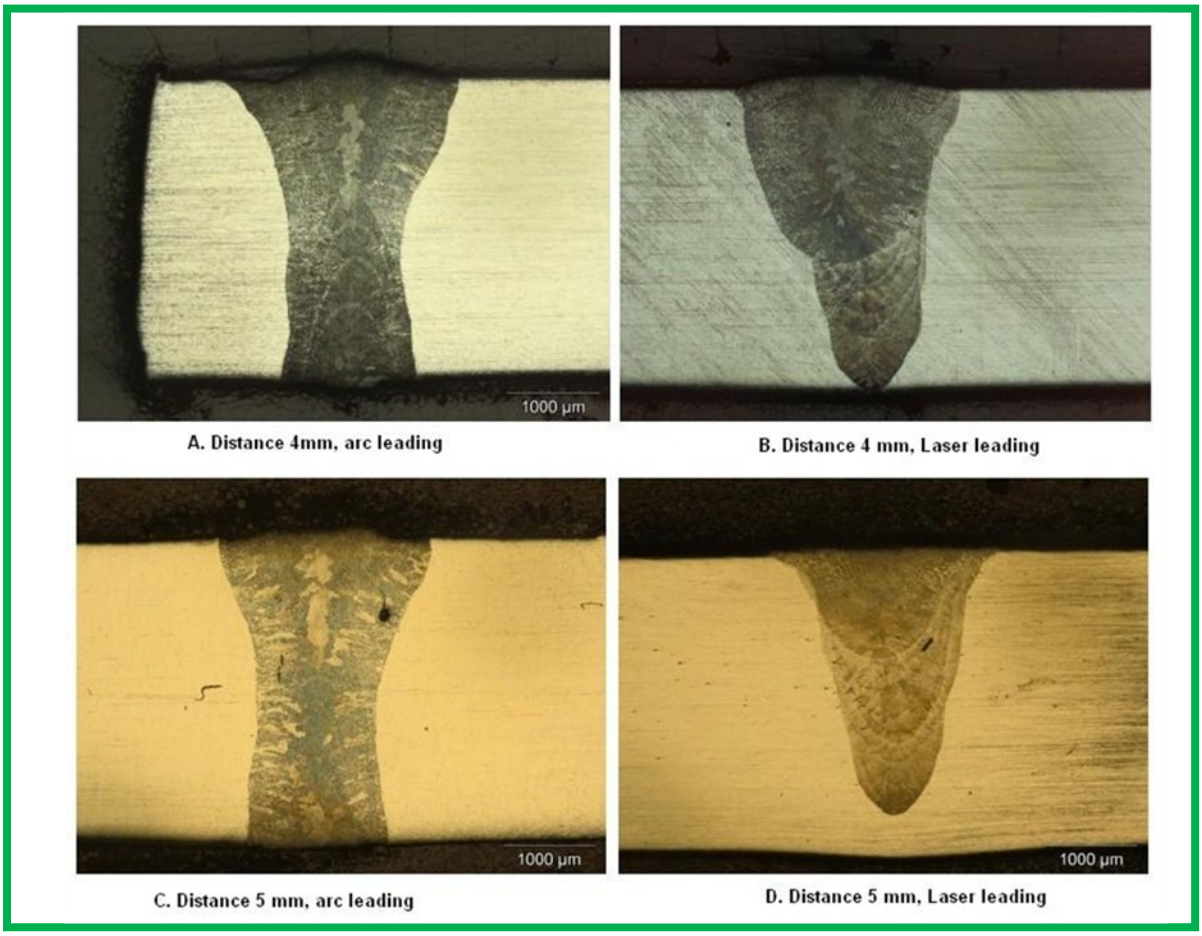

Figure 5-6 Macrostructures of arc and laser leading welds at inter heat source distances of 4 and 5 mm

Laser parameter- Peak power- 2.8 KW, Pulse duration- 10 ms, Pulse frequency- 15 pps, Arc parameters- Current- 30 A, Traverse speed- 3 mm/s

When laser and arc heat sources are kept closer, i.e. inter heat source distance lower than 2 mm, hybrid welds at both heat source positions do not show much difference in their weld geometries. At this condition, both laser and arc heat sources are acting on common point resulting in coupled heat source which is not influenced by heat source position. While laser and arc are separated more than 3 mm in keyhole mode of operation, variation in weld geometries of ALHW and LLHW positions is observed.

As ALHW retains characteristic hybrid weld contour (Figure 5-6.a and c), LLHW transforms similar to that of laser welds in their geometry and microstructures as shown in Figure 5-6.c & d. Further, macrostructure of LLHW shows distinct laser and arc solidified regions. As laser leads GTA arc, due to its nature of intense heat input, laser melted region solidifies rapidly followed by arc melting, which forms separate solidification zones as seen in Figure 5-6. b. Also the asymmetric form of laser and arc melted regions suggest weakening effect of arc rooting action towards laser acting zone with distancing of heat sources. Solidification cracks are observed at root side of these welds due to their rapid cooling rates and consequent development of thermal stresses.

5.5 EFFECT OF DEFOCUSING ON WELD GEOMETRY

Focal position is a vital process parameter in laser welding as it influences power density of the laser beam. When laser beam is focused on material surface, highest power density is achieved at this position. Defocusing the laser beam above (positive) or below (negative) the material surface decreases the power density. But, it is also practiced for attaining specific advantages like widening beam spot area, reducing spattering etc. The general recommendation to make deeper welds is keeping laser beam focused on surface (0 mm position) [6, 198]. But with respect to material, laser power and workpiece thickness, maximum penetration depth is observed at other focusing positions also. While few results show maximum penetration depth at focusing on surface, some other experiments provide evidence of deeper penetrations at negative defocusing conditions [199, 200]. Variation in focus position has been observed to change keyhole dimensions and influence weld geometry [201].

In positive defocusing condition, laser beam is focussed above material surface and the material interacts with the diverged beam. As the beam is wider and power density is reduced, depth of penetration can be decreased. In negative defocused condition, the material surface interacts with wider, converging beam. At this condition also, power density is lower and can produce welds with low penetration. But when this converged beam is capable of vaporizing sufficient material, keyhole is formed and the focused beam directly interacts on keyhole walls in deeper direction and more laser energy is absorbed effectively by multiple reflections. Therefore, few experiments have been reported to enhance depth of penetration under negative defocusing. In case of laser-arc hybrid welding, due to laser-arc interaction these phenomena can be modified.

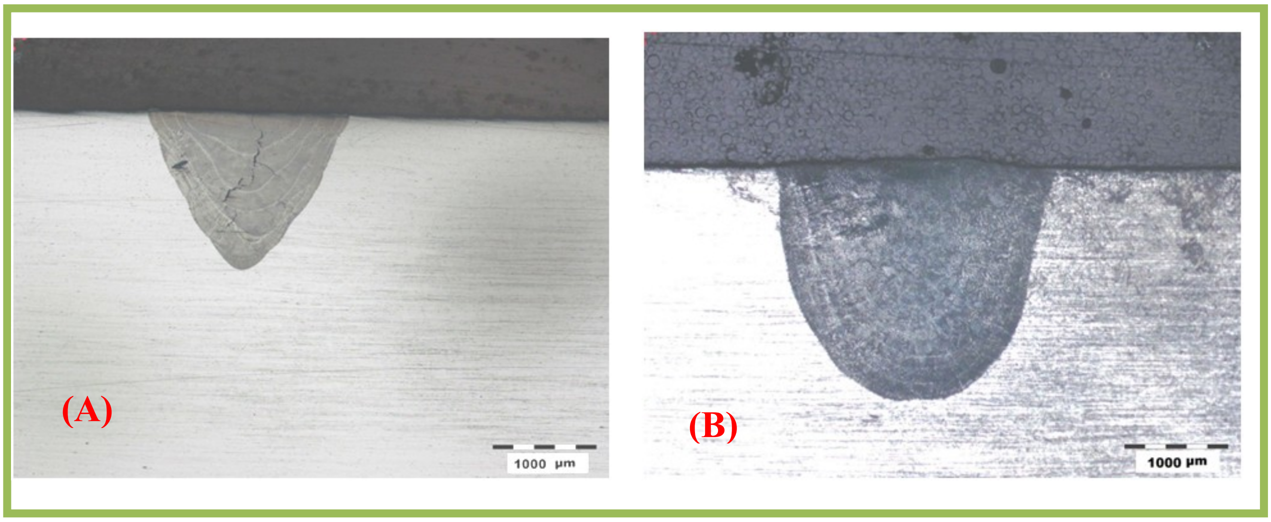

Figure 5-7 Macrostructures of welds at positive defocusing A) Laser alone, B) Hybrid
Laser parameter- Peak power- 4 KW, Pulse duration- 8 ms, Pulse frequency- 15pps, Defocus- +4 mm, Arc parameters- Current- 40 A, Traverse peed- 2.5 mm/s, Laser leading

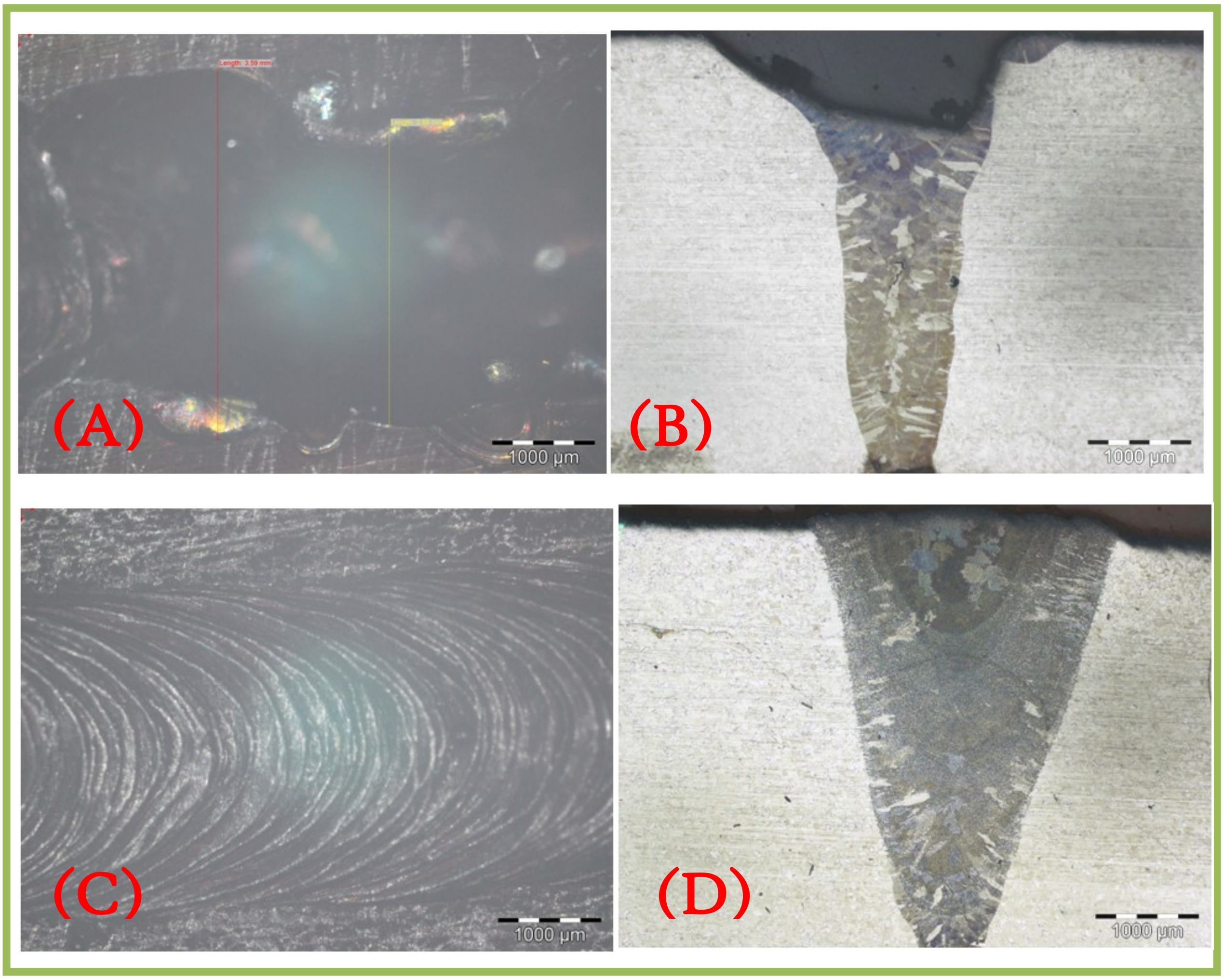

Figure 5-8 Macrostructures of welds at negative defocusing- Laser weld's A) surface and B) cross section, Hybrid weld's C) surface and D) cross section

Laser parameter- Peak power- 4 KW, Pulse duration- 8 ms, Pulse frequency- 15 pps, Defocus: -2 mm, Arc parameters- Current- 40 A, Traverse speed- 2.5 mm/s, Laser leading

Figure 5-7 shows macrostructures of positively defocused (+4mm) laser and hybrid welds. Though weld penetration is observed to be improved in positive focused hybrid welds, this increment is not as much as that of negative focusing. As Figure 5-7 shows the improvement in weld penetration is only 20-30%. It is essentially due to the reduction in power density of laser beam at positive defocusing which is not capable to produce sufficient and stable keyhole. The addition of arc plasma does not seem to enhance keyhole formation effectively and which is demonstrated in geometry of hybrid weld. As shown from the macrostructures of laser welds performed in negative defocusing (Figure 5-8), weld penetration is observed to be enhanced drastically. But these laser welds are with heavy spattering and surface defects like undercut as shown in Figure 5-8.a,b. In hybrid welding, under the interaction of laser photons with laser and arc plasmas, spattering is reduced significantly and deeper welds with smooth surfaces are achieved as shown from the surface and cross-sectional macrostructures of laser and hybrid welds in Figure 5-8.c and d. It indicates that hybrid welds with high depth of penetration can be made at keyhole mode of operation in negative defocusing condition. Further study is needed to understand this improvement.

5.6 INFLUENCE OF ARC CURRENT IN PULSED LASER-ARC HYBRID WELDING

In laser-arc hybrid welding, either laser or arc can be primary heat source and assisted by other heat source. The experiments presented so far utilizes laser as primary heat source and arc was used to augment laser beam characteristics. In the present experiments, laser was employed to enhance the GTAW arc and the welds were made by keeping laser power 180W and increasing arc current from 20 to 70A. The resultant welds were analysed and the plots drawn between arc current and weld geometry parameters; depth of penetration, aspect ratio and melt area are shown in Figure 5-9. a-c respectively. From the graphs it is clear that with increase in arc current both GTAW and hybrid weld's depth, aspect ratio and melt area increases linearly. In GTAW, this increment is up to 60A and above that only melt area is enlarged but penetration depth and aspect ratio tends to be saturated. At all the current levels, hybrid weld depth, aspect ratio and melt area are larger than GTA welds of same arc current. However at 70A, hybrid weld shows sharp increment in depth, aspect ratio and melt area. It shows that up to 60A arc current, heat transfer primarily takes place as heat conduction in radial direction and convective forces which enhance depth of penetration are not effective. Therefore in only GTAW, increasing arc current beyond 60A does not enhance depth of penetration and aspect ratio but enlarges melt area. But in hybrid weld with 70A GTAW arc current, although the improvement in met area is insignificant, enormous increase in weld depth, aspect ratio occurs.

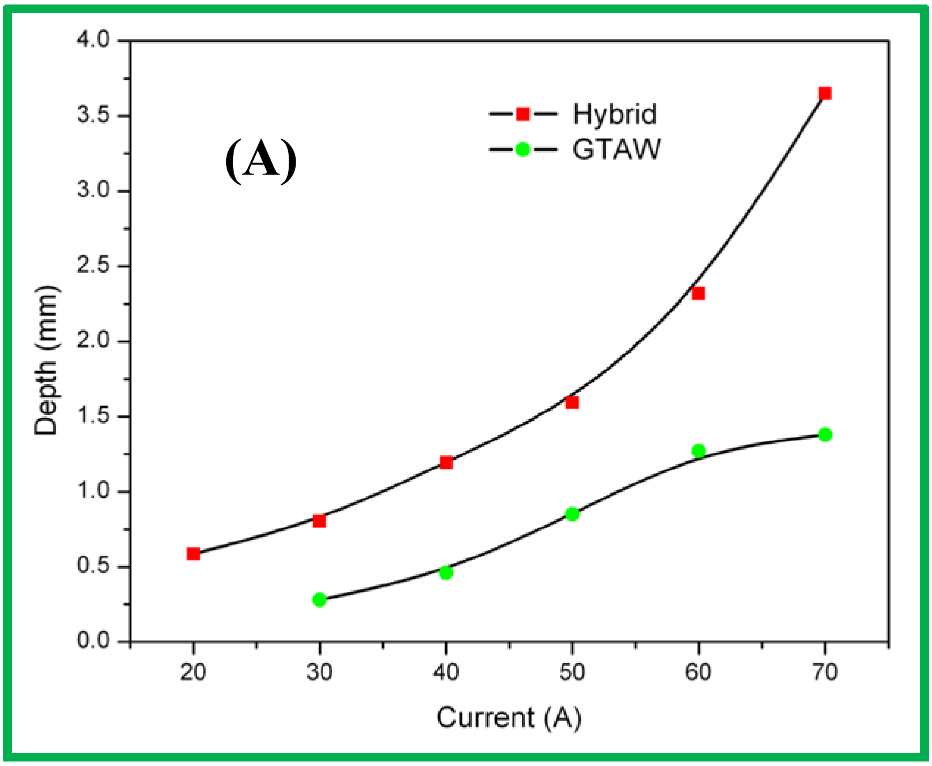

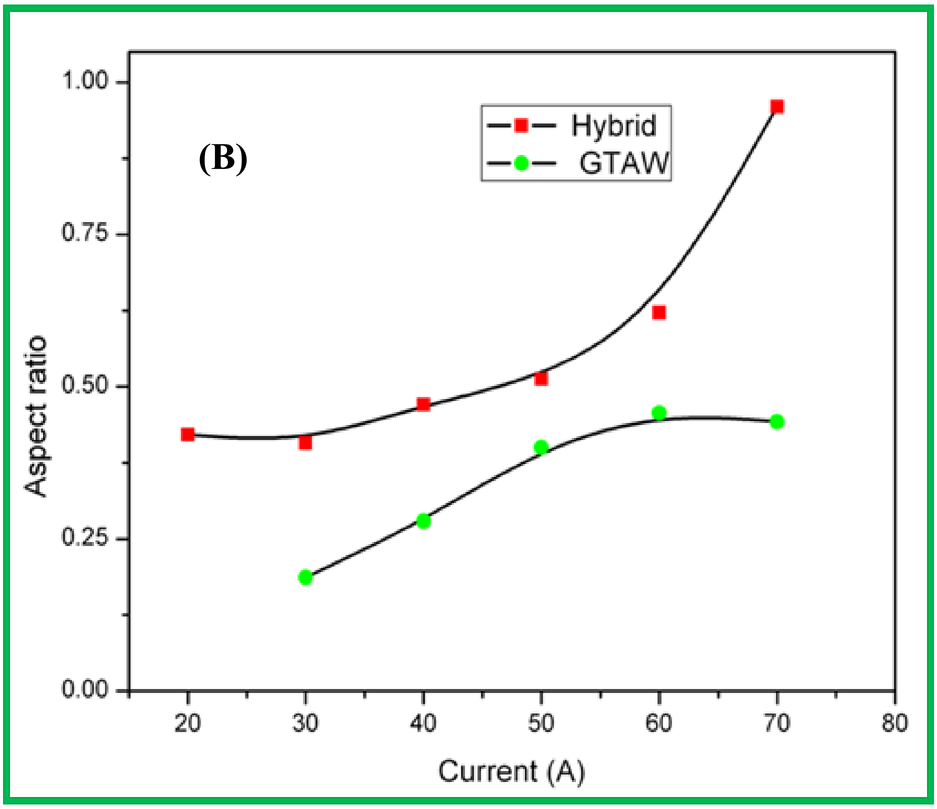

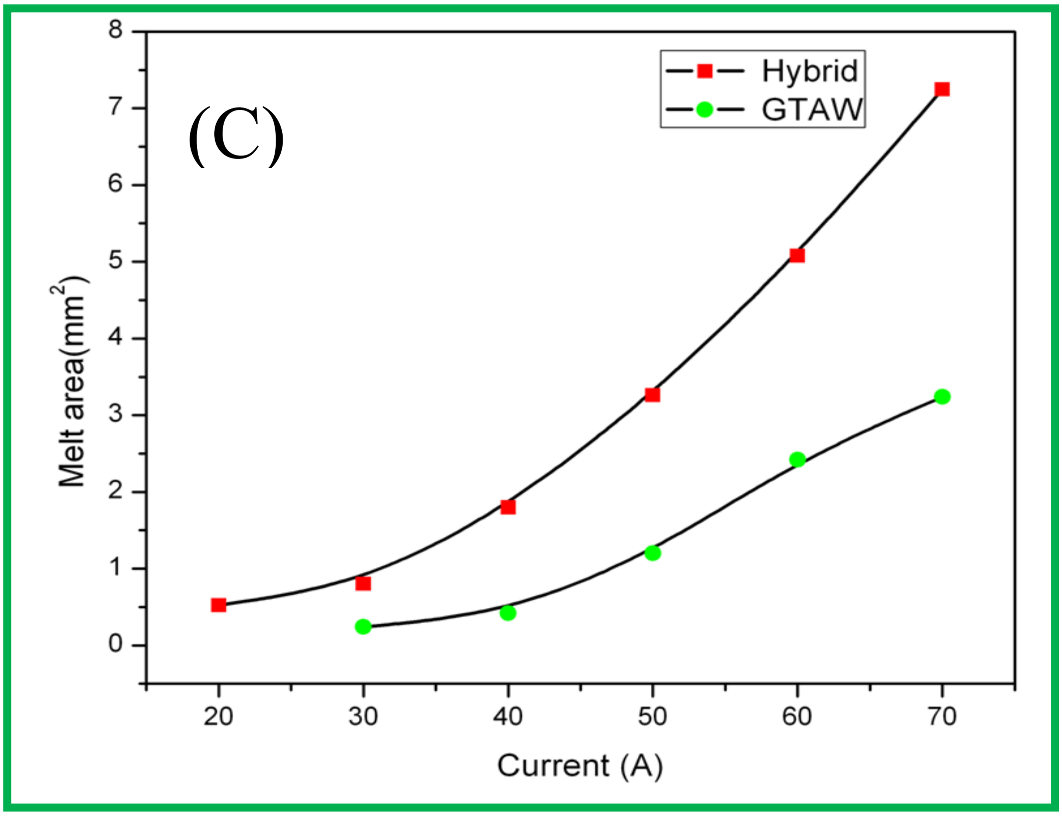

Figure 5-9 Effect of arc current on pulsed laser- GTA hybrid weld geometry
Arc current vs. A) Depth of penetration, B Aspect ratio and C) Melt area

The macrostructures of laser, GTA and hybrid welds of 70A current shown in Figure 5-10.A-C obviously explain hybrid phenomena. More than 150% improvement in depth of penetration in hybrid weld as shown in Figure 5-10.C, is not mere addition of laser and GTA processes. It strongly demonstrates the effect of synergistic action of laser and arc heat sources. Laser pulses of peak power 1.5 KW and mean power 180 W was used for these experiments. Moreover, laser was kept in leading GTAW arc position at which enhancement of keyhole formation is not efficient. These rationales indicate that the improvement is not from laser beam rather due to the action of arc. In addition to these, the reverse-bell shape hybrid weld geometry also suggests the possible arc constriction due to laser-arc interaction. The constriction of bell shape arc is beneficial to produce deep penetration welds with high aspect ratio. In activated TIG (A-TIG) welding process, arc constriction is considered to occur due to the presence of unique flux.

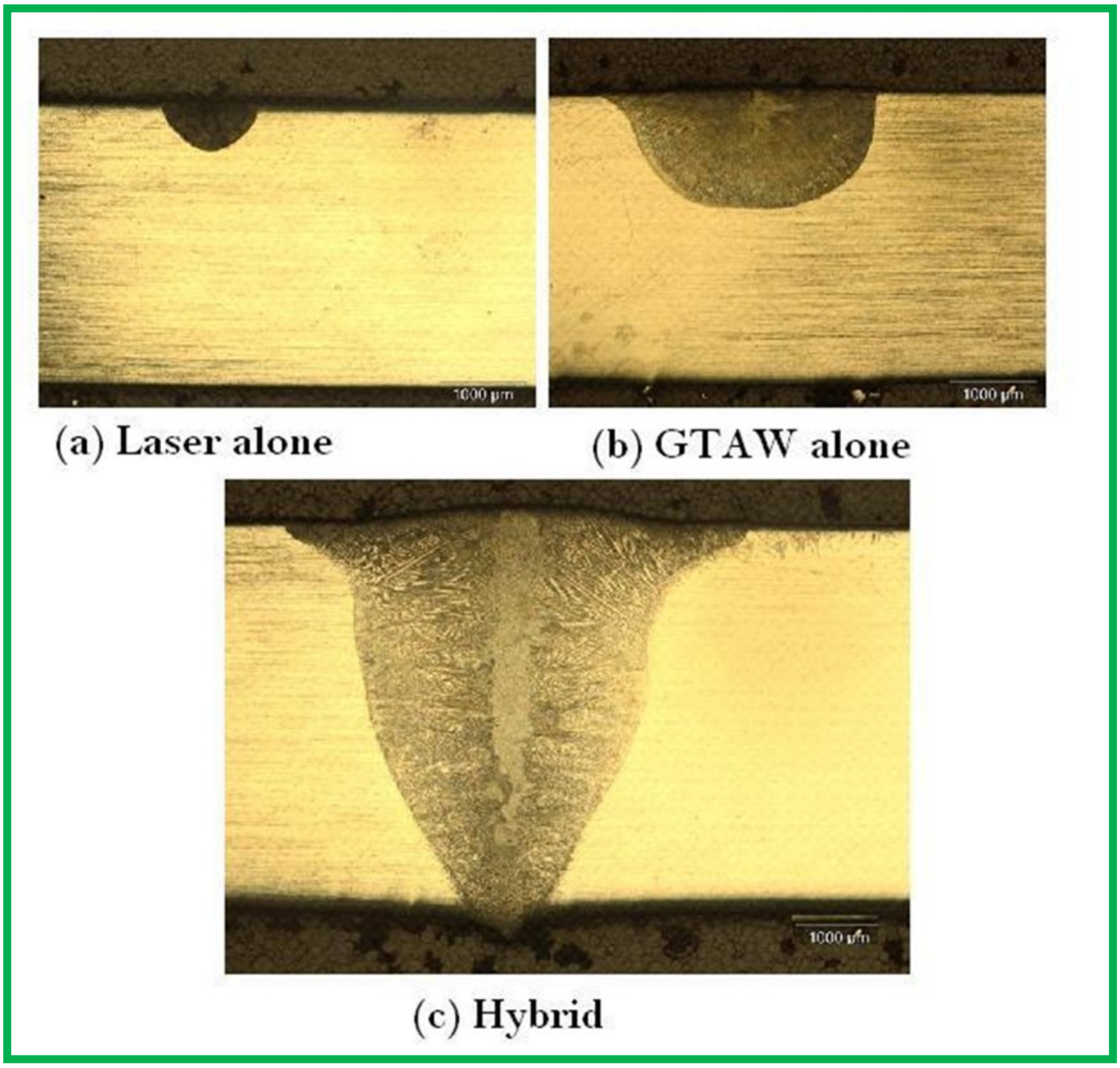

Figure 5-10 Macrostructures of a) Laser alone (Mean power 180W), b) GTAW alone (arc current 70 A) and c) hybrid (coupled) welds

In the present case, as laser beam is coupled with GTAW arc in leading position, the plasma generated by laser facilities arc constriction. When the dense laser plasma interacts with arc plasma, arc tends to be rooted on laser acting spot in accordance with 'minimum voltage' principle. As electricity will pass through least resistance path made by laser plasma, arc rooting and arc constriction occur. As arc current was raised from 30 A to 70 A, drop in arc voltage was observed. At 30 A current, voltage was 9.2 V and as arc current increased to 70 A, voltage reduced to 8.8 V. Therefore heat source density is enhanced which leads to improvement in penetration depth and aspect ratio of welds.

5.7 MICROSTRUCTURAL AND MECHANICAL PROPERTIES OF HYBRID, LASER AND GTA WELDS

As specified above, pulsed laser-arc hybrid welds have benefits like improved penetration depth, good surface etc. Unless better microstructural and mechanical properties are obtained, hybrid welds may not see actual application. Therefore, microstructural and mechanical properties of hybrid welds at keyhole mode of operation have been examined and compared with laser and GTAW processes. For comparison of these processes, minimum heat input required to make full penetration welds at same traverse speed was used. These process parameters were optimised from several trial experiments and are given in Table 5-2.

5.7.1 Weld geometry

As the power density of GTAW, laser and hybrid heat sources is different, the heat input required to achieve same depth of penetration varies with processes. The heat input given in GTAW, laser and hybrid processes is estimated as following:

Heat input $_{\text{GTAW}}$ (J/mm) = [Current × Voltage/ Traverse speed] × Energy transfer efficiency

Heat input $_{\text{Laser}}$ (J/mm) = [Mean Power/ Traverse speed] × Energy transfer efficiency

Heat input $_{\text{Hybrid}}$ (J/mm) = Heat input $_{\text{Nd: YAG}}$ + Heat input $_{\text{GTAW}}$

Energy transfer efficiency of GTAW process is taken as 80% [202] and that of Nd: YAG laser is assumed to be 65% [203, 204]. In hybrid welding, the net heat inputs from laser and GTAW sources are summed up while taking their efficiencies also into account.

Table 5-2 Process parameters used in Laser, GTA and hybrid processes

Parameters	Pulsed Laser	GTAW	Hybrid
Peak power, KW	3	--	2.2
Pulse duration, ms	9		8
Frequency, pps	18		20
Pulse energy, J	27		17.6
Mean power, W	486		352
Arc current, A	--	126	40
Voltage, V	--	12.5	12
Inter heat source distance, mm	--	--	3
Torch angle, °	--	90	60
Heat source position	--	--	Arc leading
Defocusing distance, mm	0	--	0
Spot diameter, mm	0.8	--	0.8
Electrode diameter, mm	--	3.4	2.4
Arc gap, mm	--	1.5	1.5
Shielding gas	99.99% Pure argon		
Flow rate, lpm	10	10	5
Traverse speed, mm/s	3	3	3

The cross-section macrostructures of laser, hybrid and GTAW welds are shown in Figure 5-11. In Table 5-3, the details of macro and microstructures are given. The minimum heat input required to make full penetration joints in laser, hybrid and GTAW processes are observed from trial experiments to be 105, 204 and 420 J/mm respectively. The geometry of weld is primarily determined by the nature and power density of heat sources. While GTAW weld has hemispherical shape, laser and hybrid welds show their characteristic keyhole geometry. Further, hybrid weld cross-section can be clearly distinguished as laser and arc

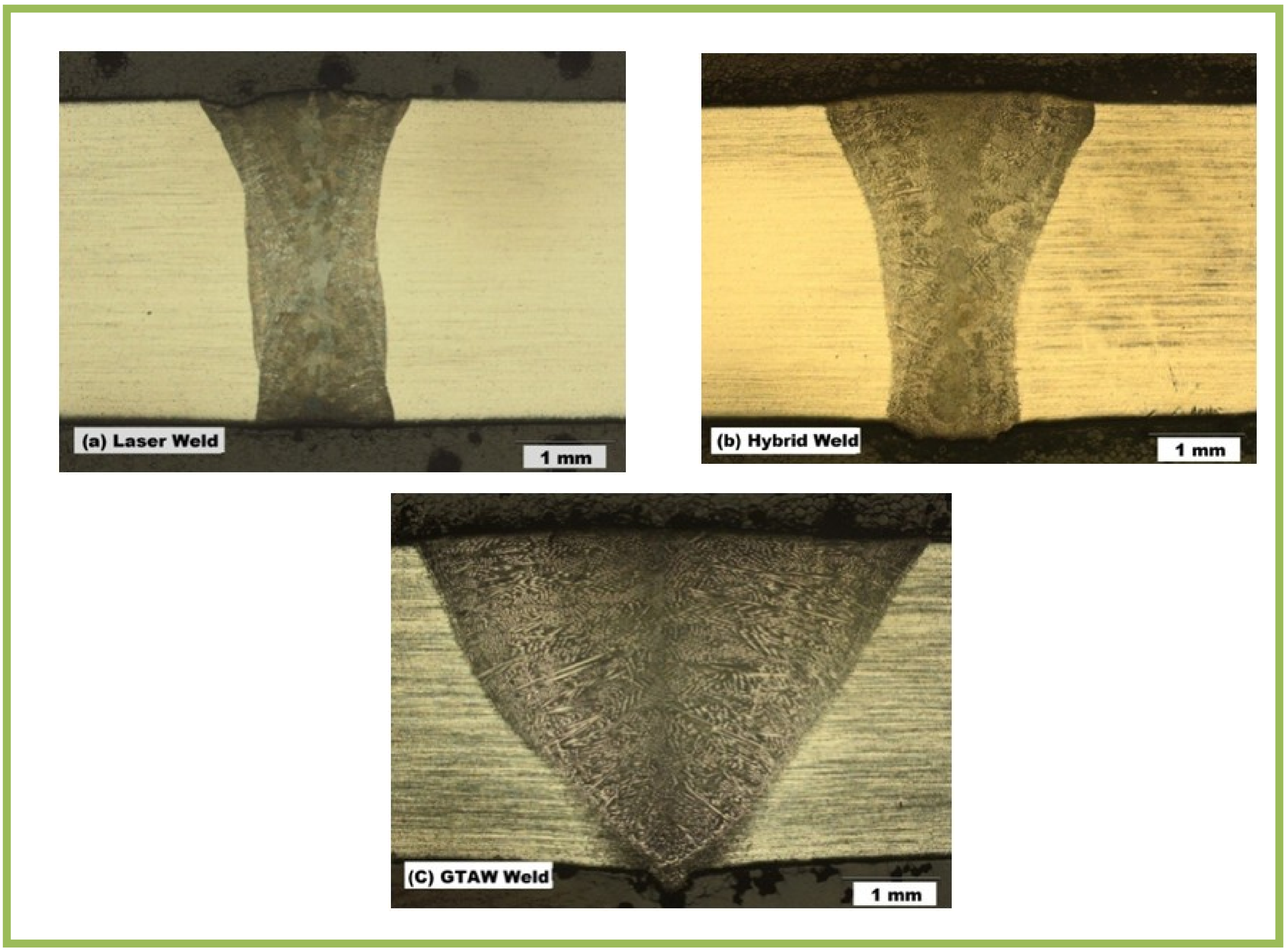

Figure 5-11 Weld geometries of full penetration a) Laser, b) Hybrid and c) GTA welds

combined zone at top and laser only acting zone at bottom. While the width and melt area of GTAW is largest, laser is least and that of hybrid lies in between GTAW and laser. Formation of shallow GTAW weld is attributed to the wide bell shaped arc plasma and resultant large heat input. The narrow, keyhole geometry of hybrid welds corresponds to the increase in laser energy absorption due to arc preheating. It shows that as GTAW is substituted by hybrid process, size of the molten zone can be reduced considerably.

Table 5-3 Comparison of Microstructures of Laser, GTA and hybrid welds

Processes	Heat input, J/mm	Weld geometry		Mean cell size, μm		Cooling rate, K/S	
		width , mm	area, mm^2	Top	Root	Top	Root
Laser	105.3	2.1	4.5	6.54	4.86	1.97×10^3	4.86×10^3
Hybrid	204.3	2.8	6.1	10.15	7.46	5.21×10^2	1.33×10^3
GTAW	420	5.3	10.5	15.0		1.60×10^2	

5.7.2 Microstructural Analysis

The microstructure of base metal shows fully austenitic phase as seen in Figure 5-12.a. The average grain size measured by grain intercept method is approximately 40 μm, which corresponds to ASTM G7. As microstructure of welds is influenced by welding process and their operating parameters, the change in process determines microstructures and consequent mechanical properties. As shown in microstructures of welds in Figure 5-12.b-e, it is observed that all these welds solidify in primary austenitic mode due to low Chromium equivalent to Nickel equivalent chemical composition of material. The retained δ-ferrite was measured by ferritescope and found to be almost nil in all the welds. Primary austenitic mode solidification together with rapid solidification tends to cause solidification cracking in laser and hybrid welds. However, no such cracks are observed in these welds. It is attributed to the reduction in cooling rate and associated thermal stresses at two dimensional heat transfer condition as stated in chapter 4. Both laser and hybrid welds show cellular-dendritic structure growing from fusion boundary to weld centre in the direction opposite to heat removal.

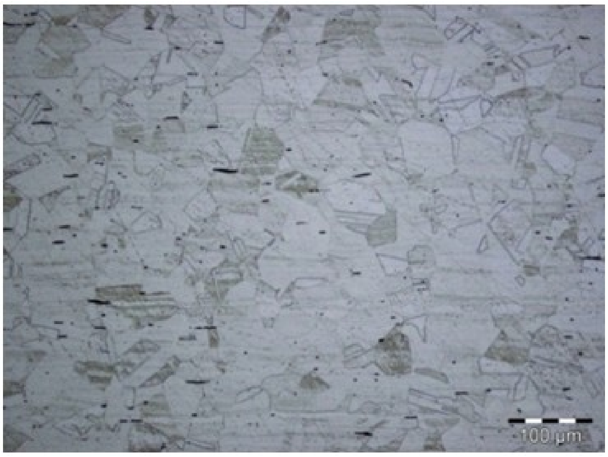

(a) Base metal

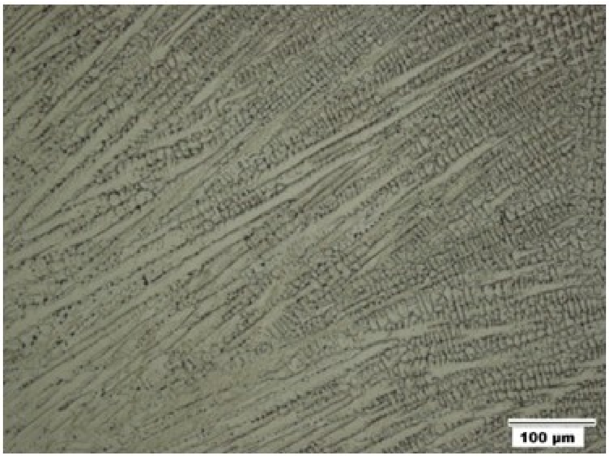

(b) Hybrid- Top zone

(c) Hybrid- bottom zone

(d) Laser centre zone

(e) Hybrid centre zone

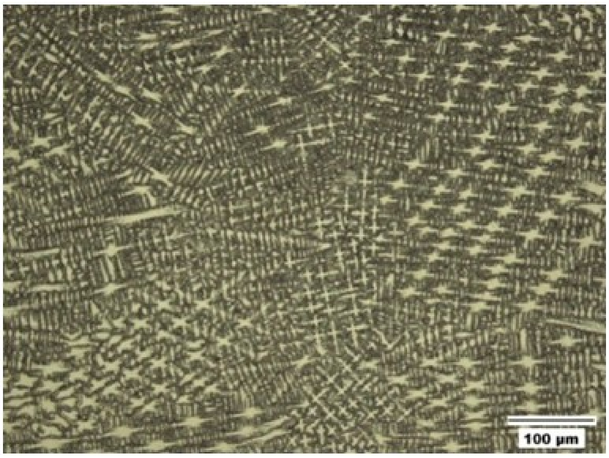

(f) GTAW centre zone

Figure 5-12 Microstructures of full penetration Laser, Hybrid and GTAW welds

But in GTA weld, columnar-dendritic grains were observed. At the centre of laser and hybrid welds, characteristic fine equiaxed like grains are observed throughout the thickness as shown in Figure 5-12.d&e. However GTA weld is noticed to have only columnar- dendritic morphology even at centre as seen in Figure 5-12.f. The intercellular spacing was determined in all the welds except at weld centre and is found to be smallest in laser and largest in GTAW as depicted in Table 5-3. In hybrid welds, intercellular spacing is found to be in between laser and GTAW. Within hybrid weld, variation in inter cellular spacing was observed as slightly wider at top than root side (Figure 5-12.b and c).

It is well known that solidification microstructure depends on Temperature gradient (G) and Solidification rate (R) attained in weld pool. While the morphology of weld microstructure is dictated by G/R ratio, intercellular spacing is determined by cooling rate (G×R). As G/R decreases, solidification morphology can be changed from planer to equiaxed-dendritic structure. When the cooling rate inside the weld pool decreases, solidification grain size increases. Temperature gradient, G is high in weld fusion boundary and it decreases towards weld centre and reaches its lower limit there. Solidification rate, R is low at fusion boundary and increases towards centre and it attains its upper limit of traverse speed at weld centre-line [84]. Since high power density laser is used in laser and hybrid welds, large value of G/R (G is high) is reached at fusion boundary and results in fine cellular-dendritic structure. In case of GTAW, G/R is lower than that of laser and hybrid welds due to its nature of wider and high heat input. Therefore, the morphology changes to columnar-dendritic. At centre of laser and hybrid welds equiaxed like microstructure is observed. However, the microstructures along weld line show that these are cellular-dendritic grains growing parallel to weld line as shown in Figure 4-3.d. In GTA weld, columnar- dendritic grains evolving from fusion boundaries converges at weld centre as shown in Figure 5-12.f.

The intercellular spacing is influenced by cooling rate encountered in weld pool. The cooling rate inside weld pool can be estimated using Katayama's relation between intercellular spacing and cooling rate [25, 205]. The relationship is given as $\lambda=80\Delta T^{-0.33}$, where λ- primary arm spacing in μm and ΔT- Cooling rate in K/s. The cell spacing and calculated cooling rates of all welds are shown in Table 5-3. The cooling rate is determined to be highest in laser and lowest in GTA welds. Hybrid weld indicates in-between laser and hybrid welds. At the top side, the cooling rate is lower and is in the order of GTA weld. At root side, cooling rate is higher and is equivalent to laser weld. This order of cooling rate is in accordance with power density of welding processes. As the power density of heat source decreases, cooling rate also decreases.

5.7.3 Tensile properties of weldments

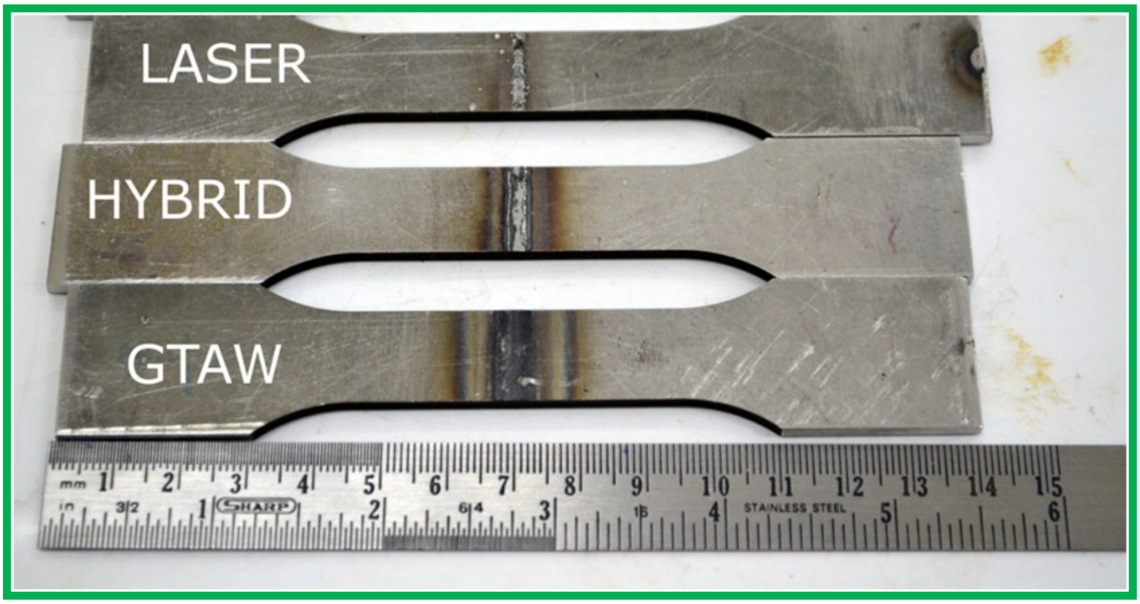

Figure 5-13 Traverse tensile test samples of Laser, GTA and hybrid welds

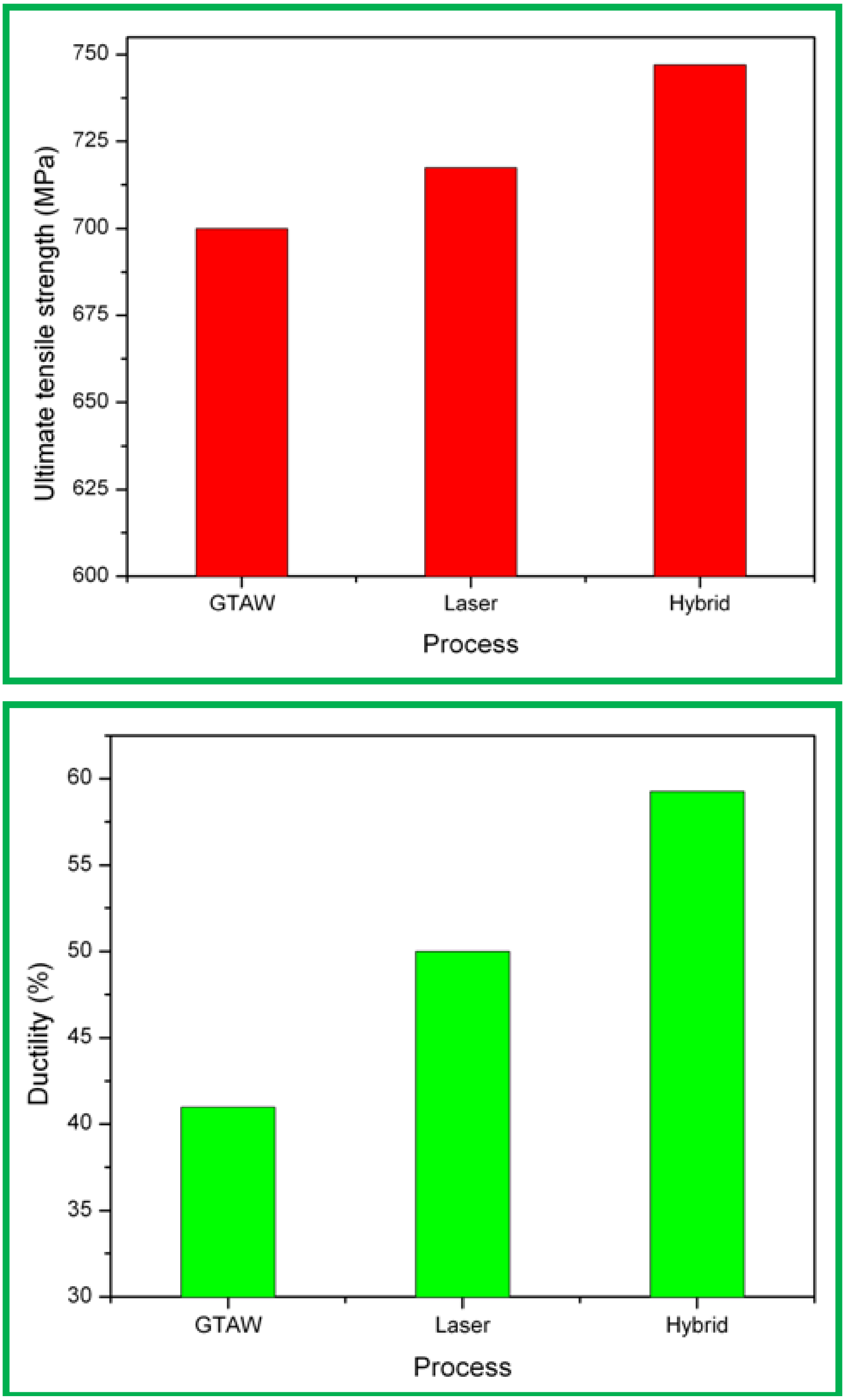

Figure 5-14 Tensile test results of laser, GTA and hybrid welds-(a) Joint strength, (b) Ductility

Tensile test samples prepared from weld pads are shown in Figure 5-13 and the results are reported in Figure 5-14. While Yield strength of all the welds is observed to be the same value of 412 MPa, the ultimate tensile strength (UTS) and ductility of hybrid weld are superior to other welds. Though little variation is observed in UTS, the ductility of GTA weld is much lower than other welds. The variation in mechanical properties is due to the differences in microstructures. The fine cellular-dendritic microstructure produced in laser and hybrid welds enhances the strength and ductility of welds. Another possible reason for better mechanical properties are due to reduced segregation in Laser and hybrid welds than GTA welds. The grain size variation in the HAZ of weldment causes reduction in strength of weldment. However, the wider columnar-dendritic profile in GTA weld is prone to premature failure and resulted in least joint strength and ductility. It shows that hybrid weld can be substituted for GTA welds for its superior mechanical properties.

5.7.4 Residual Stress Measurements

Residual stresses developed due to non-uniform heating and cooling of materials during welding can develop serious issues in material's service condition. Presence of tensile residual stresses in stress corrosion cracking (SCC) environment that accelerates failure of components [206]. Moreover, fatigue life of fabricated components will also be reduced substantially due to tensile-residual stresses build up during welding [207]. The variation of locked-in residual stresses across the welds of all the three processes, determined by X-ray diffraction (XRD) residual stress measurement system, is shown in Figure 5-15. Among the processes, due to high heat input of GTA weld, highest residual stress pattern is formed in this weld than other processes [206]. One of the reasons could be due to weld pool shape hence molten pool variation with non-uniform pattern of heat flow causes more amount of residual stress in the resultant weld. Due to high power density of laser heat source and narrow weld geometry, residual stress developed is much lesser in laser welding. In the case of hybrid welding, the addition of arc heat source with laser is expected to enhance residual stresses. But, the Figure 5-15 shows that residual stress developed in hybrid weld shows less variation compared with laser weldment. It is primarily due to the synergistic nature of hybrid process, where, in place of addition of two heat sources, a 'hybrid heat source' is made. As the power density of this 'hybrid heat source' is closer to that of laser, the thermo-mechanically induced residual stresses are similar.

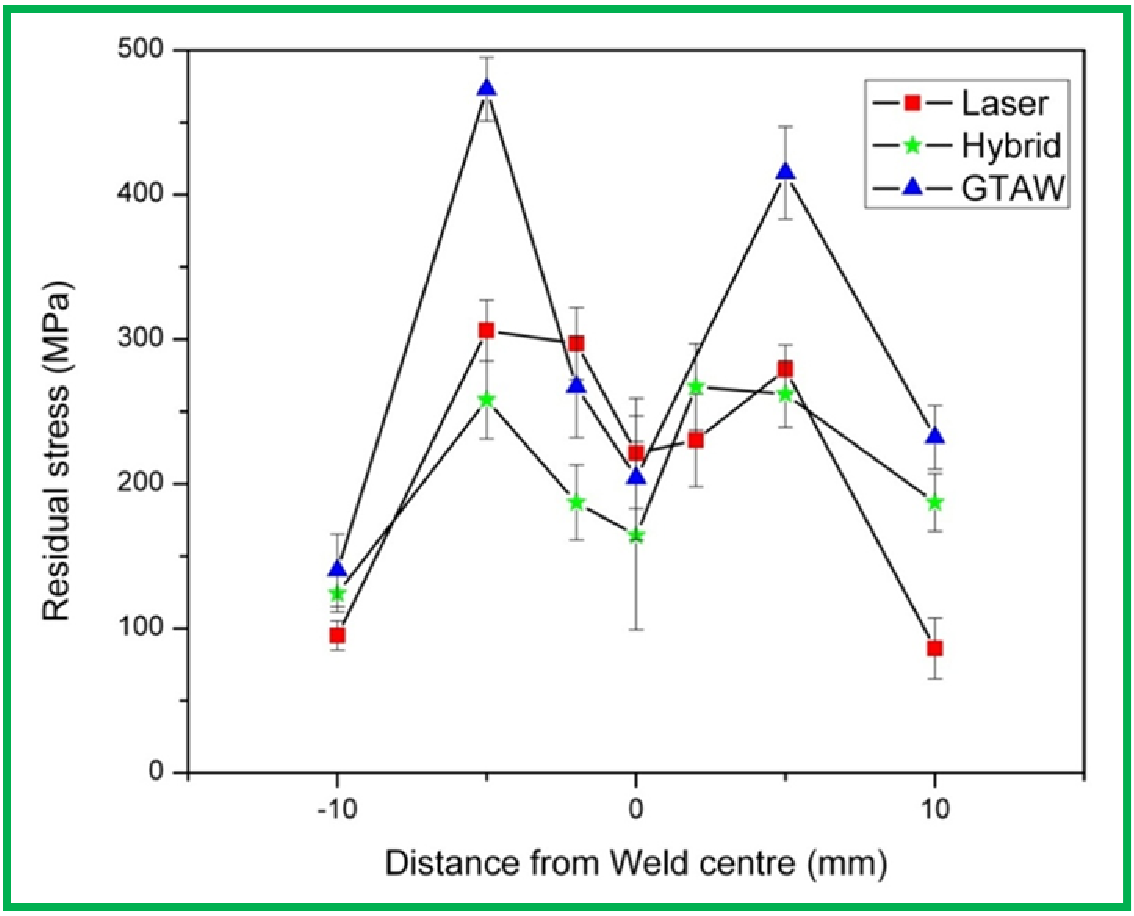

Figure 5-15 Residual stress distribution in Laser, GTA and Hybrid welds across weld line

5.8 CONCLUSIONS

Pulsed laser- GTA hybrid welding facility was established, basic hybrid parameters such as heat source position, inter heat source distance, focus position etc have been investigated and microstructural and mechanical properties of hybrid welds have been compared with laser and GTA welds.

- Hybrid welds were carried out in conduction and keyhole modes after optimisation of process parameters. The conduction mode hybrid welds are free from solidification cracks unlike laser welds due to its reduction in cooling rate. In Keyhole mode, synergistic effect of laser and arc is observed which results in enhanced weld penetration and aspect ratio.
- Heat source position is noticed to be an essential parameter to influence laser-arc interaction with material. While arc leading position imparts better penetration, laser leading position yields aesthetic surface similar to laser weld. Preheating mechanism is predominant in arc leading position and leads to enhancement of laser energy absorptivity and subsequent improvement in depth of penetration. In laser leading position, the phenomena of arc rooting and constriction occur.
- If pulsed laser and GTAW heat sources are kept more than 3mm in laser leading position, hybrid phenomenon does not occur and laser and arc operate independently.
- Defocusing of laser beam is noticed to influence pulsed laser arc hybrid welds. Positive defocusing hybrid welding produce low weld penetration and negative defocusing improves depth with better surface appearance.
- As increasing arc current at constant laser power, a great deal of improvement in depth of penetration and melt area is noticed. The weld geometry envisages GTAW arc constriction due to the interaction of arc plasma with laser beam.

- Weld geometry, microstructures and mechanical properties of hybrid welds have been observed to be superior to its competent processes laser and GTAW. Joint strength and ductility of hybrid welds are superior to laser and GTAW in due to its microstructural characteristics. The development of residual stresses in hybrid weld is almost similar to that of laser but it is much lower than of GTAW.

The part of the work presented in this chapter is discussed in [208].

CHAPTER 6 CONCLUSIONS & FUTURE DIRECTIONS

6

6.1 SUMMARY

In the present study, energy transfer modes in pulsed laser seam welding have been studied and the effect of process parameters on the transition of modes has been determined. The influence of energy transfer modes on solidification cracking has been analysed. In order to investigate the advantages of pulsed laser-arc hybrid welding for thin materials, the process was established and synergistic advantages have been observed. The conclusions of these studies have been summarised as follows:

i. Energy transfer modes in pulsed laser seam welding are identified as conduction, transition, penetration and keyhole modes based on the weld bead geometry and microstructural observations. The transition to keyhole mode is not defined by single peak power density but the threshold peak power density to form keyhole is influenced by pulse duration. As the pulse duration increases, the threshold power density decreases. In order to incorporate the influence of pulse duration on the mode transition, it is suggested that energy density should be considered along with peak power density. While weld geometry is determined by energy density within conduction zone, in keyhole regime it is influenced by peak power density. The optimum pulse duration is found to be around 8ms at which highest depth of penetration per unit peak power is attained. In shorter pulses sufficient keyhole is not formed and in longer pulses laser energy is lost in plume attenuation. As weld surface at different modes of energy transfer exhibit distinct profiles, the mode of energy transfer can be predicted empirically.

ii. Solidification cracking in pulsed laser welds of austenitic stainless steel is influenced by both heat input and energy transfer modes which affect the cooling rate and strains induced in weld pool during solidification. While keyhole mode weld is free from cracking, conduction welds have severe cracking throughout weld bead, and penetration welds show cracks only at root side of weld. Conduction welds produced with pulses of longer durations are less severe for cracking than conduction welds with higher pulse frequencies. As heat input increases and energy transfer mode changes from conduction to keyhole mode, cooling rate decreases. The resultant reduction in solidification shrinkage and thermal strains diminishes cracking severity. In addition to this, the characteristic cellular-dendritic grains along the weld line at the weld centre facilitate crack free keyhole mode welds. The threshold cooling rate of the weld pool during solidification to obtain crack free welds is 10^4 K/s.

iii. Pulsed laser- GTA hybrid welding facility was established, basic hybrid parameters such as heat source position, inter heat source distance, focus position etc have been investigated and microstructural and mechanical properties of hybrid welds have been analysed by comparing with laser and GTA welds. Hybrid welds were carried out in conduction and keyhole modes by selecting suitable process parameters. Solidification cracks were not observed in conduction limited hybrid welds for reduction in cooling rate. In keyhole mode, synergistic effect of laser and arc is observed which results in enhanced weld penetration and aspect ratio. Heat source position is noticed to be an essential parameter to influence laser-arc interaction with material. While arc leading position imparts better penetration, laser leading position yields aesthetic surface similar to laser weld. Preheating mechanism is predominant in arc leading position and leads to enhancement of laser energy absorptivity and subsequent improvement in depth of penetration. In laser leading position, the phenomena of arc rooting and constriction happen. When pulsed laser and GTAW heat sources are kept at more than 3mm in laser leading position, hybrid phenomenon does not take place and laser and arc operate independently. Defocusing of laser beam is noticed to influence pulsed laser-arc hybrid welds. Positive defocusing produce welds with low penetration but negative defocusing enhances penetration depth significantly. As increasing arc current while augmenting with low laser power (180 W), a great deal of improvement in depth of penetration and melt area is noticed. Arc constriction due to the presence of dense laser plasma is envisaged from the weld geometry and processing conditions. Microstructures and mechanical properties of hybrid welds in keyhole mode have been observed to be superior to its competent processes, laser and GTAW. Joint strength and ductility of hybrid welds are superior to laser and GTAW due to its microstructural characteristics. The development of residual stresses in hybrid weld is almost similar to that of laser but it is much lower than of GTAW.

6.2 SUGGESTIONS FOR FUTURE WORKS

i. In the present study, it has been found that solidification cracking is influenced by energy transfer modes and crack free welds are obtained in Type 316 stainless steel in keyhole mode due to reduction in cooling rate and induced strains. This methodology can be extended to study solidification cracking severity in crack susceptible stainless steels such as D9 and D9I.

ii. As the interaction of pulsed laser with GTAW arc is extremely complicated and involves several process parameters, sophisticated numerical models need to be developed to enlarge the understanding of this process.

iii. The various physical phenomena such as pulsed interaction of laser induced and arc plasmas, molten pool solidification, keyhole dynamics etc, can best be studied through experimenting with DSO (Digital storage oscilloscope), high speed camera to understand the process better.

iv. Laser assisted GTA hybrid welding (LAGTAHW) has been found to offer promising advantages. However, this study has been carried out only upto 70A for 3 mm thick stainless steels. Higher amperage arc current may be examined for higher thickness plates.

v. The established hybrid welding system can be extended for Hexcan welds of 3.2 mm wall thickness in fast breeder reactor application. Thus the advantages of narrow welds with reduced HAZ and better quality can be achieved.

REFERENCES

[1] M. K. Kulekci, "Magnesium and its alloys applications in automotive industry," *The International Journal of Advanced Manufacturing Technology,* 39, (9-10). 851-865, **2008**.

[2] I. Rötzer, "Laser beam welding makes aircraft lighter," *Fraunhofer magazine,* 1. 36-37, **2005**.

[3] S. Tsirkas, P. Papanikos, K. Pericleous, N. Strusevich, F. Boitout, and J. Bergheau, "Evaluation of distortions in laser welded shipbuilding parts using local-global finite element approach," *Science and Technology of Welding & Joining,* 8, (2). 79-88, **2003**.

[4] E. Assuncao and S. Williams, "Comparison of continuous wave and pulsed wave laser welding effects," *Optics and Lasers in Engineering,* 51, (6). 674-680, **2013**.

[5] W. Steen, K. G. Watkins, and J. Mazumder, *Laser Material Processing*: Springer, 2010.

[6] C. Dawes, *Laser welding: A practical guide*: Woodhead Publishing, 1992.

[7] G. Buvanashekaran, "A study of laser welding modes with varying beam energy levels," *Proceedings of the Institution of Mechanical Engineers, Part C: Journal of Mechanical Engineering Science,* 223, (5). 1141-1156, **2009**.

[8] X. Zhang, "Laser welding mode transition and influence of thermal focusing on mode transition," in *Proceedings of SPIE - The International Society for Optical Engineering*, Beijing, China,**1996**.

[9] V. Shankar, T. Gill, S. Mannan, and S. Sundaresan, "Solidification cracking in austenitic stainless steel welds," *Sadhana,* 28, (3-4). 359-382, **2003**.

[10] I. Masumoto, K. Tamaki, and M. Kutsuna, "Hot cracking of austenitic stainless steel weld metal," *Trans. JWS,* 41, (11) p. 1306, **1972**.

[11] T. Lienert and J. Lippold, "Improved weldability diagram for pulsed laser welded austenitic stainless steels," *Science and Technology of Welding & Joining,* 8, (1). 1-9, **2003**.

[12] J. Y. Lee, S. H. Ko, D. F. Farson, and C. D. Yoo, "Mechanism of keyhole formation and stability in stationary laser welding," *Journal of Physics D: Applied Physics,* 35, (13) p. 1570, **2002**.

[13] O. Idowu, O. Ojo, and M. Chaturvedi, "Effect of heat input on heat affected zone cracking in laser welded ATI Allvac 718Plus superalloy," *Materials Science and Engineering: A,* 454. 389-397, **2007**.

[14] L. Osoba and O. Ojo, "Influence of laser welding heat input on HAZ cracking in newly developed Haynes 282 superalloy," *Materials Science and Technology,* 28, (4). 431-436, **2012**.

[15] J. Lippold and W. Savage, "Solidification of austenitic stainless steel weldments: Part 2—The effect of alloy composition on ferrite morphology," *Welding journal,* 59, (2) p. 48s, **1980**.

[16] D. Min, J. Shen, S. Lai, J. Chen, N. Xu, and H. Liu, "Effects of heat input on the low power Nd: YAG pulse laser conduction weldability of magnesium alloy AZ61," *Optics and Lasers in Engineering,* 49, (1). 89-96, **2011**.

[17] F. C. Hull, "Effect of delta ferrite on the hot cracking of stainless steel," *Welding Journal,* 46, (9) p. 399, **1967**.

[18] K. Nishimoto and H. Mori, "Hot cracking susceptibility in laser weld metal of high nitrogen stainless steels," *Science and Technology of Advanced Materials,* 5, (1). 231-240, **2004**.

[19] J. Tusek and M. Suban, "Hybrid welding with arc and laser beam," *Science and Technology of Welding & Joining,* 4, (5). 308-311, **1999**.

[20] A. Mahrle, S. Rose, M. Schnick, E. Beyer, and U. Füssel, "Laser-assisted plasma arc welding of stainless steel," *Journal of Laser Applications,* 25, (3) **2013**.

[21] B. Hu and G. Den Ouden, "Synergetic effects of hybrid laser/arc welding," *Science and Technology of Welding & Joining,* 10, (4). 427-431, **2005**.

[22] A.-V. Bîrdeanu, C. Ciucă, and A. Puicea, "Pulsed LASER-(micro) TIG hybrid welding: Process characteristics," *Journal of Materials Processing Technology,* 212, (4). 890-902, **2012**.

[23] A.-M. El-Batahgy, "Effect of laser welding parameters on fusion zone shape and solidification structure of austenitic stainless steels," *Materials Letters,* 32, (2). 155-163, **1997**.

[24] T. Jokinen, M. Karhu, and V. Kujanpää, "Welding of thick austenitic stainless steel using Nd: yttrium–aluminum–garnet laser with filler wire and hybrid process," *Journal of Laser Applications,* 15, (4). 220-224, **2003**.

[25] S. Katayama and A. Matsunawa, "Solidification microstructure of laser welded stainless steels," *Laser Institute of America*. 60-67, **1985**.

[26] S. Mannan, S. Chetal, B. Raj, and S. Bhoje, "Selection of materials for prototype fast breeder reactor," *Transactions- Indian Institute of Metals,* 56, (2). 155-178, **2003**.

[27] B. Raj, "Materials science research for sodium cooled fast reactors," *Bulletin of Materials Science,* 32, (3). 271-283, **2009**.

[28] B. Raj, S. Mannan, P. Vasudeva Rao, and M. Mathew, "Development of fuels and structural materials for fast breeder reactors," in *Sadhana (Academy Proceedings in Engineering Sciences)*. 527-558,**2002**.

[29] N. Amanat, C. Chaminade, J. Grace, D. R. McKenzie, and N. L. James, "Transmission laser welding of amorphous and semi-crystalline poly-ether–ether–ketone for applications in the medical device industry," *Materials & design,* 31, (10). 4823-4830, **2010**.

[30] D. Anand, D. Chen, S. Bhole, P. Andreychuk, and G. Boudreau, "Fatigue behavior of tailor (laser)-welded blanks for automotive applications," *Materials Science and Engineering: A,* 420, (1). 199-207, **2006**.

[31] H.-C. Chen, A. J. Pinkerton, and L. Li, "Fibre laser welding of dissimilar alloys of Ti-6Al-4V and Inconel 718 for aerospace applications," *The International Journal of Advanced Manufacturing Technology,* 52, (9-12). 977-987, **2011**.

[32] H. Friedrich and S. Schumann, "Research for a “new age of magnesium” in the automotive industry," *Journal of Materials Processing Technology,* 117, (3). 276-281, **2001**.

[33] A. Sanderson, C. Punshon, and J. Russell, "Advanced welding processes for fusion reactor fabrication," *Fusion engineering and design,* 49. 77-87, **2000**.

[34] G. Kelkar, "Pulsed laser welding," *WJM Technologies, excellence in material joining, Cerritos, CA,* 90703, **2000**.

[35] R. Biswal, K. A. Gopal, S. Murugan, S. Venugopal, and T. Jayakumar, "Standardization of Laser Welding Parameters for Attachment of Thermocouple to Pressurized Capsule for On-Line Creep Rupture Studies," *Procedia Engineering,* 86. 560-566, **2014**.

[36] K. A. Gopal, S. Murugan, S. Venugopal, and K. V. Kasiviswanathan, "Laser welding of precision engineering components," presented at the National Welding Seminar-2009 Kolkata, India, **2009**.

[37] *Laser beam welding*. Available: http://www.joiningtech.com/industry-references/welding-types/laser-beam-welding

[38] J. Liu, D. Weckman, and H. Kerr, "The effects of process variables on pulsed Nd: YAG laser spot welds: Part I. AISI 409 stainless steel," *Metallurgical Transactions B,* 24, (6). 1065-1076, **1993**.

[39] R. Domański, M. Jaworski, and M. Rebow, "Laser radiation interaction with solids," *Journal of Power Technologies,* 79, **1995**.

[40] L. Liu and X. Hao, "Improvement of laser keyhole formation with the assistance of arc plasma in the hybrid welding process of magnesium alloy," *Optics and Lasers in Engineering,* 47, (11). 1177-1182, **2009**.

[41] E. Kannatey-Asibu Jr, *Principles of laser materials processing* vol. 4: John Wiley & Sons, 2009.

[42] M. F. Modest, "Reflectivity and absorptivity of opaque surface," in *LIA handbook of laser materials processing*, J. F. Ready, D. F. Farson, and T. Feeley, Eds., ed Orlando Laser Institute of America Orlando, **2001**, p. 182.

[43] S. Ream, "Understanding the Technology and Industrial Acceptance of Laser Surface Modifications," in *Surface Engineering*. vol. 85, R. Kossowsky and S. Singhal, Eds., ed: Springer Netherlands, **1984**. 285-299.

[44] F. O. Olsen, *Hybrid laser-arc welding*: Elsevier, 2009.

[45] S. W. S. Morgan, "Hybrid laser conduction welding," presented at the 55th Annual Assembly of International Institute of Welding, Copenhagen, Denmark, **2002**.

[46] A. K. Nath, R. Sridhar, P. Ganesh, and R. Kaul, "Laser power coupling efficiency in conduction and keyhole welding of austenitic stainless steel," *Sadhana,* 27, (3). 383-392, **2002**.

[47] S. Meco, G. Pardal, S. Ganguly, R. M. Miranda, L. Quintino, and S. Williams, "Overlap conduction laser welding of aluminium to steel," *The International Journal of Advanced Manufacturing Technology,* 67, (1-4). 647-654, **2013**.

[48] D. Assuncao, S. Ganguly, D. Yapp, and S. Williams, "Conduction mode: broadening the range of applications for laser welding," **2012**.

[49] P. W. Fuerschbach, "Melting efficiency in fusion welding," *The Metal Science of Joining,* **1992**.

[50] T. J. F. Paleocrassas A.G., "Inherent instability investigation for low speed laser welding of aluminum using a single-mode fiber laser," *Journal of Materials Processing Technology,* 210, (10). 1411-1418.

[51] P. Berger, H. Hügel, and T. Graf, "Understanding Pore Formation in Laser Beam Welding," *Physics Procedia,* 12. 241-247, **2011**.

[52] A. F. H. Kaplan and J. Powell, "Spatter in laser welding," *Journal of Laser Applications,* 23, (3) **2011**.

[53] J. Karlsson, P. Norman, A. F. H. Kaplan, P. Rubin, J. Lamas, and A. Yañez, "Observation of the mechanisms causing two kinds of undercut during laser hybrid arc welding," *Applied Surface Science,* 257, (17). 7501-7506, **2011**.

[54] A. Matsunawa, M. Mizutani, S. Katayama, and N. Seto, "Porosity formation mechanism and its prevention in laser welding," *Welding International,* 17, (6). 431-437, **2003**.

[55] X. Zhang, W. Chen, G. Bao, and L. Zhao, "Suppression of porosity in beam weaving laser welding," *Science and Technology of Welding and Joining,* 9, (4). 374-376, **2004**.

[56] J. Zhou and H.-L. Tsai, "Porosity Formation and Prevention in Pulsed Laser Welding," *Journal of Heat Transfer,* 129, (8) **2007**.

[57] W. Y. Gao. Z, Huang. J, "Analysis of weld pool dynamic during stationary laser-MIG hybrid welding," *International Journal of Advanced Manufacturing Technology,* 44, (9-10). 870-879, **2009**.

[58] D. R, "Laser welding of thin metal sheets: an integrated keyhole and weld pool model with supporting experiments," *Journal of Physics D: Applied Physics,* 27, (8). 1619-1627, **1994**.

[59] S. Katayama, *Handbook of laser welding technologies*: Elsevier, 2013.

[60] Y. Zhang, L. Li, and G. Zhang, "Spectroscopic measurements of plasma inside the keyhole in deep penetration laser welding," *Journal of Physics D: Applied Physics,* 38, (5) p. 703, **2005**.

[61] J. Kroos, U. Gratzke, M. Vicanek, and G. Simon, "Dynamic behaviour of the keyhole in laser welding," *Journal of physics D: Applied physics,* 26, (3) p. 481, **1993**.

[62] T. Klein, M. Vicanek, J. Kroos, I. Decker, and G. Simon, "Oscillations of the keyhole in penetration laser beam welding," *Journal of Physics D: Applied Physics,* 27, (10) p. 2023, **1994**.

[63] J. Kroos, U. Gratzke, and G. Simon, "Towards a self-consistent model of the keyhole in penetration laser beam welding," *Journal of physics D: Applied physics,* 26, (3) p. 474, **1993**.

[64] A. Fellman and V. Kujanpää, "The effect of shielding gas composition on welding performance and weld properties in hybrid CO2 laser–gas metal arc welding of carbon manganese steel," *Journal of Laser Applications,* 18, (1). 12-20, **2006**.

[65] Y. Naito, M. Mizutani, and S. Katayama, "Effect of oxygen in ambient atmosphere on penetration characteristics in single yttrium–aluminum–garnet laser and hybrid welding," *Journal of laser applications,* 18, (1). 21-27, **2006**.

[66] S. Bag and A. De, *Computational modelling of conduction mode laser welding process*: Intech Open Access Publisher, 2010.

[67] A. De, S. K. Maiti, C. A. Walsh, and H. K. D. H. Bhadeshia, "Finite element simulation of laser spot welding," *Science and Technology of Welding and Joining,* 8, (5). 377-384, **2003**.

[68] A. Paul and T. DebRoy, "Free Surface Flow and Heat Transfer in Conduction Mode Laser Welding," *Metallurgical and materials transactions B,* 19. 851-858.

[69] H. Zhao and T. DebRoy, "Weld metal composition change during conduction mode laser welding of aluminum alloy 5182," *Metallurgical and materials transactions B,* 32, (1). 163-172, **2001**.

[70] R. Fabbro, "Melt pool and keyhole behaviour analysis for deep penetration laser welding," *Journal of Physics D: Applied Physics,* 43, (44) **2010**.

[71] R. Fabbro and K. Chouf, "Keyhole modeling during laser welding," *Journal of applied Physics,* 87, (9). 4075-4083, **2000**.

[72] X. Jin and L. Li, "An experimental study on the keyhole shapes in laser deep penetration welding," *Optics and lasers in engineering,* 41, (5). 779-790, **2004**.

[73] J. Y. Lee, S. H. Ko, D. F. Farson, and C. D. Yoo, "Mechanism of keyhole formation and stability in stationary laser welding," *Journal of Physics D: Applied Physics,* 35, (13) **2002**.

[74] A. Matsunawa and V. Semak, "The simulation of front keyhole wall dynamics during laser welding," *Journal of physics D: Applied physics,* 30, (5) **1997**.

[75] R. Wang, Y. Lei, and Y. Shi, "Numerical simulation of transient temperature field during laser keyhole welding of 304 stainless steel sheet," *Optics & Laser Technology,* 43, (4). 870-873, **2011**.

[76] J. Ion, *Laser processing of engineering materials: principles, procedure and industrial application*: Butterworth-Heinemann, 2005.

[77] Y. Harinath, K. Gopal, S. Murugan, and S. Albert, "Study on laser welding of fuel clad tubes and end plugs made of modified 9Cr–1Mo steel for metallic fuel of Fast Breeder Reactors," *Journal of Nuclear Materials,* 435, (1). 32-40, **2013**.

[78] S. Nakamura, "Detection technique for transition between deep penetration mode and shallow penetration mode in CO2 laser welding of metals," *Journal of Physics D: Applied Physics,* 33, (22). 2941-2948, **2000**.

[79] P. Colegrove, "Evaluation of a drilling model approach to represent laser spot microwelding," in *Trends in Welding Research*, Pine Mountain, GA.,**2009**.

[80] T. Sibillano, A. Ancona, V. Berardi, E. Schingaro, G. Basile, and P. M. Lugarà, "Optical detection of conduction/keyhole mode transition in laser welding," *Journal of Materials Processing Technology,* 191, (1-3). 364-367, **2007**.

[81] N. Ahmed, *New Developments in Advanced Welding*: CRC Press, 2005.

[82] D. Weckman, H. Kerr, and J. Liu, "The effects of process variables on pulsed Nd: YAG laser spot welds: Part II. AA 1100 aluminum and comparison to AISI 409 stainless steel," *Metallurgical and Materials Transactions B,* 28, (4). 687-700, **1997**.

[83] H. Bransch, D. Weckman, and H. Kerr, "Effects of Pulse Shaping on NchYAG Spot Welds in Austenitic Stainless Steel," **1994**.

[84] S. Kou, *Welding metallurgy*: Cambridge Univ Press, 1987.

[85] S. Katayama, "Solidification phenomena of weld metals. Solidification cracking mechanism and cracking susceptibility (3rd report)," **2001**.

[86] I. Medovar, "On the nature of weld hot cracking," *Avtomatich. Svarka,* 7. 12-28, **1954**.

[87] J. Borland, "Generalized theory of super-solidus cracking in welds (and castings)," *British Welding Journal,* 7, (8). 508-512, **1960**.

[88] T. Clyne and G. Davies, "Influence of composition on solidification cracking susceptibility in binary alloy systems," *British Foundryman,* 74. 65-73, **1981**.

[89] F. Matsuda, H. Nakagawa, and K. Sorada, "Dynamic Observation of Solidification and Solidification Cracking during Welding with Optical Microscope (I): Solidification Front and Behavior of Cracking (Materials, Metallurgy & Weldability)," *Transactions of JWRI,* 11, (2). 67-77, **1982**.

[90] N. Semenyuk, D. Rabkin, and A. Korshun, "Determining the hot cracking temperature range in the welding of aluminium alloys," *Welding International,* 1, (3). 222-224, **1987**.

[91] F. Matsuda, "Hot crack susceptibility of weld metal," in *Proceedings of the 1st US-Japan Symposium on Advances in Welding Metallurgy*. 19-36,**1990**.

[92] H. Fredriksson, "Transition from Peritectic to Eutectic Reaction in Iron Base Alloys," in *Solidification and Casting of Metals* Sheffield, England. 131-138,**1979**.

[93] F. Matsuda, H. Nakagawa, T. Uehara, S. Katayama, and Y. Arata, "A new explanation for role of delta-ferrite improving weld solidification crack susceptibility in austenitic stainless steel," *Transactions of the JWRI,* 8, (1). 105-112, **1979**.

[94] A. L. Schaeffler, "Constitution diagram for stainless steel weld metal.," *Metal progress,* 56. 680-680B, **1949**.

[95] D. Kotecki and T. Siewert, "WRC-1992 constitution diagram for stainless steel weld metals: a modification of the WRC-1988 diagram," *Welding Journal,* 71, (5). 171-178, **1992**.

[96] Y. Arata, F. Matsuda, and S. Katayama, "Solidification crack susceptibility in weld metals of fully austenitic stainless steels (Report II): Effect of ferrite, P, S, C, Si and Mn on ductility properties of solidification brittleness," *Transactions of JWRI,* 6, (1). 105-116, **1977**.

[97] J. Brooks and F. Lambert Jr, "The effects of phosphorus, sulfur and ferrite content on weld cracking of type 309 stainless steel," *Welding journal,* 51, (5) **1978**.

[98] T. Takalo, N. Suutala, and T. Moisio, "Austenitic solidification mode in austenitic stainless steel welds," *Metallurgical Transactions A,* 10, (8). 1173-1181, **1979**.

[99] J. Brooks and A. Thompson, "Microstructural development and solidification cracking susceptibility of austenitic stainless steel welds," *International Materials Reviews,* 36, (1). 16-44, **1991**.

[100] S. David, J. Vitek, R. Reed, and T. Hebble, "Effect of rapid solidification on stainless steel weld metal microstructures and its implications on the Schaeffler diagram," Oak Ridge National Lab., TN (USA)1987.

[101] J. C. Lippold, "Solidification Behavior and Cracking Susceptibility of Pulsed-Laser Welds in Austenitic Stainless Steels," *Welding research supplement*. 129s-139s, **1994**.

[102] A. Mahrle and E. Beyer, "Hybrid laser beam welding—classification, characteristics, and applications," *Journal of laser applications,* 18, (3). 169-180, **2006**.

[103] T. Graf and H. Staufer, "Laser-hybrid welding drives VW improvements," *Welding Journal-New york,* 82, (1). 42-42, **2003**.

[104] C. Bagger and F. O. Olsen, "Review of laser hybrid welding," *Journal of laser applications,* 17, (1). 2-14, **2005**.

[105] W. M. Steen, "Arc augmented laser processing of materials," *Journal of Applied Physics,* 51, (11). 5636-5641, **1980**.

[106] Y. Naito, S. Kodama, T. Miyazaki, Y. Sakiyama, and T. Nose, "Current Problems and the Answer Techniques in Welding Technique of Auto Bodies—Second Part," Nippon Steel2013.

[107] C. Roepke, S. Liu, S. Kelly, and R. Martukanitz, "Hybrid laser arc welding process evaluation on DH36 and EH36 steel," *Welding Journal,* 89, (7). 140-149, **2010**.

[108] J. Defalco, "Hybrid Laser Welding," *Welding journal,* 86, (10) **2007**.

[109] H. Stauffer, M. Ruhrnossl, and G. Miessbacher, "Hybrid welding for the automotive industry," *Industrial laser solutions for manufacturing*. 7-10, **2003**.

[110] S. Herbert, "Laser-hybrid welding of ships," *Welding Journal,* 83, (6). 39-44, **2004**.

[111] U. Jasnau, J. Hoffmann, and P. Seyffarth, "Nd: YAG Laser- GMA Hybrid Welding in Shipbuilding and Steel Construction," in *Robotic Welding, Intelligence and Automation*, ed: Springer, **2004**. 14-24.

[112] S. Kelly, S. Brown, J. Tressler, R. Martukanitz, and M. Ludwig, "Using hybrid laser arc welding to reduce distortion in ship panels," *Welding Journal,* 88, (3). 32-36, **2009**.

[113] B. Ribic, T. A. Palmer, and T. DebRoy, "Problems and issues in laser-arc hybrid welding," *International Materials Reviews,* 54, (4). 223-244, **2009**.

[114] C. Casavola, C. Pappalettere, and G. Pluvinage, "Fatigue resistance of titanium laser and hybrid welded joints," *Materials & Design,* 32, (5). 3127-3135, **2011**.

[115] C. Li, K. Muneharua, S. Takao, and H. Kouji, "Fiber laser-GMA hybrid welding of commercially pure titanium," *Materials & Design,* 30, (1). 109-114, **2009**.

[116] C. Roepke and S. Liu, "Hybrid laser arc welding of HY-80 steel," *Welding Journal,* 88, (8). 159-167, **2009**.

[117] G. Song, L. Liu, M. Chi, and J. F. Wang, "Investigations on Laser-TIG Hybrid Welding of Magnesium Alloys," *Materials Science Forum,* 488-489. 371-376, **2005**.

[118] N. A. McPherson, N. Suarez-Fernandez, D. W. Moon, C. P. H. Tan, C. K. Lee, and T. N. Baker, "Laser and laser assisted arc welding processes for DH 36 microalloyed steel ship plate," *Science and Technology of Welding and Joining,* 10, (4). 460-467, **2005**.

[119] H. Engstrom, K. Nilsson, J. Flinkfeldt, T. Nilsson, A. Skirfors, and B. Gustavsson, "Laser hybrid welding of high strength steels." 125-134,**2001**.

[120] S. Matsusaka, T. Uezono, T. Tsumura, M. Tanaka, and T. Watanabe, "Laser-Arc Hybrid Welding Process of Galvanized Steel Sheets," *Materials Science Forum,* 580-582. 355-358, **2008**.

[121] J. Wang, Y. Takenaka, T. Hongu, K. Fujii, and S. Katayama, "Laser-MIG arc hybrid welding of aluminium alloy - Comparison of melting characteristics between YAG laser and diode laser," *Welding International,* 21, (1). 32-38, **2007**.

[122] D.-I. C. Thomy, "Laser-MIG Hybrid Welding of Aluminium to Steel—Effect of Process Parameters on Joint Properties," *Welding in the World,* 56, (5-6). 124-132, **2012**.

[123] M. Gao, X. Zeng, Q. Hu, and J. Yan, "Laser-TIG hybrid welding of ultra-fine grained steel," *Journal of Materials Processing Technology,* 209, (2). 785-791, **2009**.

[124] L. M. Liu, X. F. Hao, and X. Du, "Microstructure characteristics and mechanical properties of laser–TIG hybrid welding joint of TA15 titanium alloy," *Materials Research Innovations,* 12, (3). 114-118, **2008**.

[125] C. Kim, W. Choi, J. Kim, and S. Rhee, "Relationship between the weldability and the process parameters for laser-TIG hybrid welding of galvanized steel sheets," *Materials transactions,* 49, (1). 179-186, **2008**.

[126] S. Grünenwald, T. Seefeld, F. Vollertsen, and M. Kocak, "Solutions for joining pipe steels using laser-GMA-hybrid welding processes," *Physics Procedia,* 5. 77-87, **2010**.

[127] H. S. Bang, H. S. Bang, Y. C. Kim, and I. H. Oh, "A study on mechanical and microstructure characteristics of the STS304L butt joints using hybrid CO2 laser-gas metal arc welding," *Materials & Design,* 32, (4). 2328-2333, **2011**.

[128] L. M. Liu and X. Zhao, "Study on the weld joint of Mg alloy and steel by laser-GTA hybrid welding," *Materials Characterization,* 59, (9). 1279-1284, **2008**.

[129] D. Rasmussen and L. Dubourg, "Hybird laser-GMAW welding of aluminium alloys: a review,"**2005**.

[130] S. Katayama, S. Uchiumi, M. Mizutani, J. Wang, and K. Fujii, "Penetration and porosity prevention mechanism in YAG laser-MIG hybrid welding," *Welding International,* 21, (1). 25-31, **2007**.

[131] L. Liming, W. Jifeng, and S. Gang, "Hybrid laser–TIG welding, laser beam welding and gas tungsten arc welding of AZ31B magnesium alloy," *Materials Science and Engineering: A,* 381, (1-2). 129-133, **2004**.

[132] L. Liu, G. Song, G. Liang, and J. Wang, "Pore formation during hybrid laser-tungsten inert gas arc welding of magnesium alloy AZ31B—mechanism and remedy," *Materials Science and Engineering: A,* 390, (1-2). 76-80, **2005**.

[133] L. Liu, G. Song, and J. F. Wang, "Investigation on Pore Formation during Hybrid Laser-Tungsten Inert Gas Arc Welding of Magnesium Alloy AZ31B," *Materials Science Forum,* 488-489. 361-364, **2005**.

[134] G. Song, L. Liu, and P. Wang, "Overlap welding of magnesium AZ31B sheets using laser-arc hybrid process," *Materials Science and Engineering: A,* 429, (1-2). 312-319, **2006**.

[135] G. Song and Z. Luo, "The influence of laser pulse waveform on laser–TIG hybrid welding of AZ31B magnesium alloy," *Optics and Lasers in Engineering,* 49, (1). 82-88, **2011**.

[136] A. Vandewynckèle, E. Vaamonde, J. Arias, M. Pérez, and G. Quintáns, "Laser-Arc welding of duplex stainless steel," in *26th International Congress on Applications of Lasers & Electro–Optics, ICALEO, paper*,**2007**.

[137] H. Chmelíčková and H. Šebestová, *Pulsed Laser Welding*: InTech, 2012.

[138] G. Campana, A. Fortunato, A. Ascari, G. Tani, and L. Tomesani, "The influence of arc transfer mode in hybrid laser-mig welding," *Journal of Materials Processing Technology,* 191, (1-3). 111-113, **2007**.

[139] M. Gao, X. Zeng, J. Yan, and Q. Hu, "Microstructure characteristics of laser–MIG hybrid welded mild steel," *Applied Surface Science,* 254, (18). 5715-5721, **2008**.

[140] M. Gao, X. Y. Zeng, and Q. W. Hu, "Effects of welding parameters on melting energy of CO_2 laser–GMA hybrid welding," *Science and Technology of Welding and Joining,* 11, (5). 517-522, **2006**.

[141] M. Gao, X. Y. Zeng, Q. W. Hu, and J. Yan, "Weld microstructure and shape of laser–arc hybrid welding," *Science and Technology of Welding and Joining,* 13, (2). 106-113, **2008**.

[142] G. L. Qin, Z. Lei, and S. Y. Lin, "Effects of Nd:YAG laser + pulsed MAG arc hybrid welding parameters on its weld shape," *Science and Technology of Welding and Joining,* 12, (1). 79-86, **2007**.

[143] L. Liu, S. Yuan, and C. Li, "Effect of relative location of laser beam and TIG arc in different hybrid welding modes," *Science and Technology of Welding and Joining,* 17, (6). 441-446, **2012**.

[144] P. Kah, A. Salminen, and J. Martikainen, "The effect of the relative location of laser beam with arc in different hybrid welding processes," *Mechanika,* 3, (83). 68-74, **2010**.

[145] B. Hu, "Nd/YAG Laser-assisted arc welding," PhD Dissertation, Delft University of Technology, Netherlands, 2002.

[146] M. El Rayes, C. Walz, and G. Sepold, "The influence of various hybrid welding parameters on bead geometry," *Weld. J,* 83, (5). 147-153, **2004**.

[147] S. Liu, F. Liu, H. Zhang, and Y. Shi, "Analysis of droplet transfer mode and forming process of weld bead in CO_2 laser–MAG hybrid welding process," *Optics & Laser Technology,* 44, (4). 1019-1025, **2012**.

[148] M. Doi, "Coaxial hybrid process of hollow cathode TIG and YAG laser welding," *Welding International,* 24, (3). 188-196, **2010**.

[149] T. Ishide, M. Nayama, M. Watanabe, and T. Nagashima, "Coaxial TIG-YAG & MIG-YAG welding methods," *Welding international,* 15, (12). 940-945, **2001**.

[150] G. Casalino, S. L. Campanelli, U. Dal Maso, and A. D. Ludovico, "Arc Leading Versus Laser Leading in the Hybrid Welding of Aluminium Alloy Using a Fiber Laser," *Procedia CIRP,* 12. 151-156, **2013**.

[151] G. Casalino, S. Campanelli, and A. D. Ludovico, "Hybrid Welding of AA5754-H111 Alloy Using a Fiber Laser," *Advanced Materials Research,* 628. 193-198, **2012**.

[152] G. Campana, A. Ascari, A. Fortunato, and G. Tani, "Hybrid laser-MIG welding of aluminum alloys: The influence of shielding gases," *Applied Surface Science,* 255, (10). 5588-5590, **2009**.

[153] P. Kah, A. Salminen, and J. Martikainen, "The analysis of shielding gases in laser-arc hybrid welding processes," *Proceedings of the Institution of Mechanical*

Engineers, Part B: Journal of Engineering Manufacture, 225, (7). 1073-1082, **2011**.

[154] P. Sathiya, M. K. Mishra, and B. Shanmugarajan, "Effect of shielding gases on microstructure and mechanical properties of super austenitic stainless steel by hybrid welding," *Materials & Design,* 33. 203-212, **2012**.

[155] G. Tani, G. Campana, A. Fortunato, and A. Ascari, "The influence of shielding gas in hybrid LASER–MIG welding," *Applied Surface Science,* 253, (19). 8050-8053, **2007**.

[156] L. Zhao, S. Tsukamoto, G. Arakane, T. Sugino, and T. DebRoy, "Influence of oxygen on weld geometry in fibre laser and fibre laser–GMA hybrid welding," *Science and Technology of Welding and Joining,* 16, (2). 166-173, **2011**.

[157] G. Ming, Z. Xiaoyan, and H. Qianwu, "Effects of gas shielding parameters on weld penetration of CO2 laser-TIG hybrid welding," *Journal of Materials Processing Technology,* 184, (1-3). 177-183, **2007**.

[158] P. Kah, "Overview of the exploration status of laser-arc hybrid welding processes," *Reviews on Advanced Materials Science,* 30, (2). 112-132, **2012**.

[159] A. Mahrle, S. Rose, M. Schnick, E. Beyer, and U. Füssel, "Laser-assisted plasma arc welding of stainless steel," *Journal of Laser Applications,* 25, (3). 0320061-8, **2013**.

[160] A. Mahrle, S. Rose, M. Schnick, T. Pinder, E. Beyer, and U. Füssel, "Improvements of the welding performance of plasma arcs by a superimposed fibre laser beam," in *SPIE LASE*. 82390D-82390D-12,**2012**.

[161] A. Mahrle, S. Rose, M. Schnick, E. Beyer, and U. Füssel, "Laser-assisted plasma arc welding of stainless steel," *Journal of Laser Applications,* 25, (3) p. 032006, **2013**.

[162] L. Zhiyong, T. S. Srivatsan, L. Yan, and Z. Wenzhao, "Coupling of Laser with Plasma Arc to Facilitate Hybrid Welding of Metallic Materials: A Review," *Journal of Materials Engineering and Performance,* 22, (2). 384-395, **2013**.

[163] B. Hu and G. Den Ouden, "Laser induced stabilisation of the welding arc," *Science and Technology of Welding & Joining,* 10, (1). 76-81, **2005**.

[164] Y. B. Chen, Z. L. Lei, L. Q. Li, and L. Wu, "Experimental study on welding characteristics of CO_2 laser TIG hybrid welding process," *Science and Technology of Welding and Joining,* 11, (4). 403-411, **2006**.

[165] A. Mahrle, M. Schnick, S. Rose, C. Demuth, E. Beyer, and U. Füssel, "Process characteristics of fibre-laser-assisted plasma arc welding," *Journal of Physics D: Applied Physics,* 44, (34) p. 345502, **2011**.

[166] J. Paulini and G. Simon, "A theoretical lower limit for laser power in laser-enhanced arc welding," *Journal of Physics D: Applied Physics,* 26, (9) p. 1523, **1993**.

[167] M. Anand, P. Gibbon, and M. Krishnamurthy, "Laser absorption in microdroplet plasmas," *Europhysics Letters (EPL),* 80, (2) **2007**.

[168] E. Le Guen, R. Fabbro, M. Carin, F. Coste, and P. Le Masson, "Analysis of hybrid Nd:Yag laser-MAG arc welding processes," *Optics & Laser Technology,* 43, (7). 1155-1166, **2011**.

[169] S. Katayama, Y. Naito, S. Uchiumi, and M. Mizutani, "Physical phenomena and porosity prevention mechanism in laser-arc hybrid welding," *Transactions-JWRI,* 35, (1) p. 13, **2006**.

[170] L. Zhao, T. Sugino, G. Arakane, and S. Tsukamoto, "Influence of welding parameters on distribution of wire feeding elements in CO_2 laser GMA hybrid welding," *Science and Technology of Welding and Joining,* 14, (5). 457-467, **2009**.

[171] O. Bader and H. Lui, "Laser safety and the eye: hidden hazards and practical pearls," in *Poster presented at the annual meeting of the American Academy of Dermatology*,**1996**.

[172] B. Raj, T. Jayakumar, S. Mahadevan, and S. K. Rai, "X-ray Diffraction Based Residual stress measurements for assessment of fatigue damage and rejuvenation process for undercarriages of aircrafts," *Journal of Nondestructive Evaluation,* 28, (3-4). 157-162, **2009**.

[173] H. Lapsanska, H. Chmelickova, and M. Hrabovsky, "Effect of beam energy on weld geometric characteristics in Nd: YAG laser overlapping spot welding of thin AISI 304 stainless steel sheets," *Metallurgical and materials transactions B,* 41, (5). 1108-1115, **2010**.

[174] W. Suder and S. Williams, "Investigation of the effects of basic laser material interaction parameters in laser welding," *Journal of Laser Applications,* 24, (3) p. 032009, **2012**.

[175] Y. Tzeng, "Parametric analysis of the pulsed Nd: YAG laser seam-welding process," *Journal of Materials Processing Technology,* 102, (1). 40-47, **2000**.

[176] M. J. Torkamany, M. J. Hamedi, F. Malek, and J. Sabbaghzadeh, "The effect of process parameters on keyhole welding with a 400W Nd:YAG pulsed laser," *Journal of Physics D: Applied Physics,* 39, (21). 4563-4567, **2006**.

[177] E. Assuncao, S. Williams, and D. Yapp, "Interaction time and beam diameter effects on the conduction mode limit," *Optics and Lasers in Engineering,* 50, (6). 823-828, **2012**.

[178] W. Tan, N. S. Bailey, and Y. C. Shin, "Investigation of keyhole plume and molten pool based on a three-dimensional dynamic model with sharp interface formulation," *Journal of Physics D: Applied Physics,* 46, (5) p. 055501, **2013**.

[179] S. Fujinaga, H. Takenaka, T. Narikiyo, S. Katayama, and A. Matsunawa, "Direct observation of keyhole behaviour during pulse modulated high-power Nd: YAG laser irradiation," *Journal of Physics D: Applied Physics,* 33, (5) **2000**.

[180] A. M. Chelladurai, K. A. Gopal, S. Murugan, S. Venugopal, and T. Jayakumar, "Energy Transfer Modes in Pulsed Laser Seam Welding," *Materials and Manufacturing Processes,* 30, (2). 162-168, **2015**.

[181] N. Seto, S. Katayama, and A. Matsunawa, "High-speed simultaneous observation of plasma and keyhole behavior during high power CO2 laser welding: effect of shielding gas on porosity formation," *Journal of laser applications,* 12, (6). 245-250, **2000**.

[182] J. Lippold, "Centerline cracking in deep penetration electron beam welds in Type 304L stainless steel," *Welding Journal,* 64, (5). 127s-136s, **1985**.

[183] H. Zhao and T. DebRoy, "Pore formation during laser beam welding of die-cast magnesium alloy AM60B-mechanism and remedy," *Welding Journal,* 80, (8). 204-210, **2001**.

[184] J. O. Milewski, G. K. Lewis, and J. E. Wittig, "Microstructural evaluation of low and high duty cycle Nd: YAG laser beam welds in 2024-T3 aluminum," *Welding journal,* 72. 341-s -346s, **1993**.

[185] C. Bertrand and A. Poulon-Quintin, "Effect of temporal pulse shaping on the reduction of laser weld defects in a Pd–Ag–Sn dental alloy," *Dental Materials,* 27, (3). e43-e50, **2011**.

[186] J. Zhang, D. Weckman, and Y. Zhou, "Effects of temporal pulse shaping on cracking susceptibility of 6061-T6 aluminum Nd: YAG laser welds," *Welding Journal,* 87, (1) p. 18, **2008**.

[187] G. M. Goodwin, "The effects of heat input and weld process on hot cracking in stainless steel," *Welding Journal,* 67. 88s-94s, **1988**.

[188] M. Montazeri, F. Malek Ghaini, and O. Ojo, "Heat Input and the Liquation Cracking of Laser Welded IN738LC Superalloy," *Welding journal,* 92, (9). 258s-264s, **2013**.

[189] P. W. Hochanadel, T. J. Lienert, J. N. Martinez, R. J. Martinez, and M. Q. Johnson, "Weld solidification cracking in 304 to 304L stainless steel," in *Hot Cracking Phenomena in Welds III*, ed: Springer, **2011**. 145-160.

[190] T. Zacharia, S. David, J. Vitek, and T. Debroy, "Heat transfer during Nd: YAG pulsed laser welding and its effect on solidification structure of austenitic stainless steels," *Metallurgical Transactions A,* 20, (5). 957-967, **1989**.

[191] J. Vitek, A. Dasgupta, and S. David, "Microstructural modification of austenitic stainless steels by rapid solidification," *Metallurgical Transactions A,* 14, (9). 1833-1841, **1983**.

[192] T. Böllinghaus, H. Herold, C. E. Cross, and J. C. Lippold, *Hot cracking phenomena in welds II*: Springer Science & Business Media, 2008.

[193] A. M. Chelladurai, K. A. Gopal, S. Murugan, S. K. Albert, S. Venugopal, and T. Jayakumar, "Effect of energy transfer modes on solidification cracking in pulsed laser welding," *Science and Technology of Welding and Joining,* 20, (7). 578-584, **2015**.

[194] X. Hao and L. Liu, "Effect of laser pulse on arc plasma and magnesium target in low-power laser/arc hybrid welding," *Plasma Science, IEEE Transactions on,* 37, (11). 2197-2201, **2009**.

[195] R. S. Huang, L. Kang, and X. Ma, "Microstructure and phase composition of a low-power YAG laser-MAG welded stainless steel joint," *Journal of materials engineering and performance,* 17, (6). 928-935, **2008**.

[196] A. Mahrle, S. Rose, M. Schnick, E. Beyer, and U. Füssel, "Stabilisation of plasma welding arcs by low power laser beams," *Science and Technology of Welding and Joining,* 18, (4). 323-328, **2013**.

[197] A.-V. Bîrdeanu, C. Ciucă, and A. Puicea, "Pulsed LASER-(micro)TIG hybrid welding: Process characteristics," *Journal of Materials Processing Technology,* 212, (4). 890-902, **2012**.

[198] A.-M. El-Batahgy, A.-F. Khourshid, and T. Sharef, "Effect of laser beam welding parameters on microstructure and properties of duplex stainless steel," *Materials Sciences and Applications,* 2, (10) p. 1443, **2011**.

[199] M. Lee, J. Huang, and N. Ho, "Microstructural and mechanical characterization of laser-beam welding of a 8090 Al-Li thin sheet," *Journal of materials science,* 31, (6). 1455-1468, **1996**.

[200] M. Zhang, G. Chen, Y. Zhou, and S. Liao, "Optimization of deep penetration laser welding of thick stainless steel with a 10 kW fiber laser," *Materials & Design,* 53. 568-576, **2014**.

[201] M. Vänskä, F. Abt, R. Weber, A. Salminen, and T. Graf, "Effects of welding parameters onto keyhole geometry for partial penetration laser welding," *Physics Procedia,* 41. 199-208, **2013**.

[202] P. Fuerschbach and G. Knorovsky, "A study of melting efficiency in plasma arc and gas tungsten arc welding: a method for selecting optimal weld schedules to minimize net heat input is derived frm calorimetric measuremts," *Welding Journal,* 70, (11). 287-297, **1991**.

[203] T. Kim, C. E. Albright, and S. Chiang, "The energy transfer efficiency in laser welding process," *Journal of Laser Applications,* 2, (1). 23-28, **1990**.

[204] M. Vedani, "Microstructural evolution of tool steels after Nd-YAG laser repair welding," *Journal of materials science,* 39, (1). 241-249, **2004**.

[205] A. Odabaşı, N. Ünlü, G. Göller, E. S. Kayalı, and M. N. Eruslu, "Assessment of the effects of heat input on microstructure and mechanical properties in laser beam welded Haynes 188 undermatched joints," *Materials Science and Engineering: A,* 559. 731-741, **2013**.

[206] D. Akbari and I. Sattari-Far, "Effect of the welding heat input on residual stresses in butt-welds of dissimilar pipe joints," *International journal of pressure vessels and piping,* 86, (11). 769-776, **2009**.

[207] M. Mochizuki, "Control of welding residual stress for ensuring integrity against fatigue and stress–corrosion cracking," *Nuclear Engineering and Design,* 237, (2). 107-123, **2007**.

[208] A. M. Chelladurai, K. A. Gopal, S. Murugan, S. Venugopal, and T. Jayakumar, "Development of pulsed laser-GTAW hybrid welding," in *International Institute of Welding – International Welding Congress 2014 (IC 2014)*, New Delhi. 171-176,**2014**.